

# Discovery and Crystallographic Studies of Trisubstituted Piperazine Derivatives as Non-Covalent SARS-CoV-2 Main Protease Inhibitors with High Target Specificity and Low Toxicity

Shenghua Gao, Katharina Sylvester, Letian Song, Tobias Claff, Lanlan Jing, Molly Woodson, Renato H. Weiße, Yusen Cheng, Laura Schäkel, Marvin Petry, Michael Gütschow, Anke C. Schiedel, Norbert Sträter, Dongwei Kang, Shujing Xu, Karoly Toth, John Tavis, Ann E. Tollefson,\* Christa E. Müller,\* Xinyong Liu,\* and Peng Zhan\*



Cite This: <https://doi.org/10.1021/acs.jmedchem.2c01146>



Read Online

ACCESS |



Metrics & More

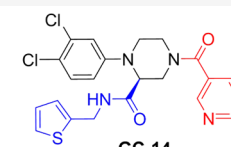
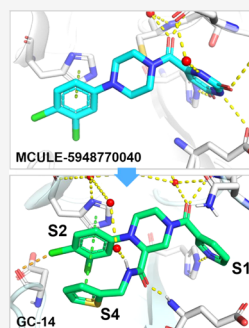


Article Recommendations



Supporting Information

**ABSTRACT:** The continuous spread of SARS-CoV-2 calls for more direct-acting antiviral agents to combat the highly infectious variants. The main protease ( $M^{Pro}$ ) is a promising target for anti-SARS-CoV-2 drug design. Here, we report the discovery of potent non-covalent non-peptide  $M^{Pro}$  inhibitors featuring a 1,2,4-trisubstituted piperazine scaffold. We systematically modified the non-covalent hit MCULE-5948770040 by structure-based rational design combined with multi-site binding and privileged structure assembly strategies. The optimized compound GC-14 inhibits  $M^{Pro}$  with high potency ( $IC_{50} = 0.40 \mu M$ ) and displays excellent antiviral activity ( $EC_{50} = 1.1 \mu M$ ), being more potent than Remdesivir. Notably, GC-14 exhibits low cytotoxicity ( $CC_{50} > 100 \mu M$ ) and excellent target selectivity for SARS-CoV-2  $M^{Pro}$  ( $IC_{50} > 50 \mu M$  for cathepsins B, F, K, L, and caspase 3). X-ray co-crystal structures prove that the inhibitors occupy multiple subpockets by critical non-covalent interactions. These studies may provide a basis for developing a more efficient and safer therapy for COVID-19.



**GC-14**  
SARS-CoV-2  $M^{Pro}$   $IC_{50} = 0.40 \mu M$ ,  
 $EC_{50} = 1.1 \mu M$ ,  $CC_{50} > 100 \mu M$

- ✓ Non-covalent, non-peptidic;
- ✓ Crystallographic study;
- ✓ High target specificity;
- ✓ Low cytotoxicity.

## INTRODUCTION

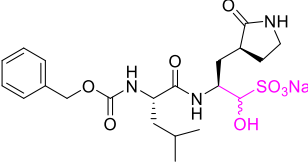
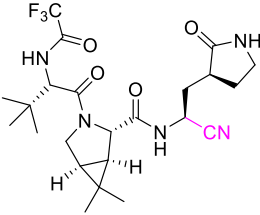
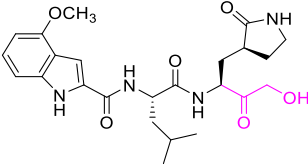
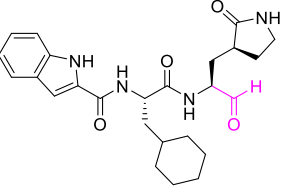
Severe acute respiratory syndrome coronavirus 2 (SARS-CoV-2), the pathogen of coronavirus disease 2019 (COVID-19), has caused a serious public health issue and continues to be a global health concern. This pathogen, emerging from the  $\beta$ -coronavirus family, is characterized by a positive-sense single-stranded RNA and has affected more people than any other human coronavirus to date.<sup>1</sup> By the end of June 2022, there have been a total of 546 million confirmed infections and 6.3 million deaths reported worldwide.<sup>2</sup> SARS-CoV-2 invades its host through the respiratory tract via interactions with the human angiotensin-converting enzyme 2 (ACE2) receptor causing symptoms that range from fever to pneumonia, multiorgan failure, and even death.<sup>3,4</sup> The advancement of vaccines has proven helpful in building up the population's immunity and reducing severe symptoms. However, the efficacy of approved COVID-19 vaccines has shown a dramatic decline within a few months after vaccination, and moreover, they display only moderate efficacy toward the emerging omicron variants.<sup>5–7</sup> Furthermore, the percentage of vaccinated people has remained moderate to low in many countries. Thus, effective therapeutic agents are urgently required to treat infected patients suffering from severe symptoms. However,

therapeutic small-molecule drugs approved for the treatment of COVID-19 are still limited.

The life cycle of SARS-CoV-2 includes the expression of four structural proteins (S/N/M/E) and two overlapping polyproteins (pp1a and pp1ab). Two cysteine proteases, the main protease [ $M^{Pro}$ , also termed 3C-like (3CL) protease] and the papain-like protease ( $PL^{Pro}$ ), are responsible for cleaving polyproteins into sequences, generating non-structural proteins.<sup>8</sup>  $M^{Pro}$  has thus been confirmed to play an indispensable role in SARS-CoV-2 reproduction, and almost no mutations have occurred in the  $M^{Pro}$  active site among the existing SARS-CoV-2 mutant strains (Alpha, Beta, Gamma, Delta, and Omicron), which makes this enzyme an attractive drug target. Moreover,  $M^{Pro}$  cleaves polypeptide sequences exclusively after a glutamine residue; to the best of our knowledge, no human host-cell protease is known with this substrate specificity, and

Received: July 17, 2022

Table 1. Representative Peptidomimetic SARS-CoV-2 M<sup>Pro</sup> Inhibitors<sup>21–23</sup>

Covalent M <sup>Pro</sup> inhibitor	Clinical stage	SARS-CoV-2 M <sup>Pro</sup> , IC <sub>50</sub> (nM)	Off-target activity, IC <sub>50</sub> (nM)
 <b>GC-376</b>	Phase III	33 nM	Cathepsin L (990 nM) Cathepsin I (74 nM) Cathepsin K (0.56 nM)
 <b>PF-07321332</b> <b>(Nirmatrelvir)</b>	Approved	75 nM	N.D. <sup>a</sup>
 <b>PF-00835231</b>	Phase III (Prodrug)	5 nM	Cathepsin L (146 nM) Cathepsin B (1300 nM)
 <b>11a</b>	Phase I	8 nM	Cathepsin L (210 nM)

<sup>a</sup>N.D. = no data available.

the human genome does not encode any homogeneous analogue to M<sup>Pro</sup>, making it a rational target for anti-SARS-CoV-2 drug development. The central part of the active site in M<sup>Pro</sup> is formed by His41 and Cys145 serving as the catalytic dyad to promote peptide bond hydrolysis, around which four pockets containing key amino acid residues are arranged.<sup>9–11</sup>

The M<sup>Pro</sup> inhibitors described so far are mainly based on peptidomimetics with electrophilic covalent warheads targeting Cys145.<sup>12–14</sup> This class of compounds includes Nirmatrelvir (PF-07321332),<sup>15</sup> PF-07304814,<sup>16</sup> GC-376,<sup>17</sup> and 11a,<sup>18</sup> which have been developed as clinical candidates or were already approved to treat COVID-19 (Table 1). In addition, covalently binding small-molecule M<sup>Pro</sup> inhibitors, such as chloropyridyl esters of indole derivatives, have been

described.<sup>13,14,19,20</sup> However, it was indicated that some of the developed covalently binding peptidomimetics additionally inhibit certain host proteases.<sup>21,22</sup> The reactive warhead-equipped peptidic scaffolds are responsible for those off-target activities, which have become a serious concern for most covalent peptidomimetic inhibitors (see Table 1).<sup>22,23</sup>

In contrast, de novo designed non-covalent non-peptide inhibitors have shown promising selectivity and drug-like properties but in many cases still lack satisfactory antiviral activity. Examples include compounds 21,<sup>24</sup> 23R,<sup>25</sup> and recently disclosed compound S-217622 (Figure 1), which showed promising safety and antiviral potency profiles in a phase II clinical trial.<sup>26</sup> S-217622 was proven to be effective against most SARS-CoV-2 variants and to show remarkable

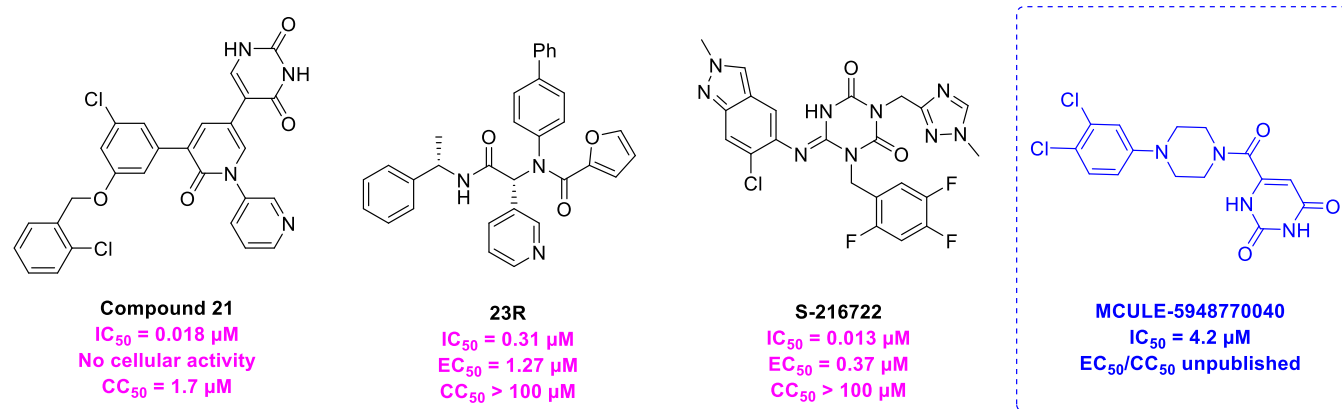


**Figure 1.** Representative non-covalent SARS-CoV-2  $M^{\text{Pro}}$  inhibitors.

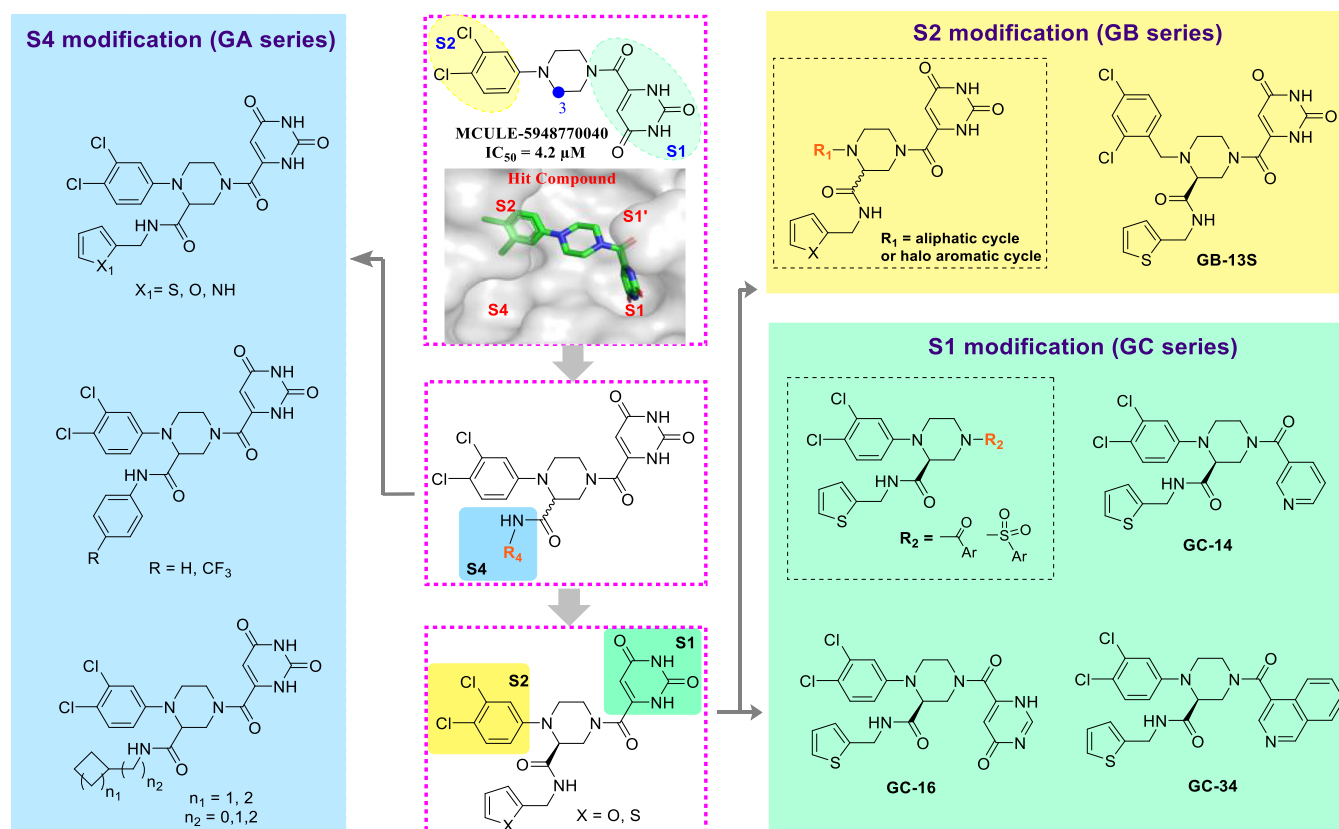


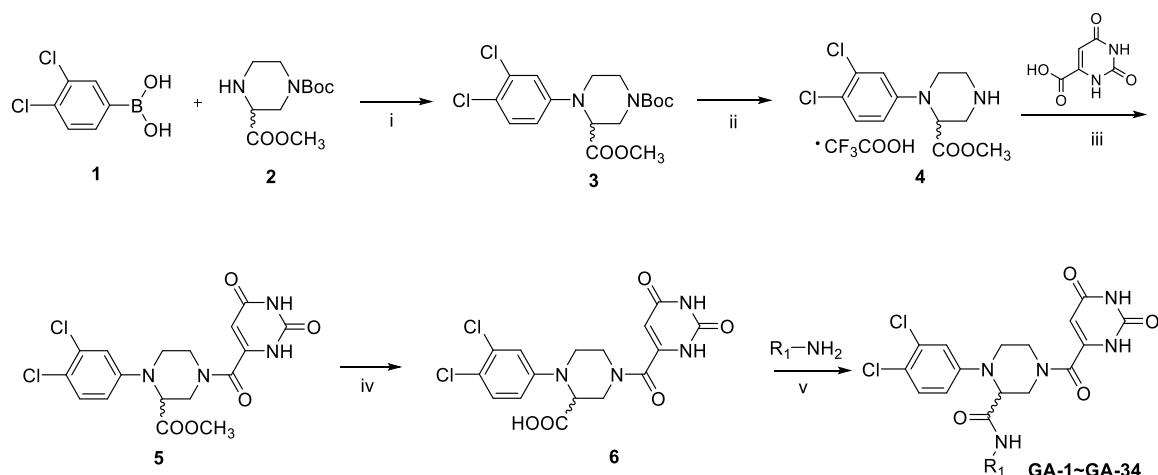
**Figure 2.** Illustration of the general design concepts and structures of representative compounds of the three designed series of compounds: GA series (blue), GB series (yellow), and GC series (green).

selectivity for  $M^{\text{Pro}}$  versus host proteases, suggesting great potential for non-covalent non-peptide inhibitors. However, development of non-covalent inhibitors is still very limited, although an urgent need for potent non-covalent inhibitors with improved properties and therapeutic effects continues to exist; to date, no such drug has been approved for clinical use. In view of the necessity to create a wide range of options and due to the anticipated clinical requirements, novel  $M^{\text{Pro}}$  inhibitors with diverse chemical scaffolds, increased target specificity, and improved pharmaceutical profile need to be further explored and developed.

MCULE-5948770040 was identified by high-throughput virtual screening showing moderate inhibition against  $M^{\text{Pro}}$  ( $IC_{50} = 4.2 \mu\text{M}$ , Figure 1), as reported by Clyde et al.<sup>27</sup> Its co-

crystal structure revealed that the compound that contains a piperazine ring as the skeleton occupies only the S1 and S2 pockets of the  $M^{\text{Pro}}$  active site, but no interactions within the S4 pocket were observed. The piperazine ring lacks additional functional groups that could bind within the S3 and S4 pockets, which are considered vital sites as revealed in previous structure–activity relationships (SARs) analysis and computational studies.<sup>10,24</sup> These features make MCULE-5948770040 a promising lead structure for further systematic structure-based modification.

Our objective was to investigate non-covalent  $M^{\text{Pro}}$  inhibitors based on novel scaffolds that could combine enhanced antiviral activity and reduced adverse effects with an improved pharmaceutical profile. To maximally occupy the

Scheme 1. Synthetic Route to the Intermediates and Target Compounds in the GA Series<sup>a</sup>

<sup>a</sup>Reagents and conditions: (i)  $\text{Cu}(\text{OAc})_2$ ,  $\text{O}_2$ , pyridine, DCM, r.t.; (ii)  $\text{CF}_3\text{COOH}$ , DCM, r.t.; (iii) orotic acid, HATU, DIPEA, DCM, r.t.; (iv)  $\text{LiOH}$ ,  $\text{MeOH}$ ,  $\text{THF}$ , water, r.t.; (v) various amines, HATU, DIPEA, DCM, r.t.

entire active site of  $\text{M}^{\text{Pro}}$  and to interact with key amino acid residues, multi-site binding and privileged structure assembly strategies were employed to combine diverse fragments with the lead structure.<sup>28,29</sup> Accordingly, we introduced a carboxamide group protruding from the piperazine ring of the hit compound, attaching privileged substituents to occupy the S4 pocket. By modifying substitutions on the piperazine nitrogen atoms and the carboxyl side chain, respectively, three series of derivatives were designed and successively synthesized. The new compounds were characterized by enzymatic and cellular activity evaluation, selectivity determination, and structural biology studies. Two final compounds were discovered with high in vitro inhibitory activity and selectivity, whose co-crystal structures with  $\text{M}^{\text{Pro}}$  revealed a multi-valent binding mode with their target, confirming our rational design approach. The synthetic procedures, experimental details, and characterization of the compounds are provided within the [Supporting Information](#). These results indicated the great potential of non-covalent  $\text{M}^{\text{Pro}}$  inhibitors based on novel 1,2,4-trisubstituted piperazine scaffold, which warrants their further optimization, in vivo studies, and development toward novel clinical candidates against SARS-CoV-2.

## RESULTS AND DISCUSSION

MCULE-5948770040 is a promising inhibitor identified by an in silico screening, showing moderate activity against  $\text{M}^{\text{Pro}}$  of SARS-CoV-2 ( $\text{IC}_{50} = 4.2 \mu\text{M}$ ).<sup>27</sup> Co-crystallization of the compound with  $\text{M}^{\text{Pro}}$  indicated that the piperazine derivative displays interactions with the S1 and S2 pockets of the  $\text{M}^{\text{Pro}}$  active site, while the S4 pocket remains unoccupied. This observation provided a basis for our subsequent structural modifications. In order to fully occupy each pocket of the active site and to enhance the compound's binding affinity for  $\text{M}^{\text{Pro}}$ , the hit compound MCULE-5948770040 was systematically modified. The rationale for the design of novel  $\text{M}^{\text{Pro}}$  inhibitors is illustrated in [Figure 2](#).

### General Design Concept and Synthetic Route.

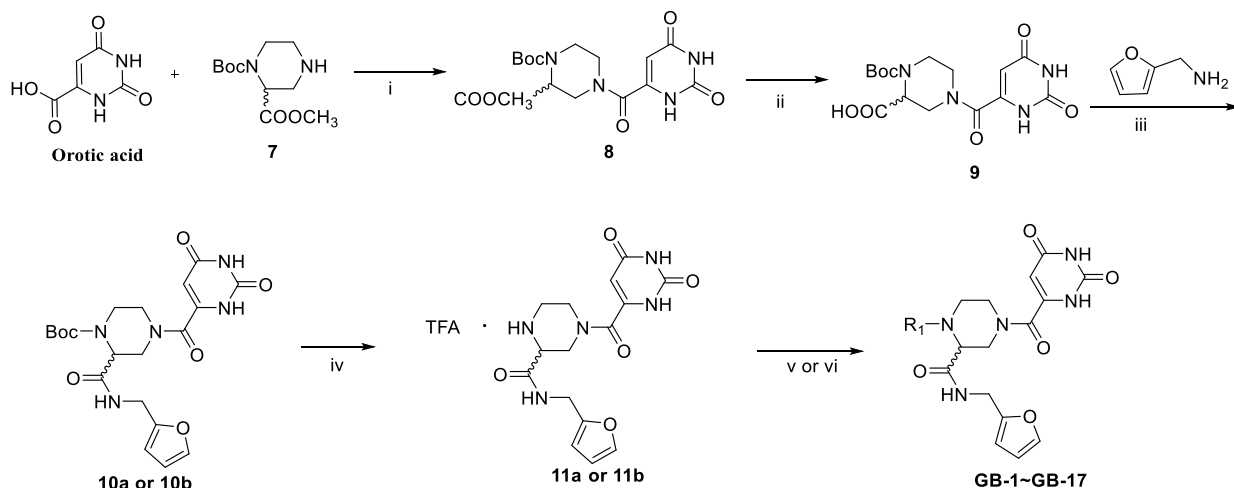
Structure-based drug design is a powerful approach to develop antiviral agents that can be specifically tailored to a target. Three-dimensional X-ray crystallographic structures of  $\text{M}^{\text{Pro}}$  have provided valuable insights into its substrate binding and enzymatic mechanism<sup>10</sup> and have enabled target-based design

strategies. As described above, we have primarily taken into consideration an occupation of the S4 hydrophobic site of  $\text{M}^{\text{Pro}}$  with the aim to design novel inhibitors with enhanced antiviral activity. Based on analyzing the co-crystal structure of our lead compound, we introduced several privileged S4-occupying components of known  $\text{M}^{\text{Pro}}$  inhibitors into the 3-position of the piperazine skeleton, using the "multi-site binding" strategy. Subsequently, a variety of amines containing lipophilic substituents, such as substituted phenyl, aliphatic carbocycle, and aromatic heterocyclic residues, were selected to explore the preferred groups for interacting with the S4 pocket ([Figure 2](#), GA series).

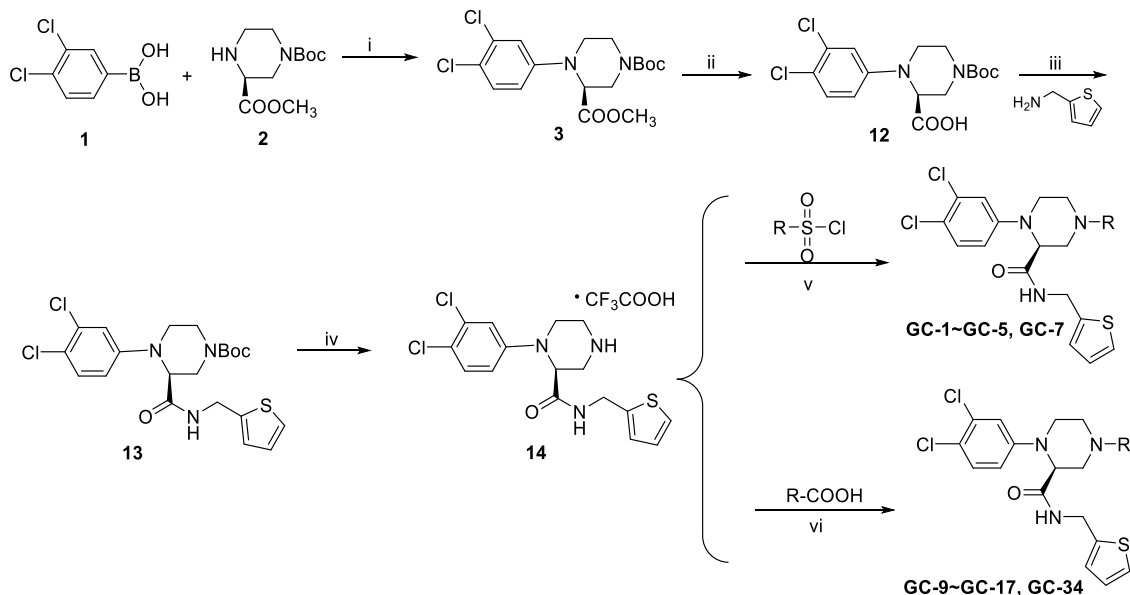
Moreover, a second series was designed to ascertain the tolerability of changes to S2 pocket binding, adjust the rigidity of the compounds, and determine the optimal substituents. From the co-crystal structure of the non-covalent inhibitor **23R**,<sup>25</sup> we realized that extra chemical space should be present in the S2 pocket, which could accommodate bulky groups such as a biphenyl residue. Therefore, the lipophilic groups were selected for attachment to the parent scaffold ([Figure 2](#), GB series).

Furthermore, given the poor antiviral activity of the lead compound (for details see below), membrane permeability prediction was conducted, leading to the discovery that the orotic acid fragment interacting with the S1 pocket was the major factor for lacking cell permeability. Therefore, the orotic acid moiety was replaced by less polar groups still containing H-bond acceptors to sustain the interaction with His163. Additionally, some privileged fragments of existing  $\text{M}^{\text{Pro}}$  inhibitors with high lipophilicity interacting with the S1 pocket were introduced. Considering the insignificant activity improvement in the GB series and potential metabolism-sensitive site on benzyl  $-\text{CH}_2-$ , 3,4-dichlorophenyl moiety was unchanged in the S2 pocket. Based on molecular hybridization and computer-aided drug design strategies, we selected pyridine formamide, isoquinoline formamide, and an aromatic sulfonamide to substitute for orotic acid ([Figure 2](#), GC series).

Synthetic routes were designed and elaborated to prepare these target compounds in three series. [Scheme 1](#) shows the synthesis of intermediates and target compounds of the GA series, as listed in [Table S1](#). The starting material, 1-(*tert*-butyl)

Scheme 2. Synthetic Route to the Intermediates and Target Compounds in the GB Series<sup>4f</sup>

<sup>4f</sup>Reagents and conditions: (i) HATU, DIPEA, DCM, r.t.; (ii) LiOH, MeOH, THF, water, r.t.; (iii) HATU, DIPEA, DCM, r.t.; (iv) TFA, DCM, r.t.; (v) various benzyl bromides, MeOH, K<sub>2</sub>CO<sub>3</sub>, r.t. (vi) NEt<sub>3</sub>, DCM, r.t.

Scheme 3. Synthetic Route to the Intermediates and Target Compounds in the GC Series<sup>4f</sup>

<sup>4f</sup>Reagents and conditions: (i) Cu(OAc)<sub>2</sub>, O<sub>2</sub>, pyridine, DCM, r.t.; (ii) LiOH, MeOH, THF, water, r.t.; (iii) HATU, *N,N*-diisopropyl ethylamine, DCM, r.t.; (iv) CF<sub>3</sub>COOH, DCM, r.t.; (v) various sulfonyl chlorides, *N,N*-diisopropyl ethylamine, DCM, r.t.; (vi) various carboxylic acids, HATU, *N,N*-diisopropyl ethylamine, DCM, r.t.

3-methylpiperazine-1,3-dicarboxylate, was treated with 3,4-dichlorophenylboronic acid to obtain the C–N coupling product 3. The Boc group was then removed to give trifluoroacetate of intermediate 4, which was then acylated by orotic acid in the presence of HATU to yield 5. Subsequently, the ester group of 5 was hydrolyzed under alkaline conditions to afford 6, followed by treatment with various amines, which gave all target compounds in GA series.

Scheme 2 shows a likewise synthetic route to the GB series in Table S2. 1-(*tert*-Butyl)-2-methylpiperazine-1,2-dicarboxylate (7) was acylated by orotic acid to obtain the intermediate 8. The intermediate was hydrolyzed to remove the methyl ester group and treated with furan-2-yl methylamine or thiophen-2-yl methylamine to yield the acylated products 10a and 10b. The Boc group was then cleaved to afford 11a/

11b in the form of trifluoroacetate. Finally, 11a/11b was converted to target compounds by nucleophilic substitution or acylation.

Scheme 3 shows the synthesis of compounds in the GC series, shown in Table S4. The (*S*)-enantiomer of intermediate 3 was prepared as described above using 1-(*tert*-butyl) 2-methyl (*S*)-piperazine-1,2-dicarboxylate and then hydrolyzed to give carboxylic acid intermediate 12. Treatment of 12 with thiophen-2-yl methylamine yielded 13, which was then processed by trifluoroacetic acid to give 14 as a trifluoroacetate. 14 was treated by carboxylic acids or sulfonyl chlorides to afford final compounds in the GC series.

**Enzyme Inhibition and SAR Analysis of the GA Series.** Altogether 34 synthesized novel compounds (see Table S1 in the Supporting Information) were initially tested as racemic

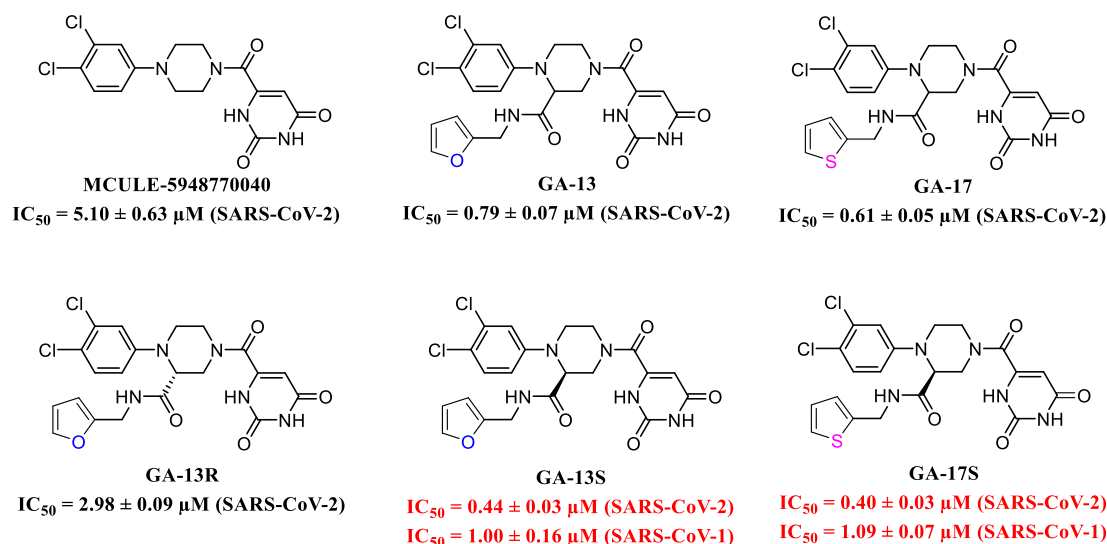


**Figure 3.** Inhibition of  $M^{pro}$  activity by MCULE-5948770040, GA-13, GA-13S, GA-13R, GA-17, and GA-17S. For GA-13S and GA-17S,  $M^{pro}$  inhibition of SARS-CoV-1 has additionally been determined. Error bars represent the mean  $\pm$  SD values of three independent experiments.

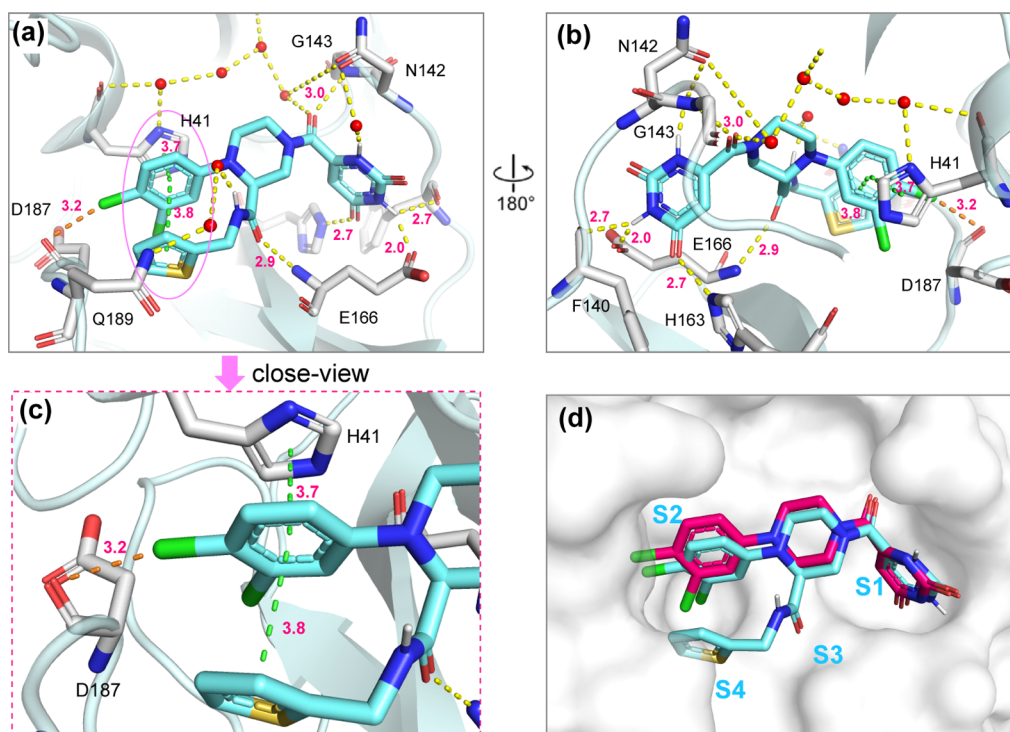


**Figure 4.** X-ray co-crystal structure of GA-17S and  $M^{pro}$  (PDB ID: 8ACD). (a,b) View of GA-17S (cyan) from an inward/backward angle of the active pocket. Water molecules are shown as red spheres. Hydrogen bonds are indicated as yellow dashed lines;  $\pi$ - $\pi$  stacking is indicated as green dashed lines; a halogen bond is indicated as an orange dashed line; (c) close-up view of a sandwich-like stacking structure across the S2 and S4 pockets; (d) binding pose comparison of GA-17S (cyan) and MCULE-5948770040 (magenta) (PDB ID: 7LTJ).

mixtures against  $M^{pro}$  in a fluorescence resonance energy transfer (FRET)-based enzymatic assay at 10  $\mu M$  concentration. Several compounds displayed significantly improved enzyme inhibition compared to the lead compound MCULE-5948770040 (Figure S1 in the Supporting Information). For compounds showing an inhibition of  $>80\%$ , we also determined the  $IC_{50}$  values. The inhibitory activities of several compounds toward  $M^{pro}$  were significantly higher than that of MCULE-5948770040 ( $IC_{50} = 5.1 \pm 0.63 \mu M$ ) (Figures 3 and S2), among which GA-13 ( $IC_{50} = 0.79 \pm 0.07 \mu M$ ) and GA-17 ( $IC_{50} = 0.61 \pm 0.05 \mu M$ ) displayed the best potency. These

activity data were the first evidence to prove our design hypothesis.

SAR analysis revealed that the activities of phenylethylamine- (GA-4 and GA-14) and benzylamine-bearing compounds (GA-2, GA-10, GA-11, and GA-12) were significantly lower than those of the aniline-substituted analogues (GA-18, GA-19, and GA-27) or heterocycle analogues (GA-13, GA-17, and GA-25). Elongation of the carbon chains was detrimental for protease inhibition. A rigid aromatic moiety joint with carboxamide by two or more carbons may clash with residues around the S4 pocket and lead to a solvent exposed

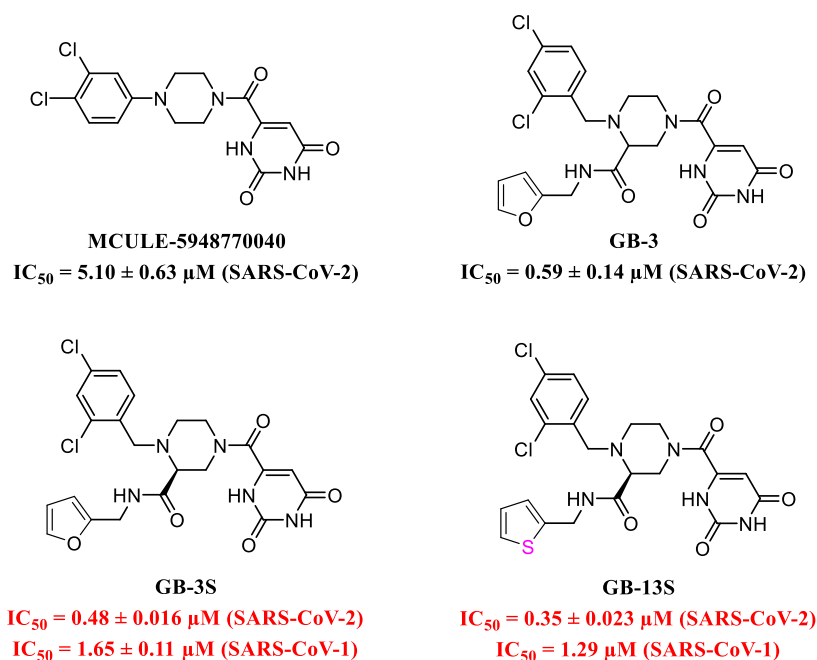


**Figure 5.** Enzymatic inhibitory activity of **GB-3**, **GB-3S**, and **GB-13S** against  $M^{pro}$  of SARS-CoV-2 and SARS-CoV-1.

orientation. Likewise, additional substituents on the aromatic heterocycles led to a decrease in inhibitory activity (**GA-20** and **GA-24**). These data imply that the tailored ability of the S4 pocket to accommodate inhibitor substructures is the major factor governing the potency of various GA compounds. In order to further explore the stereoselectivity of the compounds' interaction, two isomers of **GA-17** and **GA-13** were synthesized from chiral sources. Superimposition of co-crystal structures suggested that S4-directed side chain of the *S*-enantiomer adapts an equatorial conformation stretching out from the piperazine heterocycle into an unoccupied cavity and should thus provide a more favorable binding mode of the *S*- than the *R*-enantiomer. In fact, the *S*-enantiomer possessed the advantageous configuration, and **GA-17S** ( $IC_{50} = 0.40 \pm 0.03 \mu M$ ) was superior to the racemate. Moreover, **GA-13S** and **GA-17S** also proved to be active against SARS-CoV-1  $M^{pro}$  (see Figure 3).

**Crystallographic Studies of GA-17S in Complex with  $M^{pro}$ .** To investigate the interaction mode between compounds of the GA series and  $M^{pro}$ , especially with the S4 pocket, a co-crystal structure of **GA-17S** was obtained (see Figure 4a,b). The piperazine skeleton maintained the original binding mode of MCULE-5948770040. The orotic acid moiety occupies the S1 pocket, forming a hydrogen bond network with surrounding amino acids such as Glu166 (side chain), His163, and Gly143. The 3,4-dichlorophenyl residue extends into the hydrophobic S2 pocket, forming stacking interactions with the side chain of His41. Additionally, 4-chlorine atom of the dichlorophenyl residue displays a weak halogen bonding interaction with the backbone carbonyl group of Asp187 (distance of 3.2 Å, angle C–Cl...O of 166.4°); in the previous co-crystal structure of MCULE-5948770040, the geometry (distance of 3.4 Å, angle C–Cl...O of 136.4°) is below the thresholds of an energetically relevant interaction.<sup>27,30</sup> The newly introduced (thiophen-2-ylmethyl) carbamoyl group extends to the previously unoccupied S4 pocket, and a hydrogen bond is built between C=O and the backbone NH of the key residue Glu166. Concurrently, a sandwich-like  $\pi$ – $\pi$  stacking interaction over

thiophene, dichlorophenyl ring, and the imidazole side chain of His41 is formed (Figure 4c). Similar sandwich-like interaction was first reported and described in  $M^{pro}$  inhibitor 23R.<sup>25</sup> Here, the triple stacking leads to a stabilized conformation of S4 side chain, meanwhile increasing overall target affinity of **GA-17S**. The extended interaction toward the S3 and S4 sites are the key factors contributing to the activity improvement of **GA-17S**. The enzyme inhibitory activities of compounds with aromatic substituents were higher than those with aliphatic substituents, which confirms the assumption that the newly generated  $\pi$ – $\pi$  stacking interactions improve biological activity. Comparing the X-ray crystallographic structure of **GA-17S** with that of MCULE-5948770040 (Figure 4d) shows that the new compound displaying higher activity occupies multiple pockets in the active site of the enzyme, which provides compelling evidence for the success of the application “multi-site binding” strategy.

**Enzyme Inhibition and SAR Analysis of the GB Series.** The GB series of compounds was aimed at exploring the tolerability of the S2 pocket, adjusting the rigidity of the designed compounds and determining the optimal substituents. Thus, 15 novel compounds with diverse lipophilic groups were designed and synthesized (Scheme 1 and Table S2 of the Supporting Information). Unexpectedly, the enzymatic assay showed that most of these compounds had reduced inhibitory activity toward  $M^{pro}$  (Figure S3 in the Supporting Information), except for two compounds in this series, **GB-3S** ( $IC_{50} = 0.48 \pm 0.016 \mu M$ ) and **GB-13S** ( $IC_{50} = 0.35 \pm 0.023 \mu M$ ), containing a 2,4-dichlorobenzyl substituent (Figures 5 and S4). Their potency was similar to that of **GA-17S**, with  $IC_{50}$  values being 1 order of magnitude lower compared to MCULE-5948770040 ( $IC_{50} = 5.1 \pm 0.63 \mu M$ ). However, when a 2,4-dichlorobenzyl or a 4-chlorophenylsulfonamide residue was connected to the piperazine skeleton via amide or sulfonamide linkage, the activity was completely lost (**GB-16** and **GB-17**). Moreover, if one of the chlorine atoms was replaced by a fluorine atom or a nitro group, inactive compounds (**GB-1**, **GB-2**, and **GB-4**) were obtained. A decrease in activity by

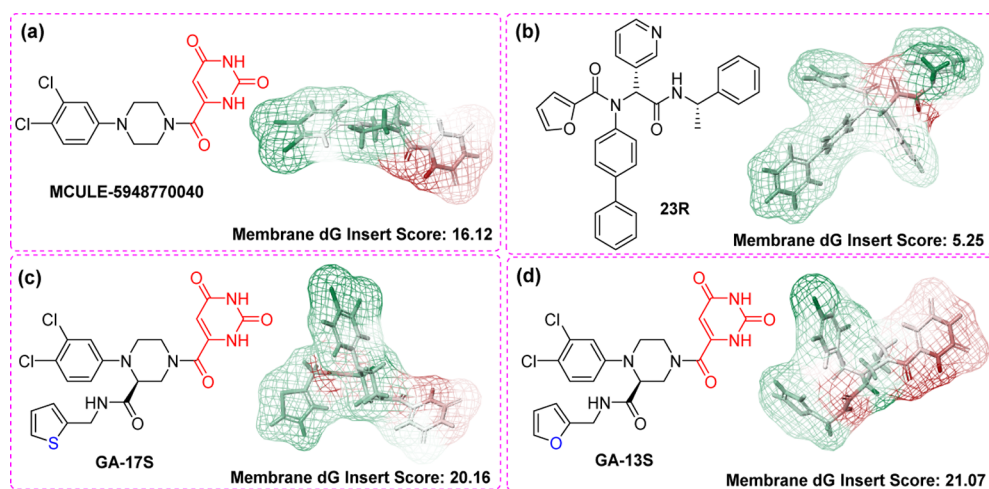


**Figure 6.** Predicted membrane permeability of MCULE-5948770040 (a), 23R (b), GA-17S (c), and GA-13S (d) by Schrödinger. A more positive Membrane dG Insert value indicates a larger energy required for the compound to penetrate the cell membrane; red surfaces indicate structures likely limiting permeability.

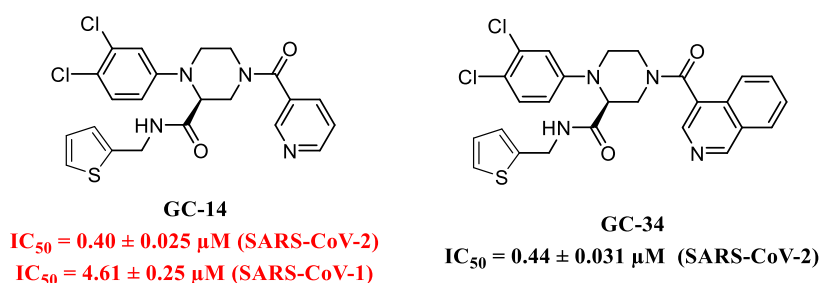


**Figure 7.** Inhibition of  $M^{pro}$  of SARS-CoV-2 and SARS-CoV-1 by GC-14 and GC-34.

altering S2 substituents is consistent with reported observations by Han et al.,<sup>31</sup> which can be attributed to clashes within the S2 pocket. The enzyme inhibitory activity also decreased when cyclohexyl or biphenyl residues, existing in several highly active  $M^{pro}$  inhibitors and therefore classified as privileged structures, were attached to the piperazine skeleton (GB-10 and GB-12; see Figure S3). The most favorable substitution for interaction with the S2 pocket was 3,4-dichlorophenyl or 2,4-dichlorobenzyl, which was irreplaceable by any other of the explored substituents.

**Antiviral Activity and Prediction of Membrane Permeability of Representative Compounds of the GA and GB Series.** Subsequently, a method was established to evaluate the antiviral activity of selected compounds with potent enzymatic inhibitory activity in SARS-CoV-2-infected Vero E6 cells (Figure S5 in the Supporting Information). While the selected compounds had no obvious cytotoxicity ( $CC_{50} > 100 \mu\text{M}$ , Figure S6), they did not exhibit satisfactory antiviral activity ( $EC_{50} > 50 \mu\text{M}$ ) investigated in our established assay (see the Supporting Information). Considering that there are many amide fragments in the structure, we presumed that the high polarity of the compounds might result in low membrane permeability and thus unsatisfactory antiviral activity. To test this assumption, we first calculated the membrane permeability of representative compounds of the GA series and of MCULE-5948770040 by computer simulation, and the Membrane dG Insert index from the Schrödinger suite was taken as the evaluation index.<sup>32,33</sup> The calculated value correlates with the required energy for compounds to penetrate the cell membrane and thus with

low membrane permeability. The prediction results are displayed in Figure 6. Red surface areas in the figures represent the groups predicted to confer poor membrane permeability, indicating that the orotic acid fragment to be the major factor resulting in poor membrane permeability. However, the predicted membrane permeability of a reported  $M^{pro}$  inhibitor, that is, 23R ( $EC_{50} = 1.27 \mu\text{M}$ ,<sup>25</sup> Membrane dG Insert score = 5.25) was significantly better than that of our compounds GA-13S and GA-17S, which prompted us to conduct further structural modifications to achieve high cell permeation and the desired good antiviral activity.

**Biochemical Activity, Antiviral Assay, and SAR Analysis of the GC Series.** According to the predictions of membrane permeability, the orotic acid fragment located in the S1 pocket was the major factor leading to poor antiviral activity. Therefore, the orotic acid moiety of GA-17S was replaced by less polar groups but featuring H-bond acceptors to sustain interaction with His163. The prediction results of membrane permeability for the designed virtual compound library, obtained with the Schrödinger software, are shown in Table S3. Finally, based on molecular hybridization and computer-aided drug design strategies, a series of 16 piperazine-typed  $M^{pro}$  inhibitors were synthesized with a maintained dichlorophenyl portion at one nitrogen but various acyl and sulfonyl groups at the other nitrogen (GC series, Scheme 1 and Table S4). Results of  $M^{pro}$  inhibition assays showed that the nicotiny (GC-14) and isoquinolinyl (GC-34) fragments caused strongest enzyme inhibitory potency and  $IC_{50}$  values of 0.40 and 0.44  $\mu\text{M}$ , respectively (Figures 7 and S8). Hence, the replacement of the orotic acid fragment was



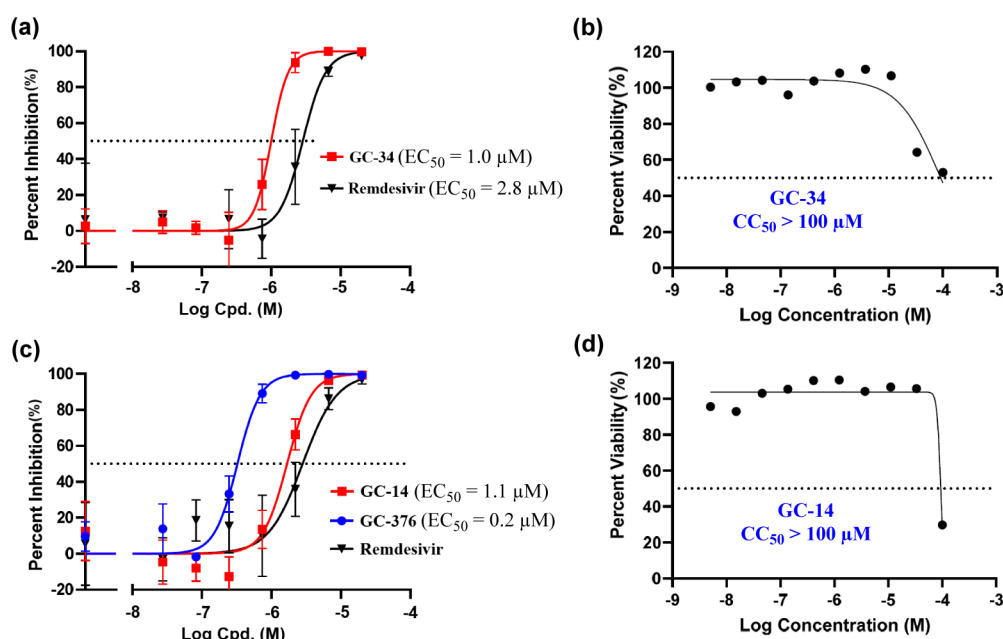


**Figure 8.** Antiviral activity and cytotoxicity of GC-34 (a,b) and GC-14 (c,d) against SARS-CoV-2 in Vero E6 cells. GC-376 (for structure, see Table 1) and Remdesivir were used as positive controls ( $n = 3$  biological replicates). Error bars represent the SD values of three independent experiments.

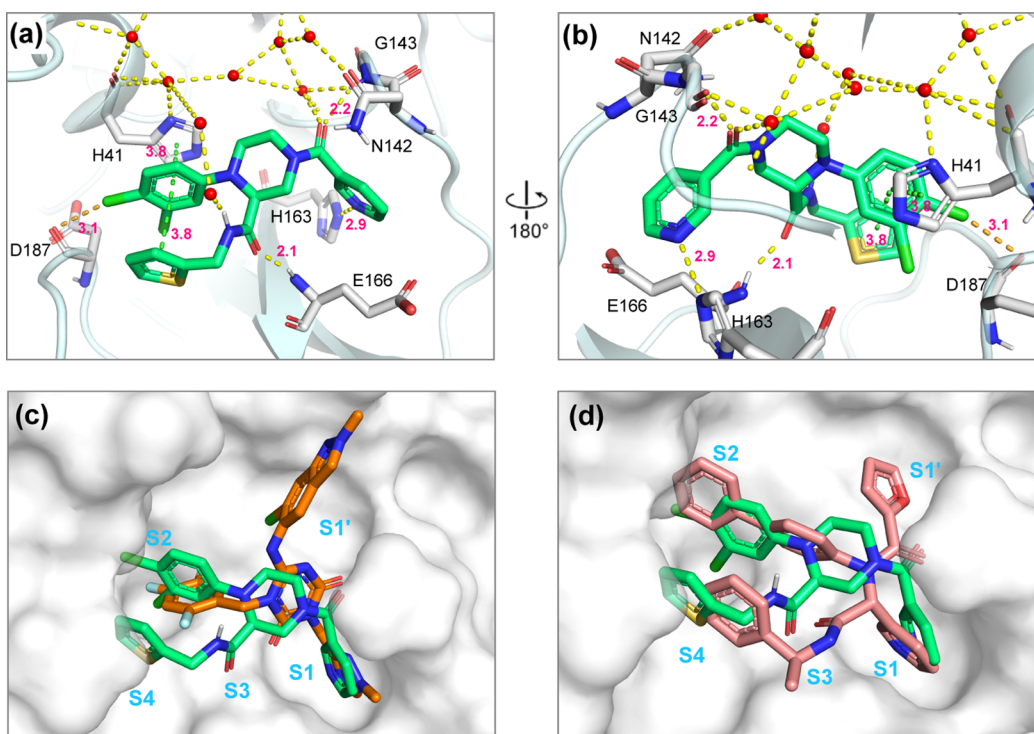


**Figure 9.** X-ray co-crystal structure of GC-14 and  $M^{\text{pro}}$  (PDB ID: 8ACL). (a,b) View of GC-14 (green) from an inward/backward angle of the active pocket. Water molecules are shown as red spheres. Hydrogen bonds are indicated as yellow dashed lines,  $\pi$ - $\pi$  stacking as green dashed lines, and halogen bonds as orange dashed lines; (c) binding pose comparison of GC-14 (green) and S-217622 (orange, PDB ID: 7VU6); (d) comparison of GC-14 and 23R (pink, PDB ID: 7KX5).

well tolerated. However, the inhibition by the picolinoyl derivative GC-13 at  $10 \mu\text{M}$  was much weaker than that by GC-14, which may be due to its inability of GC-13 to form a hydrogen bond with His163 (Figure S7). Analogously, sulfonamides (GC-1 to GC-7) were inactive (Figure S7).

Antiviral activity of GC-14 and GC-34 against SARS-CoV-2 in Vero E6 cells confirmed our design hypothesis (Figure 8a,c).

The  $EC_{50}$  values of GC-14 and GC-34 were  $1.1 \pm 0.2$  and  $1.0 \pm 0.1 \mu\text{M}$ , respectively, displaying a huge improvement as compared to GA-17S ( $EC_{50} > 100 \mu\text{M}$ ). GC-34 was more potent than the approved drug Remdesivir ( $EC_{50} = 2.8 \pm 0.3 \mu\text{M}$ ), which was used as a control. GC-34 has lower antiviral activity compared to the covalent  $M^{\text{pro}}$  inhibitor GC-376 ( $EC_{50} = 0.2 \pm 0.05 \mu\text{M}$ ); however, GC-376 displays poor

target selectivity. We then considered the EC<sub>50</sub> ratio between Remdesivir and reported M<sup>Pro</sup> inhibitors. Comparison of the EC<sub>50</sub> ratio between Remdesivir (RDV) and reported M<sup>Pro</sup> inhibitors is listed in Table S5. The antiviral potency of GC-34 versus Remdesivir [EC<sub>50</sub>(RDV)/EC<sub>50</sub>(GC-34) = 2.8] is comparable to that of S-217622 [EC<sub>50</sub>(RDV)/EC<sub>50</sub>(S-217622) = 5.0], the currently most advanced non-covalent M<sup>Pro</sup> inhibitor, and it is also superior to other inhibitors (see Table S5).<sup>31,34</sup> More specifically, GC-14 and GC-34 displayed an at least 100-fold increase in antiviral activity, most likely due to the improvement of the membrane permeability profile. Additionally, neither of them exhibited notable cytotoxicity in Vero E6 cells (CC<sub>50</sub> > 100 μM), as shown in Figure 8b,d.

**Crystallographic Study of GC-14 in Complex with M<sup>Pro</sup>.** Next, we obtained an X-ray co-crystal structure of GC-14, which demonstrated the accommodation of the dichlorophenyl moiety in the S2 pocket and of the (thiophen-2-ylmethyl)carbamoyl group in the S4 pocket. The piperazine ring of GC-14 resides in a similar position as in the case of the M<sup>Pro</sup>-GA-17S complex (Figures 9a,b and 4). The hydrogen bonding with Glu166 and stacking with the imidazole ring of His41 in the hydrophobic S2 pocket are also unaltered in the GC-14 and GA-17S complexes. The newly introduced nicotinic acid group in GC-14 occupies the S1 pocket perfectly and maintains hydrogen bonding with the imidazole NH of His163. Compared with GA-17S, replacement of the uracil fragment by a pyridine reduced the hydrogen bonds and water bridges with the hydrophilic area around the S1. GC-14 possesses nearly equipotent enzyme inhibitory activity, but it is endowed with higher membrane permeability. The direct comparison of uracil and pyridine targeting the S1 cavity demonstrated that the limited but crucial H-bond interaction with His163 in this sub-pocket is overall beneficial for antiviral activity. Consequently, this modification clearly increased cellular activity, indicating the success of our design strategy. Figure 9c,d displays a comparison of the X-ray co-crystal structures of GC-14, S-217622, and 23R. Although their skeletons are different, the compounds occupy multiple pockets of the active site in a similar manner and interact with key amino acids, exemplified by Glu166, His163, Gly143, and His41.

**Target Selectivity.** Most of the existing covalent M<sup>Pro</sup> inhibitors display poor target selectivity by reactive warheads prone to covalent interactions, such in the representative inhibitors GC-376, PF-00835231, and 11a,<sup>17</sup> which may result in many side effects upon clinical application. Some side effects may be ignored in an emergency situation when no efficient drugs are available, but in the current research and future developments, specificity of M<sup>Pro</sup> inhibitors should be taken into consideration. Thus, the target selectivity of our non-covalent M<sup>Pro</sup> inhibitors was further evaluated. Human cathepsins B, F, K, and L and caspase 3 were selected to assess potential inhibition by GC-14 and GC-34. To our delight, both compounds did not inhibit the host proteins at a high concentration of 50 μM (Table S6), suggesting that GC-14 and GC-34 have excellent target specificity toward coronavirus proteases, which also indicates a low risk of side effects in therapy.

**In Vivo Pharmacokinetic Study.** In microsomal stability tests, GC-14 showed relatively high clearance, which measured the Cl<sub>int</sub> to be 994 mL/min/kg in rat liver microsomes (Tables S13 and S14 in the Supporting Information). Finally, the pharmacokinetic profile of GC-14 was examined in Sprague–

Dawley rats to evaluate its potential for therapeutic application (Table 2). After a single 2 mg/kg i.v. dose of GC-14 in

**Table 2. Pharmacokinetic Parameters of GC-14<sup>a</sup>**

parameter	units	i.v. <sup>b</sup>	p.o. <sup>b</sup>
<i>t</i> <sub>1/2</sub>	h	0.36 ± 0.05	1.73 ± 0.25
<i>T</i> <sub>max</sub>	h	0.08 ± 0.00	0.5 ± 0.0
<i>C</i> <sub>max</sub>	ng/mL	1310 ± 120	74.6 ± 12.5
<i>C</i> <sub>0</sub>	ng/mL	1760 ± 208	
AUC <sub>0–<i>t</i></sub>	h ng/mL	627 ± 76	235 ± 27
AUC <sub>0–∞</sub>	h ng/mL	637 ± 80	230 ± 28
MRT <sub>0–∞</sub>	h	0.40 ± 0.05	2.45 ± 0.16
CL	mL/h/kg	3140 ± 500	
<i>F</i>	%		7.2

<sup>a</sup>PK parameters (mean ± SD, *n* = 3). <sup>b</sup>Dosed orally at 10 mg/kg. Dosed intravenously at 2 mg/kg.

Sprague–Dawley rats, clearance rate (CL), mean residence time (MRT), and half-life (*t*<sub>1/2</sub>) were determined to be 3140 mL/h/kg, 0.40 h, and 0.36 h, respectively. GC-14 (10 mg/kg) was rapidly absorbed after oral dosing, with a time-to-maximum concentration (*T*<sub>max</sub>) of 0.5 h, and showed a moderate pharmacokinetic profile including a favorable *t*<sub>1/2</sub> (1.73 h), a maximum concentration (*C*<sub>max</sub>) 74.6 ng/mL, and an area under curve (AUC<sub>0–*t*</sub>) of 235 ng h/mL. Given the structural electron-rich aromatic rings in GC-14, the results above were not unexpected. The oral bioavailability of GC-14 was only 7.2%, which is unfortunately insufficient for oral administration. We speculated that limited solubility might also be responsible for the unsatisfactory pharmacokinetic data. Thus, the kinetic solubility of GC-14 was determined in phosphate buffer solution (pH = 7.3) and was found to be 0.0041 ± 0.0003 mg/mL (8.7 μM). The promising pharmacokinetic properties of GC-14 indicate that 1,2,4-trisubstituted piperazine derivatives deserve further study, and future efforts of our laboratory will be focused on improving their metabolic stability and oral bioavailability.

## CONCLUSIONS

According to the classical lock-and-key model for drug design, an ideal binder should efficiently enter and maximally occupy the drug target, thereby maximizing favorable interactions with its complementary pocket. The concept of “multi-site binding” was based on the idea that affinity and specificity could be greatly improved by designing complementary ligands that fully utilize topographical features near the main binding site. In this study, using the highly conserved SARS-CoV-2 main protease as the drug target, we systematically modified the structure of the hit compound, the non-covalent inhibitor MCULE-S948770040, using the multi-site binding concept and privileged fragment assembly strategy.

First, aiming at the S4 pocket of the M<sup>Pro</sup>, the privileged fragments of the existing M<sup>Pro</sup> inhibitors addressing this pocket were assembled, keeping the piperazine skeleton of MCULE-S948770040, and the compounds in GA series with multi-site binding characteristics were designed and synthesized. Most of the newly synthesized non-covalent M<sup>Pro</sup> inhibitors maintained better enzyme inhibitory activity against M<sup>Pro</sup> than that of the lead structure, the best inhibitors being GA-13S and GA-17S. An X-ray crystallography of GA-17S and M<sup>Pro</sup> complex revealed that the newly introduced (thiophen-2-ylmethyl)-carbamoyl moiety did extend into the previously unoccupied

S4 pocket and generated hydrogen bond and stacking interactions, which increased inhibitory potency.

To further explore the internal chemical space of the S2 pocket, the 3,4-dichlorophenyl unit was replaced according to the bioisosterism principle. The enzyme inhibitory activity demonstrated that 2,4-dichlorobenzyl and 3,4-dichlorophenyl were the optimum fragments for the S2 pocket. Unfortunately, bioactive representatives of our GA and GB series failed to exhibit obvious antiviral activity due to their poor membrane permeability. Thus, for improving membrane permeability, the GC series was designed, out of which GC-14 maintained high  $M^{pro}$  inhibition ( $IC_{50} = 0.40 \mu M$ ) and showed excellent antiviral activity ( $EC_{50} = 1.1 \mu M$ ), which was significantly better than that of GA-17S and the approved drug Remdesivir. Notably, all the tested compounds showed extraordinarily low cytotoxicity ( $CC_{50} > 100 \mu M$ ). Furthermore, GC-14 and GC-34 exhibited no inhibitory activity against the human proteases cathepsins B, F, K, and L and caspase-3, implying their specificity for  $M^{pro}$ . The co-crystal structure of GC-14 and  $M^{pro}$  showed that GC-14 was bound to the active site in a non-covalent mode and provides a foundation for further structural improvement of related  $M^{pro}$  inhibitors. Finally, the pharmacokinetic profile of GC-14 was evaluated in rats. Further structural optimization to improve its water solubility and oral bioavailability is in progress. In summary, a non-covalent  $M^{pro}$  inhibitor with excellent anti-SARS-CoV-2 activity and high target specificity was developed. Multi-site binding and privileged fragment assembly as major drug discovery strategies have successfully been applied in this study.

## EXPERIMENTAL SECTION

**Chemistry.** All chemical reagents and reaction solvents were purchased from commercial suppliers. All melting points were determined on a micro-melting point apparatus (RY-1G, Tianjin TianGuang Optical Instruments).  $^1H$  NMR and  $^{13}C$  NMR spectra were recorded in DMSO- $d_6$  on a Bruker AV-400 spectrometer, with tetramethyl silane (TMS) as the internal standard. Coupling constants were given in hertz, and chemical shifts were reported in  $\delta$  values (ppm) from TMS; signals were abbreviated as s (singlet), d (doublet), t (triplet), q (quarter), and m (multiplet). A G1313A Standard LC autosampler (Agilent) was used to collect samples for measurement of mass spectra. All reactions were routinely monitored by thin-layer chromatography (TLC) on silica gel GF254. Flash column chromatography was performed on columns packed with silica gel (200–300 mesh), purchased from Qingdao Haiyang Chemical Company. The purity of representative final compounds was tested on a Shimadzu HPLC system. HPLC conditions: Agilent ZORBAX, SB-C18 column (250 mm  $\times$  4.6 mm  $\times$  5  $\mu m$ ). Isocratic elution method: mobile phase A: methanol (80%); mobile phase B: water (20%); flow rate 1.0 mL/min; wavelength: 254 nm, temperature, 30  $^{\circ}C$ ; injection volume, 10  $\mu L$ . The purities of tested compounds was >95%.

**General Synthesis Procedure for the GA Series Compounds.** *General Synthesis Procedure for Intermediates 3–6.* 1-(3,4-Dichlorobenzoyl)-4-Boc piperazine-2-carboxylic Acid Methylate (3). A 250 mL round-bottom flask was charged with compound 1 (7.8 g, 41.1 mmol) and compound 2 (5.0 g, 20.5 mmol), which were dissolved with 80 mL of dichloromethane under stirring. Anhydrous cupric acetate (3.75 g, 20.7 mmol) and pyridine (3.24 g, 41.0 mmol) were then added to the mixture simultaneously. The mixture was stirred under oxygen atmosphere and room temperature for 12 h, then washed with water (4  $\times$  60 mL) to remove copper salt and pyridine. The resulting organic phase was separated, dried over anhydrous  $Na_2SO_4$ , then organic solvent removed in vacuo successively to produce a dark-green oil as a residue. It was purified through silica gel column chromatography (EtOAc/hexane = 1:20) to give compound 3

(4.05 g, 10.4 mmol, 51%) as a colorless oil. ESI-MS:  $m/z$  389.2  $[M + H]^+$ .  $C_{17}H_{22}Cl_2N_2O_4$  (388.1).

1-(3,4-Dichlorobenzoyl) Piperazine-2-carboxylic Acid Methylate Trifluoroacetate (4). To a solution of compound 3 (4.05 g, 10.4 mmol) in DCM (70 mL) was added TFA (25% solution in DCM, 28 mL, 62.3 mmol) dropwise. Then, the mixture was stirred under room temperature for 8 h. When the reaction was finished monitoring by TLC, DCM and trifluoroacetic acid were removed under reduced pressure. To the remaining purple oil, 15 mL of EtOAc was added upon stirring. The resulting suspension was filtered and washed with 2 mL of EtOAc to yield compound 4 (3.91 g, 9.73 mmol, 94%) as a white granular solid. ESI-MS:  $m/z$  289.2  $[M + H]^+$ .  $C_{12}H_{14}Cl_2N_2O_2$  (288.1).

1-(3,4-Dichlorobenzoyl)-4-(2,6-dioxo-1,2,3,6-tetrahydropyrimidine-4-carbonyl) Piperazine-2-carboxylic Acid Methylate (5). To a suspension of orotic acid (1.67 g, 10.7 mmol) in DCM (60 mL), O-(7-azabenzotriazol-1-yl)-N,N,N',N'-tetramethyluronium hexafluorophosphate (HATU, 5.66 g, 14.6 mmol) was added under an ice bath. The mixture was stirred for 10 min and then added with N,N-diisopropyl ethylamine (DIPEA, 5.01 g, 38.8 mmol) and compound 4 (3.91 g, 9.73 mmol). The reaction was allowed to warm to room temperature for 6 h. When the reaction was finished monitoring by TLC, all precipitates were separated by filtering and washed with 15 mL of DCM to yield compound 5 (3.25 g, 7.63 mmol, 78%) as a gray-white solid, without further purification. ESI-MS:  $m/z$  427.2  $[M + H]^+$ .  $C_{17}H_{16}Cl_2N_4O_5$  (426.1).

1-(3,4-Dichlorobenzoyl)-4-(2,6-dioxo-1,2,3,6-tetrahydropyrimidine-4-carbonyl) Piperazine-2-carboxylic Acid (6). To a stirred solution of compound 5 (3.25 g, 7.63 mmol) in THF/MeOH (60 mL, v/v = 1/1) was added LiOH (1 M aqueous solution, 38.2 mL, 38.2 mmol) dropwise under an ice bath. Then, the mixture was allowed to react under room temperature for 5 h with stirring. When the reaction finished, the mixture was concentrated under reduced pressure until the remaining mixture was less than 50 mL. The resulting solution was then cooled under an ice bath and added with 1 M HCl dropwise accompanied with stirring. The resulting suspension was filtered, to afford compound 6 (2.9 g, 7.04 mmol, 92%) as a light-yellow solid. mp 275–277  $^{\circ}C$ .  $^1H$  NMR (400 MHz, DMSO- $d_6$ ):  $\delta$  13.16 (s, 1H), 11.27 (d,  $J = 29.1$  Hz, 2H), 7.42 (d,  $J = 9.0$  Hz, 1H), 7.14 (d,  $J = 2.9$  Hz, 1H), 6.91 (d,  $J = 11.9$  Hz, 1H), 5.52 (s, 1H), 4.80 (d,  $J = 20.8$  Hz, 1H), 4.24 (dd,  $J = 62.0, 12.5$  Hz, 1H), 3.95–3.46 (m, 3H), 3.02 (d,  $J = 13.4$  Hz, 1H). ESI-MS:  $m/z$  411.1  $[M - H]^-$ .  $C_{16}H_{14}Cl_2N_4O_5$  (412.03).

**General Synthesis Procedure for GA-1 to GA-34.** A suspension of compound 6 (0.24 mmol, 1.0 equiv), HATU (0.36 mmol, 1.5 equiv), and DCM (8 mL) was stirred for 30 min under 0  $^{\circ}C$ . DIPEA (0.72 mmol, 3 equiv) and side-chain amines (0.29 mmol, 1.2 equiv) were added to the system. The mixture was stirred for 4 h at room temperature. When the reaction was finished monitoring by TLC, the mixture was washed by 1 M HCl, saturated  $NaHCO_3$  solution, and saturated NaCl solution successively. The organic layer was dried over anhydrous  $Na_2SO_4$  and concentrated in vacuo. The residue was purified by flash column chromatography on silica gel to afford the final products.

N-Cyclohexylmethyl-1-(3,4-dichlorobenzoyl)-4-(2,6-dioxo-1,2,3,6-tetrahydropyrimidine-4-carbonyl) Piperazine-2-carboxamide (GA-1). Off-white solid. 55% yield. mp 211–213  $^{\circ}C$ .  $^1H$  NMR (600 MHz, DMSO- $d_6$ ):  $\delta$  11.20 (s, 2H), 8.09 (dt,  $J = 28.9, 5.9$  Hz, 1H), 7.41 (d,  $J = 9.0$  Hz, 1H), 7.00 (d,  $J = 18.2$  Hz, 1H), 6.82 (d,  $J = 9.1$  Hz, 1H), 5.42 (d,  $J = 16.2$  Hz, 1H), 4.35 (d,  $J = 39.6$  Hz, 1H), 4.06 (dd,  $J = 44.4, 13.5$  Hz, 1H), 3.86–3.67 (m, 1H), 3.66–3.42 (m, 3H), 3.28–3.15 (m, 1H), 3.01–2.71 (m, 2H), 1.64–1.49 (m, 5H), 1.36–0.98 (m, 6H), 0.77 (d,  $J = 8.5$  Hz, 2H).  $^{13}C$  NMR (150 MHz, DMSO- $d_6$ ):  $\delta$  169.88, 164.16, 161.64, 151.48, 149.86, 147.17, 131.98, 130.91, 120.02, 115.86, 114.88, 99.40, 58.07, 47.52, 45.29, 43.18, 41.55, 37.77, 30.78, 26.41, 25.86. HRMS (ESI)  $m/z$   $[M + H]^+$  calcd for  $C_{23}H_{27}Cl_2N_5O_4$ , 507.1440; found, 508.1513. HPLC purity: 98.90%.

N-(2-Phenylethyl)-1-(3,4-dichlorobenzoyl)-4-(2,6-dioxo-1,2,3,6-tetrahydropyrimidine-4-carbonyl) Piperazine-2-carboxamide

**(GA-2).** White solid, 72% yield. mp 177–180 °C.  $^1\text{H}$  NMR (600 MHz, DMSO- $d_6$ ):  $\delta$  11.37–11.11 (m, 2H), 8.20 (d,  $J$  = 16.7 Hz, 1H), 7.40 (d,  $J$  = 9.1 Hz, 1H), 7.27 (t,  $J$  = 7.4 Hz, 2H), 7.22–7.11 (m, 3H), 7.02 (d,  $J$  = 2.9 Hz, 1H), 6.76 (td,  $J$  = 9.7, 9.1, 2.9 Hz, 1H), 5.52–5.42 (m, 1H), 4.37 (d,  $J$  = 36.6 Hz, 1H), 4.10 (d,  $J$  = 13.4 Hz, 1H), 3.74–3.55 (m, 2H), 3.47 (d,  $J$  = 39.0 Hz, 2H), 3.32 (d,  $J$  = 10.2 Hz, 1H), 3.18 (s, 1H), 2.66 (qt,  $J$  = 14.0, 7.4 Hz, 2H).  $^{13}\text{C}$  NMR (150 MHz, DMSO- $d_6$ ):  $\delta$  169.7, 164.2, 161.7, 151.5, 149.9, 147.2, 139.8, 132.0, 130.9, 129.1, 128.7, 126.5, 119.9, 115.8, 114.7, 99.4, 58.0, 47.5, 43.1, 41.4, 40.8, 35.3. HRMS (ESI)  $m/z$  [ $M + H$ ] $^+$  calcd for  $\text{C}_{24}\text{H}_{23}\text{Cl}_2\text{N}_5\text{O}_4$ , 515.1127; found, 516.1201. HPLC purity: 97.29%.

***N*-(Indol-3-yl-methyl)-1-(3,4-dichlorobenzoyl)-4-(2,6-dioxo-1,2,3,6-tetrahydropyrimidine-4-carbonyl) Piperazine-2-carboxamide (GA-3).** Gray-white solid, 59% yield. mp 242–244 °C.  $^1\text{H}$  NMR (600 MHz, DMSO- $d_6$ ):  $\delta$  11.22 (d,  $J$  = 37.6 Hz, 2H), 10.90 (s, 1H), 8.37 (d,  $J$  = 32.0 Hz, 1H), 7.46–7.30 (m, 3H), 7.19 (d,  $J$  = 28.9 Hz, 1H), 7.07 (t,  $J$  = 7.0 Hz, 1H), 7.00 (dd,  $J$  = 11.9, 3.0 Hz, 1H), 6.92 (t,  $J$  = 7.4 Hz, 1H), 6.84–6.73 (m, 1H), 5.47 (d,  $J$  = 11.4 Hz, 1H), 4.56 (dd,  $J$  = 14.6, 6.4 Hz, 1H), 4.50–4.29 (m, 2H), 4.23–4.04 (m, 2H), 3.71–3.58 (m, 2H), 3.52–3.41 (m, 1H), 3.27–3.11 (m, 1H).  $^{13}\text{C}$  NMR (150 MHz, DMSO- $d_6$ ):  $\delta$  173.00, 170.03, 164.22, 152.62, 149.92, 146.95, 137.76, 136.86, 132.04, 130.88, 126.84, 124.23, 122.08, 121.65, 119.04, 116.69, 115.26, 114.87, 111.89, 100.06, 47.75, 43.24, 41.39, 34.89. HRMS (ESI)  $m/z$  [ $M + H$ ] $^+$  calcd for  $\text{C}_{24}\text{H}_{23}\text{Cl}_2\text{N}_5\text{O}_4$ , 540.1080; found, 541.1073. HPLC purity: 95.09%.

***N*-(4-Fluorophenylmethyl)-1-(3,4-dichlorobenzoyl)-4-(2,6-dioxo-1,2,3,6-tetrahydropyrimidine-4-carbonyl) Piperazine-2-carboxamide (GA-4).** White solid, 66% yield. mp 244–246 °C.  $^1\text{H}$  NMR (600 MHz, DMSO- $d_6$ ):  $\delta$  11.22 (s, 2H), 8.69 (d,  $J$  = 23.7 Hz, 1H), 7.42 (d,  $J$  = 9.1 Hz, 1H), 7.18 (dd,  $J$  = 8.4, 5.5 Hz, 2H), 7.13–7.00 (m, 3H), 6.83 (d,  $J$  = 9.2 Hz, 1H), 5.42 (d,  $J$  = 14.2 Hz, 1H), 4.51–4.31 (m, 2H), 4.09 (d,  $J$  = 15.6 Hz, 1H), 3.91–3.70 (m, 1H), 3.66–3.45 (m, 3H), 3.29–3.16 (m, 1H).  $^{13}\text{C}$  NMR (150 MHz, DMSO- $d_6$ ):  $\delta$  170.51, 169.99, 164.28, 162.46, 161.83, 160.85, 151.64, 149.85, 147.38, 135.63, 132.03, 130.95, 129.66, 129.60, 129.51, 120.00, 116.24, 115.85, 115.51, 115.37, 114.83, 99.37, 58.26, 47.36, 43.10, 42.14, 41.50. HRMS (ESI)  $m/z$  [ $M + H$ ] $^+$  calcd for  $\text{C}_{23}\text{H}_{20}\text{Cl}_2\text{FN}_5\text{O}_4$ , 519.0876; found, 520.0954. HPLC purity: 97.72%.

***N*-(4,4-Difluorocyclohexyl)-1-(3,4-dichlorobenzoyl)-4-(2,6-dioxo-1,2,3,6-tetrahydropyrimidine-4-carbonyl) Piperazine-2-carboxamide (GA-5).** White solid, 71% yield. mp 162–164 °C.  $^1\text{H}$  NMR (600 MHz, DMSO- $d_6$ ):  $\delta$  11.40–11.07 (m, 2H), 8.11 (dd,  $J$  = 37.5, 7.7 Hz, 1H), 7.41 (d,  $J$  = 9.0 Hz, 1H), 7.01 (s, 1H), 6.80 (d,  $J$  = 9.0 Hz, 1H), 5.45 (s, 1H), 4.54–4.11 (m, 2H), 3.90–3.67 (m, 2H), 3.67–3.38 (m, 3H), 3.16 (t,  $J$  = 9.4 Hz, 1H), 1.96 (s, 2H), 1.86 (d,  $J$  = 15.9 Hz, 2H), 1.70 (d,  $J$  = 13.4 Hz, 2H), 1.42 (d,  $J$  = 11.7 Hz, 2H).  $^{13}\text{C}$  NMR (150 MHz, DMSO- $d_6$ ):  $\delta$  169.62, 163.34, 161.60, 151.50, 149.91, 147.08, 132.00, 130.95, 119.92, 115.67, 114.65, 99.91, 57.60, 57.10, 47.68, 45.62, 43.68, 41.44, 31.77, 31.61, 28.32, 27.94. HRMS (ESI)  $m/z$  [ $M + H$ ] $^+$  calcd for  $\text{C}_{22}\text{H}_{23}\text{Cl}_2\text{F}_2\text{N}_5\text{O}_4$ , 529.1095; found, 530.1173. HPLC purity: 98.99%.

***N*-(3,5-Dimethylphenyl)-1-(3,4-dichlorobenzoyl)-4-(2,6-dioxo-1,2,3,6-tetrahydropyrimidine-4-carbonyl) Piperazine-2-carboxamide (GA-6).** White solid, 71% yield. mp 196–198 °C.  $^1\text{H}$  NMR (600 MHz, DMSO- $d_6$ ):  $\delta$  11.24 (s, 1H), 11.21 (s, 1H), 9.97 (d,  $J$  = 126.1 Hz, 1H), 7.43 (d,  $J$  = 8.9 Hz, 1H), 7.16–7.07 (m, 3H), 6.88 (dd,  $J$  = 9.0, 2.9 Hz, 1H), 6.69 (s, 1H), 5.40 (d,  $J$  = 73.7 Hz, 1H), 4.67–4.56 (m, 1H), 4.22 (dd,  $J$  = 81.3, 13.6 Hz, 1H), 3.95–3.73 (m, 1H), 3.68 (d,  $J$  = 12.7 Hz, 1H), 3.61–3.41 (m, 2H), 3.23–3.17 (m, 1H), 2.21 (s, 6H).  $^{13}\text{C}$  NMR (150 MHz, DMSO- $d_6$ ):  $\delta$  161.76, 151.53, 149.97, 147.30, 138.08, 133.59, 130.16, 127.41, 126.35, 118.53, 117.91, 116.03, 114.89, 99.49, 98.97, 58.51, 57.42, 49.07, 47.50, 44.32, 43.54, 43.19, 41.43, 21.44. HRMS (ESI)  $m/z$  [ $M + H$ ] $^+$  calcd for  $\text{C}_{24}\text{H}_{23}\text{Cl}_2\text{N}_5\text{O}_4$ , 515.1127; found, 516.1209. HPLC purity: 97.27%.

***N*-(2-(Indol-3-yl)-ethyl)-1-(3,4-dichlorobenzoyl)-4-(2,6-dioxo-1,2,3,6-tetrahydropyrimidine-4-carbonyl) Piperazine-2-carboxamide (GA-7).** White solid, 68% yield. mp 143–145 °C.  $^1\text{H}$  NMR (600 MHz, DMSO- $d_6$ ):  $\delta$  11.19 (d,  $J$  = 11.7 Hz, 1H), 10.79 (d,  $J$  = 6.8 Hz, 1H), 8.24 (q,  $J$  = 6.3, 5.7 Hz, 1H), 7.52 (d,  $J$  = 7.9 Hz, 1H), 7.36

(d,  $J$  = 8.8 Hz, 1H), 7.33 (d,  $J$  = 8.1 Hz, 1H), 7.12 (d,  $J$  = 33.6 Hz, 1H), 7.06 (t,  $J$  = 7.5 Hz, 1H), 7.02 (d,  $J$  = 3.0 Hz, 1H), 6.96 (t,  $J$  = 7.4 Hz, 1H), 6.75 (dd,  $J$  = 18.7, 7.7 Hz, 1H), 5.47 (d,  $J$  = 12.6 Hz, 1H), 4.37 (d,  $J$  = 39.9 Hz, 1H), 4.16–4.04 (m, 1H), 3.72–3.56 (m, 2H), 3.51 (d,  $J$  = 9.1 Hz, 1H), 3.39 (q,  $J$  = 6.9 Hz, 2H), 3.27–3.15 (m, 2H), 2.76 (dd,  $J$  = 15.9, 9.2 Hz, 2H).  $^{13}\text{C}$  NMR (150 MHz, DMSO- $d_6$ ):  $\delta$  169.69, 164.22, 162.53, 151.32, 149.88, 147.83, 136.78, 132.00, 130.94, 127.66, 123.11, 121.37, 119.78, 118.69, 115.66, 114.52, 112.12, 111.83, 99.93, 58.20, 47.39, 42.92, 41.55, 38.72, 25.50. HRMS (ESI)  $m/z$  [ $M + H$ ] $^+$  calcd for  $\text{C}_{24}\text{H}_{23}\text{Cl}_2\text{N}_5\text{O}_4$ , 554.1236; found, 555.1313. HPLC purity: 99.56%.

***N*-(2-Cyclohexylethyl)-1-(3,4-dichlorobenzoyl)-4-(2,6-dioxo-1,2,3,6-tetrahydropyrimidine-4-carbonyl) Piperazine-2-carboxamide (GA-8).** White solid, 72% yield. mp 222–224 °C.  $^1\text{H}$  NMR (600 MHz, DMSO- $d_6$ ):  $\delta$  11.19 (s, 2H), 8.09–7.98 (m, 1H), 7.41 (d,  $J$  = 9.1 Hz, 1H), 7.00 (d,  $J$  = 10.4 Hz, 1H), 6.81 (t,  $J$  = 9.5 Hz, 1H), 5.43 (d,  $J$  = 25.6 Hz, 1H), 4.33 (d,  $J$  = 32.7 Hz, 1H), 4.08–4.02 (m, 1H), 3.85–3.64 (m, 1H), 3.64–3.54 (m, 2H), 3.46 (d,  $J$  = 12.6 Hz, 1H), 3.26–3.11 (m, 1H), 3.05 (tp,  $J$  = 13.5, 6.7 Hz, 1H), 2.92 (dq,  $J$  = 12.8, 6.5 Hz, 1H), 1.60 (t,  $J$  = 10.3 Hz, 5H), 1.22 (q,  $J$  = 7.0 Hz, 2H), 1.08 (t,  $J$  = 8.5 Hz, 4H), 0.80 (t,  $J$  = 12.8 Hz, 2H).  $^{13}\text{C}$  NMR (150 MHz, DMSO- $d_6$ ):  $\delta$  169.60, 164.15, 161.66, 151.47, 149.89, 147.54, 147.51, 147.16, 131.98, 130.91, 120.31, 119.98, 116.21, 115.84, 115.12, 114.79, 99.40, 98.90, 58.15, 47.47, 43.13, 41.48, 36.82, 34.89, 33.14, 32.85, 26.57, 26.17, 26.10. HRMS (ESI)  $m/z$  [ $M + H$ ] $^+$  calcd for  $\text{C}_{24}\text{H}_{29}\text{Cl}_2\text{N}_5\text{O}_4$ , 521.1597; found, 522.1669. HPLC purity: 96.30%.

***N*-(Cyclohexyl)-1-(3,4-dichlorobenzoyl)-4-(2,6-dioxo-1,2,3,6-tetrahydropyrimidine-4-carbonyl) Piperazine-2-carboxamide (GA-9).** White solid, 63% yield. mp 196–198 °C.  $^1\text{H}$  NMR (600 MHz, DMSO- $d_6$ ):  $\delta$  11.23 (s, 1H), 11.20 (s, 1H), 7.97 (dd,  $J$  = 29.0, 7.9 Hz, 1H), 7.41 (d,  $J$  = 9.0 Hz, 1H), 7.00 (d,  $J$  = 9.4 Hz, 1H), 6.79 (d,  $J$  = 9.2 Hz, 1H), 5.44 (d,  $J$  = 1.9 Hz, 1H), 4.45–4.12 (m, 2H), 4.08–3.97 (m, 1H), 3.89–3.68 (m, 1H), 3.67–3.53 (m, 2H), 3.52–3.38 (m, 2H), 1.62 (d,  $J$  = 10.4 Hz, 4H), 1.51 (d,  $J$  = 14.7 Hz, 1H), 1.26–1.18 (m, 2H), 1.10 (q,  $J$  = 11.3, 10.6 Hz, 3H).  $^{13}\text{C}$  NMR (150 MHz, DMSO- $d_6$ ):  $\delta$  169.15, 164.08, 161.60, 151.46, 149.91, 147.04, 131.98, 130.93, 119.86, 115.64, 114.63, 99.53, 57.61, 48.16, 47.75, 43.20, 41.48, 32.81, 32.34, 25.63, 24.84. HRMS (ESI)  $m/z$  [ $M + H$ ] $^+$  calcd for  $\text{C}_{22}\text{H}_{25}\text{Cl}_2\text{N}_5\text{O}_4$ , 493.1284; found, 494.1359. HPLC purity: 97.51%.

***N*-(2-(4-Fluorophenyl)-ethyl)-1-(3,4-dichlorobenzoyl)-4-(2,6-dioxo-1,2,3,6-tetrahydropyrimidine-4-carbonyl) Piperazine-2-carboxamide (GA-10).** White solid, 79% yield. mp 184–186 °C.  $^1\text{H}$  NMR (600 MHz, DMSO- $d_6$ ):  $\delta$  11.24 (q,  $J$  = 13.4, 12.1 Hz, 2H), 8.23–8.10 (m, 1H), 7.39 (d,  $J$  = 9.1 Hz, 1H), 7.23–7.15 (m, 2H), 7.07 (t,  $J$  = 8.9 Hz, 2H), 7.00 (d,  $J$  = 3.0 Hz, 1H), 6.74 (d,  $J$  = 9.1 Hz, 1H), 5.46 (d,  $J$  = 16.3 Hz, 1H), 4.36 (d,  $J$  = 29.3 Hz, 1H), 4.10 (d,  $J$  = 12.6 Hz, 1H), 3.71–3.54 (m, 2H), 3.53–3.38 (m, 2H), 3.32–3.26 (m, 1H), 3.25–3.10 (m, 2H), 2.70–2.59 (m, 2H).  $^{13}\text{C}$  NMR (150 MHz, DMSO- $d_6$ ):  $\delta$  169.71, 164.22, 162.12, 161.67, 160.51, 151.52, 149.87, 147.17, 135.89, 132.00, 130.88, 119.87, 115.44, 115.31, 114.67, 99.41, 98.92, 57.97, 47.54, 43.06, 41.36, 40.78, 34.40. HRMS (ESI)  $m/z$  [ $M + H$ ] $^+$  calcd for  $\text{C}_{24}\text{H}_{22}\text{Cl}_2\text{FN}_5\text{O}_4$ , 533.1033; found, 534.1108. HPLC purity: 95.10%.

***N*-(2-(4-Chlorophenyl)-ethyl)-1-(3,4-dichlorobenzoyl)-4-(2,6-dioxo-1,2,3,6-tetrahydropyrimidine-4-carbonyl) Piperazine-2-carboxamide (GA-11).** White solid, 77% yield. mp 214–216 °C.  $^1\text{H}$  NMR (600 MHz, DMSO- $d_6$ ):  $\delta$  11.26 (s, 1H), 11.22 (d,  $J$  = 10.5 Hz, 1H), 8.17 (q,  $J$  = 5.7 Hz, 1H), 7.39 (d,  $J$  = 9.0 Hz, 1H), 7.30 (d,  $J$  = 8.5 Hz, 2H), 7.18 (t,  $J$  = 9.6 Hz, 2H), 7.00 (d,  $J$  = 2.9 Hz, 1H), 6.73 (t,  $J$  = 10.7 Hz, 1H), 5.46 (d,  $J$  = 20.1 Hz, 1H), 4.35 (d,  $J$  = 27.1 Hz, 1H), 4.10 (d,  $J$  = 13.6 Hz, 1H), 3.70–3.54 (m, 2H), 3.54–3.38 (m, 2H), 3.30 (d,  $J$  = 6.8 Hz, 1H), 3.20–3.09 (m, 1H), 2.72–2.57 (m, 2H).  $^{13}\text{C}$  NMR (150 MHz, DMSO- $d_6$ ):  $\delta$  169.72, 164.24, 161.70, 151.58, 149.86, 147.26, 138.82, 132.00, 131.24, 130.98, 130.90, 128.63, 119.86, 115.77, 114.64, 99.38, 57.95, 47.54, 43.05, 41.35, 40.54, 34.54. HRMS (ESI)  $m/z$  [ $M + H$ ] $^+$  calcd for  $\text{C}_{22}\text{H}_{25}\text{Cl}_2\text{N}_5\text{O}_4$ , 549.0737; found, 550.0814. HPLC purity: 98.14%.

***N*-(2-(3,5-Dichlorophenyl)-ethyl)-1-(3,4-dichlorobenzoyl)-4-(2,6-dioxo-1,2,3,6-tetrahydropyrimidine-4-carbonyl) Piperazine-2-car-**

boxamide (**GA-12**). White solid, 70% yield. mp 212–214 °C.  $^1\text{H}$  NMR (600 MHz, DMSO- $d_6$ ):  $\delta$  11.23 (t,  $J$  = 15.0 Hz, 2H), 8.20 (dt,  $J$  = 20.8, 5.8 Hz, 1H), 7.45–7.32 (m, 2H), 7.28 (d,  $J$  = 29.8 Hz, 2H), 6.99 (s, 1H), 6.72 (t,  $J$  = 7.0 Hz, 1H), 5.48 (d,  $J$  = 17.2 Hz, 1H), 4.47–4.29 (m, 1H), 4.10 (d,  $J$  = 12.0 Hz, 1H), 3.70–3.55 (m, 2H), 3.53–3.46 (m, 1H), 3.43 (d,  $J$  = 17.9 Hz, 1H), 3.27–3.10 (m, 2H), 2.70 (tt,  $J$  = 14.6, 6.7 Hz, 2H).  $^{13}\text{C}$  NMR (150 MHz, DMSO- $d_6$ ):  $\delta$  169.77, 164.25, 161.67, 151.54, 149.84, 147.18, 144.21, 134.28, 132.03, 130.86, 128.00, 126.32, 119.88, 115.74, 114.55, 99.40, 57.96, 57.11, 47.53, 43.04, 41.32, 34.46. HRMS (ESI)  $m/z$  [ $M + H$ ] $^+$  calcd for  $\text{C}_{24}\text{H}_{21}\text{Cl}_4\text{N}_5\text{O}_4$ , 583.0348; found, 584.0417. HPLC purity: 99.00%.

*N*-((Furan-2-yl)-methyl)-1-(3,4-dichlorobenzoyl)-4-(2,6-dioxo-1,2,3,6-tetrahydropyrimidine-4-carbonyl) Piperazine-2-carboxamide (**GA-13**). White solid, 63% yield. mp 214–216 °C.  $^1\text{H}$  NMR (600 MHz, DMSO- $d_6$ ):  $\delta$  9.56 (d,  $J$  = 47.6 Hz, 2H), 7.52 (d,  $J$  = 25.0 Hz, 1H), 7.38 (t,  $J$  = 9.7 Hz, 1H), 6.97 (d,  $J$  = 2.9 Hz, 1H), 6.79 (dd,  $J$  = 9.1, 2.9 Hz, 1H), 6.34 (d,  $J$  = 15.1 Hz, 1H), 6.14 (dd,  $J$  = 56.3, 3.1 Hz, 1H), 5.07 (d,  $J$  = 40.8 Hz, 1H), 4.56–4.34 (m, 2H), 4.34–4.14 (m, 2H), 4.10 (d,  $J$  = 13.1 Hz, 1H), 3.66–3.57 (m, 1H), 3.57–3.50 (m, 1H), 3.47 (d,  $J$  = 12.0 Hz, 1H), 3.17–2.98 (m, 1H).  $^{13}\text{C}$  NMR (150 MHz, DMSO- $d_6$ ):  $\delta$  170.23, 168.36, 167.13, 159.18, 153.00, 150.42, 142.19, 131.86, 130.16, 119.28, 115.55, 114.58, 110.36, 106.75, 95.23, 93.85, 58.45, 46.92, 43.14, 41.18, 36.24. HRMS (ESI)  $m/z$  [ $M + H$ ] $^+$  calcd for  $\text{C}_{21}\text{H}_{19}\text{Cl}_2\text{N}_5\text{O}_5$ , 491.0763; found, 492.0831. HPLC purity: 99.59%.

*N*-((1,1'-Biphenyl)-4-ylmethyl)-1-(3,4-dichlorobenzoyl)-4-(2,6-dioxo-1,2,3,6-tetrahydropyrimidine-4-carbonyl) Piperazine-2-carboxamide (**GA-14**). White solid, 68% yield. mp 266–268 °C.  $^1\text{H}$  NMR (600 MHz, DMSO- $d_6$ ):  $\delta$  11.24 (d,  $J$  = 24.7 Hz, 2H), 8.76 (d,  $J$  = 47.1 Hz, 1H), 7.63 (d,  $J$  = 7.6 Hz, 2H), 7.60–7.51 (m, 2H), 7.45 (q,  $J$  = 9.4, 8.6 Hz, 3H), 7.35 (t,  $J$  = 7.4 Hz, 1H), 7.23 (d,  $J$  = 8.0 Hz, 2H), 7.06 (dd,  $J$  = 16.0, 3.0 Hz, 1H), 6.87 (t,  $J$  = 9.7 Hz, 1H), 5.45 (s, 1H), 4.49 (d,  $J$  = 19.7 Hz, 1H), 4.37–4.21 (m, 1H), 4.19–4.08 (m, 2H), 3.64 (t,  $J$  = 12.7 Hz, 1H), 3.58 (p,  $J$  = 6.7 Hz, 2H), 3.49 (d,  $J$  = 8.4 Hz, 1H), 3.25 (t,  $J$  = 9.2 Hz, 1H).  $^{13}\text{C}$  NMR (150 MHz, DMSO- $d_6$ ):  $\delta$  170.08, 164.25, 161.57, 151.54, 149.89, 147.24, 140.46, 139.31, 138.67, 132.06, 130.99, 129.40, 128.57, 128.25, 128.08, 127.80, 127.05, 115.88, 114.87, 99.45, 58.20, 53.76, 47.50, 42.03, 12.71. HRMS (ESI)  $m/z$  [ $M + H$ ] $^+$  calcd for  $\text{C}_{29}\text{H}_{25}\text{Cl}_2\text{N}_5\text{O}_4$ , 577.1284; found, 578.1353. HPLC purity: 96.12%.

*N*-(2-Boc-2-Azaspiro[3.3]heptan-6-yl)-1-(3,4-dichlorobenzoyl)-4-(2,6-dioxo-1,2,3,6-tetrahydropyrimidine-4-carbonyl) Piperazine-2-carboxamide (**GA-15**). White solid, 78% yield. mp 268–270 °C.  $^1\text{H}$  NMR (600 MHz, DMSO- $d_6$ ):  $\delta$  11.20 (d,  $J$  = 39.4 Hz, 2H), 8.39 (dd,  $J$  = 36.3, 7.1 Hz, 1H), 7.40 (d,  $J$  = 8.8 Hz, 1H), 7.01 (d,  $J$  = 3.0 Hz, 1H), 6.79 (dd,  $J$  = 9.0, 3.1 Hz, 1H), 5.41 (s, 1H), 4.52–4.24 (m, 1H), 4.11 (t,  $J$  = 13.3 Hz, 1H), 3.95 (hept,  $J$  = 7.8 Hz, 1H), 3.77 (d,  $J$  = 64.6 Hz, 4H), 3.68–3.62 (m, 1H), 3.56 (d,  $J$  = 9.6 Hz, 1H), 3.46 (t,  $J$  = 9.3 Hz, 2H), 3.12 (t,  $J$  = 9.9 Hz, 1H), 2.43–2.30 (m, 2H), 2.11–1.92 (m, 2H), 1.35 (s, 9H).  $^{13}\text{C}$  NMR (150 MHz, DMSO- $d_6$ ):  $\delta$  169.08, 164.25, 161.83, 155.86, 151.75, 150.01, 131.96, 130.92, 119.83, 115.81, 114.78, 99.43, 78.86, 57.77, 57.08, 47.58, 45.51, 43.44, 43.13, 41.34, 40.76, 31.78, 28.54. HRMS (ESI)  $m/z$  [ $M + H$ ] $^+$  calcd for  $\text{C}_{27}\text{H}_{32}\text{Cl}_2\text{N}_5\text{O}_6$ , 606.1760; found, 607.1828. HPLC purity: 99.44%.

1-(3,4-Dichlorobenzoyl)-2-(4,4-difluoropiperidine-1-carbonyl)-4-(2,6-dioxo-1,2,3,6-tetrahydropyrimidine-4-carbonyl) Piperazine (**GA-16**). White solid, 78% yield. mp 218–220 °C.  $^1\text{H}$  NMR (600 MHz, DMSO- $d_6$ ):  $\delta$  11.29 (s, 1H), 11.22 (d,  $J$  = 10.9 Hz, 1H), 7.48–7.35 (m, 1H), 7.10 (s, 1H), 6.88 (d,  $J$  = 9.0 Hz, 1H), 5.37 (d,  $J$  = 70.1 Hz, 1H), 5.21 (d,  $J$  = 60.1 Hz, 1H), 4.40 (dd,  $J$  = 115.4, 13.1 Hz, 1H), 3.97–3.85 (m, 1H), 3.81–3.55 (m, 4H), 3.45 (d,  $J$  = 10.3 Hz, 1H), 3.06 (t,  $J$  = 14.5 Hz, 1H), 1.90 (q,  $J$  = 57.1, 52.9 Hz, 4H).  $^{13}\text{C}$  NMR (150 MHz, DMSO- $d_6$ ):  $\delta$  169.29, 164.08, 161.75, 151.45, 149.69, 147.24, 132.11, 131.18, 120.39, 116.24, 115.10, 98.88, 53.92, 53.50, 47.21, 45.80, 44.35, 43.72, 43.17, 42.11, 40.94. HRMS (ESI)  $m/z$  [ $M + H$ ] $^+$  calcd for  $\text{C}_{21}\text{H}_{21}\text{Cl}_2\text{F}_2\text{N}_5\text{O}_4$ , 515.0939; found, 516.1010. HPLC purity: 98.04%.

*N*-(Thiophen-2-ylmethyl)-1-(3,4-dichlorobenzoyl)-4-(2,6-dioxo-1,2,3,6-tetrahydropyrimidine-4-carbonyl) Piperazine-2-carboxy-

amide (**GA-17**). White solid, 78% yield. mp 176–178 °C.  $^1\text{H}$  NMR (600 MHz, DMSO- $d_6$ ):  $\delta$  11.21 (d,  $J$  = 16.6 Hz, 2H), 8.85–8.70 (m, 1H), 7.40 (d,  $J$  = 9.0 Hz, 1H), 7.36 (d,  $J$  = 4.8 Hz, 1H), 7.00 (d,  $J$  = 3.0 Hz, 1H), 6.94–6.91 (m, 1H), 6.89 (s, 1H), 6.83–6.78 (m, 1H), 5.42 (d,  $J$  = 15.6 Hz, 1H), 4.54 (dd,  $J$  = 15.4, 6.6 Hz, 1H), 4.46–4.36 (m, 2H), 4.26 (dd,  $J$  = 15.4, 5.1 Hz, 1H), 4.15–4.05 (m, 1H), 3.82–3.59 (m, 2H), 3.60–3.44 (m, 2H).  $^{13}\text{C}$  NMR (150 MHz, DMSO- $d_6$ ):  $\delta$  169.32, 164.23, 161.71, 151.08, 149.34, 147.14, 142.56, 132.84, 130.91, 128.30, 125.68, 125.45, 119.91, 115.75, 114.29, 99.91, 58.24, 47.30, 43.07, 41.47, 37.94. HRMS (ESI)  $m/z$  [ $M + H$ ] $^+$  calcd for  $\text{C}_{21}\text{H}_{19}\text{Cl}_2\text{N}_5\text{O}_4\text{S}$ , 507.0535; found, 508.0605. HPLC purity: 99.67%.

*N*-(3,5-Difluorophenyl)-1-(3,4-dichlorobenzoyl)-4-(2,6-dioxo-1,2,3,6-tetrahydropyrimidine-4-carbonyl) Piperazine-2-carboxamide (**GA-18**). White solid, 69% yield. mp 174–176 °C.  $^1\text{H}$  NMR (600 MHz, DMSO- $d_6$ ):  $\delta$  11.17 (d,  $J$  = 44.7 Hz, 2H), 10.55 (d,  $J$  = 179.4 Hz, 1H), 7.43 (d,  $J$  = 8.8 Hz, 1H), 7.26 (d,  $J$  = 9.1 Hz, 2H), 7.15 (d,  $J$  = 12.1 Hz, 1H), 6.90 (dq,  $J$  = 18.4, 10.0, 9.3 Hz, 2H), 5.36 (d,  $J$  = 126.9 Hz, 1H), 4.68 (t,  $J$  = 25.8 Hz, 1H), 4.28 (dd,  $J$  = 80.4, 13.6 Hz, 1H), 3.96–3.74 (m, 1H), 3.73–3.54 (m, 2H), 3.54–3.40 (m, 2H), 3.13 (dd,  $J$  = 16.0, 9.5 Hz, 1H).  $^{13}\text{C}$  NMR (150 MHz, DMSO- $d_6$ ):  $\delta$  170.06, 169.26, 164.31, 163.89, 163.67, 163.30, 162.05, 161.66, 151.47, 150.31, 147.38, 147.10, 132.09, 131.02, 120.77, 119.89, 116.23, 115.05, 103.21, 103.04, 99.34, 99.29, 58.53, 53.90, 47.52, 43.36. HRMS (ESI)  $m/z$  [ $M + H$ ] $^+$  calcd for  $\text{C}_{22}\text{H}_{17}\text{Cl}_2\text{F}_2\text{N}_5\text{O}_4$ , 523.0626; found, 524.0700. HPLC purity: 98.44%.

*N*-(4-(Trifluoromethyl)phenyl)-1-(3,4-dichlorobenzoyl)-4-(2,6-dioxo-1,2,3,6-tetrahydropyrimidine-4-carbonyl) Piperazine-2-carboxamide (**GA-19**). White solid, 78% yield. mp 220–222 °C.  $^1\text{H}$  NMR (600 MHz, DMSO- $d_6$ ):  $\delta$  11.27 (d,  $J$  = 53.2 Hz, 1H), 11.17 (d,  $J$  = 52.1 Hz, 1H), 10.47 (d,  $J$  = 137.1 Hz, 1H), 7.73 (d,  $J$  = 8.4 Hz, 2H), 7.64 (dd,  $J$  = 35.4, 8.5 Hz, 2H), 7.44 (dd,  $J$  = 9.3, 4.0 Hz, 1H), 7.15 (d,  $J$  = 9.2 Hz, 1H), 6.91 (s, 1H), 5.39 (d,  $J$  = 101.8 Hz, 1H), 4.67 (s, 1H), 4.27 (dd,  $J$  = 86.9, 13.8 Hz, 1H), 3.86 (dd,  $J$  = 72.4, 11.5 Hz, 1H), 3.69 (dd,  $J$  = 38.8, 12.0 Hz, 1H), 3.62–3.44 (m, 2H), 3.17 (td,  $J$  = 17.6, 15.8, 9.0 Hz, 1H).  $^{13}\text{C}$  NMR (150 MHz, DMSO- $d_6$ ):  $\delta$  169.25, 164.17, 163.93, 161.77, 151.52, 149.91, 146.75, 142.30, 132.09, 131.03, 126.33, 124.39, 120.38, 116.21, 115.03, 99.40, 58.59, 47.43, 43.36, 41.29. HRMS (ESI)  $m/z$  [ $M + H$ ] $^+$  calcd for  $\text{C}_{23}\text{H}_{18}\text{Cl}_2\text{F}_3\text{N}_5\text{O}_4$ , 555.0688; found, 556.0763. HPLC purity: 94.42%.

*N*-((4-Methylthiophen)-2-ylmethyl)-1-(3,4-dichlorobenzoyl)-4-(2,6-dioxo-1,2,3,6-tetrahydropyrimidine-4-carbonyl) Piperazine-2-carboxamide (**GA-20**). Light-yellow solid, 68% yield. mp 208–210 °C.  $^1\text{H}$  NMR (600 MHz, DMSO- $d_6$ ):  $\delta$  11.21 (d,  $J$  = 17.2 Hz, 2H), 8.71 (d,  $J$  = 22.0 Hz, 1H), 7.40 (d,  $J$  = 9.0 Hz, 1H), 6.99 (d,  $J$  = 8.4 Hz, 1H), 6.81 (d,  $J$  = 9.1 Hz, 1H), 6.65 (d,  $J$  = 3.3 Hz, 1H), 6.57 (s, 1H), 5.41 (d,  $J$  = 15.3 Hz, 1H), 4.44–4.33 (m, 2H), 4.21 (ddd,  $J$  = 60.6, 15.3, 5.3 Hz, 1H), 4.08 (t,  $J$  = 12.5 Hz, 1H), 3.81–3.69 (m, 1H), 3.64 (d,  $J$  = 12.6 Hz, 1H), 3.56–3.42 (m, 2H), 3.28–3.17 (m, 1H), 2.36 (s, 3H).  $^{13}\text{C}$  NMR (150 MHz, DMSO- $d_6$ ):  $\delta$  170.20, 169.11, 164.23, 161.69, 151.52, 149.79, 147.16, 140.09, 138.09, 132.03, 130.91, 125.52, 125.08, 115.82, 114.76, 99.45, 58.59, 47.35, 42.63, 41.88, 38.08, 15.37. HRMS (ESI)  $m/z$  [ $M + H$ ] $^+$  calcd for  $\text{C}_{22}\text{H}_{21}\text{Cl}_2\text{N}_5\text{O}_4\text{S}$ , 521.0961; found, 522.0764. HPLC purity: 99.15%.

*N*-(Cyclobutylmethyl)-1-(3,4-dichlorobenzoyl)-4-(2,6-dioxo-1,2,3,6-tetrahydropyrimidine-4-carbonyl) Piperazine-2-carboxamide (**GA-21**). White solid, 56% yield. mp 222–224 °C.  $^1\text{H}$  NMR (600 MHz, DMSO- $d_6$ ):  $\delta$  11.21 (d,  $J$  = 9.7 Hz, 2H), 8.10 (s, 1H), 7.41 (s, 1H), 6.98 (s, 1H), 6.80 (s, 1H), 5.42 (s, 1H), 4.34 (d,  $J$  = 46.5 Hz, 1H), 4.06 (dd,  $J$  = 23.3, 13.4 Hz, 1H), 3.90–3.67 (m, 1H), 3.66–3.39 (m, 3H), 3.28–2.86 (m, 3H), 2.34 (p,  $J$  = 7.5 Hz, 1H), 1.86 (qt,  $J$  = 7.7, 3.3 Hz, 2H), 1.82–1.65 (m, 2H), 1.61–1.48 (m, 2H).  $^{13}\text{C}$  NMR (150 MHz, DMSO- $d_6$ ):  $\delta$  169.98, 163.54, 161.64, 150.89, 148.70, 146.04, 131.99, 130.92, 119.89, 115.66, 114.64, 99.42, 58.11, 47.48, 44.05, 43.05, 41.52, 35.04, 25.43, 18.14. HRMS (ESI)  $m/z$  [ $M + H$ ] $^+$  calcd for  $\text{C}_{21}\text{H}_{23}\text{Cl}_2\text{N}_5\text{O}_4$ , 479.1127; found, 480.1198. HPLC purity: 97.70%.

*N*-Cyclobutyl-1-(3,4-dichlorobenzoyl)-4-(2,6-dioxo-1,2,3,6-tetrahydropyrimidine-4-carbonyl) Piperazine-2-carboxamide (**GA-22**). White solid, 64% yield. mp 188–190 °C.  $^1\text{H}$  NMR (600 MHz, DMSO- $d_6$ ):  $\delta$  10.86 (s, 2H), 8.37 (dd,  $J$  = 41.2, 7.5 Hz, 1H), 7.36 (dd,  $J$  = 58.1, 9.0 Hz, 1H), 7.01 (d,  $J$  = 2.9 Hz, 1H), 6.79 (dd,  $J$  = 9.1, 2.9

Hz, 1H), 5.41 (s, 1H), 4.37–4.25 (m, 1H), 4.19–4.05 (m, 2H), 3.83–3.57 (m, 2H), 3.43 (d,  $J = 71.3$  Hz, 2H), 3.12 (t,  $J = 11.8$  Hz, 1H), 2.10 (t,  $J = 8.2$  Hz, 2H), 1.91–1.74 (m, 2H), 1.69–1.49 (m, 2H).  $^{13}\text{C}$  NMR (150 MHz, DMSO- $d_6$ ):  $\delta$  168.74, 164.17, 161.65, 151.55, 150.02, 147.20, 131.97, 130.93, 119.83, 115.80, 114.77, 99.51, 57.65, 47.74, 44.53, 43.16, 41.36, 30.13, 27.86, 15.13. HRMS (ESI)  $m/z$   $[\text{M} + \text{H}]^+$  calcd for  $\text{C}_{20}\text{H}_{21}\text{Cl}_2\text{N}_5\text{O}_4$ , 465.0971; found, 466.1045. HPLC purity: 99.11%.

*N*-Cyclopentyl-1-(3,4-dichlorobenzoyl)-4-(2,6-dioxo-1,2,3,6-tetrahydropyrimidine-4-carbonyl) Piperazine-2-carboxamide (GA-23). White solid, 71% yield. mp 176–178 °C.  $^1\text{H}$  NMR (600 MHz, DMSO- $d_6$ ):  $\delta$  11.21 (s, 2H), 8.05 (dd,  $J = 28.8, 7.2$  Hz, 1H), 7.41 (d,  $J = 9.0$  Hz, 1H), 7.10–6.91 (m, 1H), 6.80 (t,  $J = 11.3$  Hz, 1H), 5.44 (s, 1H), 4.49–4.13 (m, 2H), 3.92 (q,  $J = 6.8$  Hz, 1H), 3.87–3.67 (m, 1H), 3.63 (d,  $J = 12.3$  Hz, 1H), 3.59–3.38 (m, 2H), 1.72 (dp,  $J = 13.1, 7.1, 6.3$  Hz, 2H), 1.58 (d,  $J = 16.8$  Hz, 2H), 1.54–1.39 (m, 3H), 1.39–1.23 (m, 2H).  $^{13}\text{C}$  NMR (150 MHz, DMSO- $d_6$ ):  $\delta$  169.42, 164.10, 161.58, 151.49, 150.01, 147.09, 131.98, 130.93, 115.71, 114.70, 100.68, 99.53, 57.49, 50.90, 43.24, 41.46, 33.03, 32.32, 23.90. HRMS (ESI)  $m/z$   $[\text{M} + \text{H}]^+$  calcd for  $\text{C}_{21}\text{H}_{23}\text{Cl}_2\text{N}_5\text{O}_4$ , 479.1127; found, 480.1196. HPLC purity: 95.12%.

*N*-(4-Methylfuran)-2-ylmethyl-1-(3,4-dichlorobenzoyl)-4-(2,6-dioxo-1,2,3,6-tetrahydropyrimidine-4-carbonyl) Piperazine-2-carboxamide (GA-24). White solid, 73% yield. mp 188–190 °C.  $^1\text{H}$  NMR (600 MHz, DMSO- $d_6$ ):  $\delta$  11.21 (d,  $J = 9.3$  Hz, 2H), 8.58 (d,  $J = 30.2$  Hz, 1H), 7.41 (d,  $J = 9.0$  Hz, 1H), 7.00 (t,  $J = 3.8$  Hz, 1H), 6.81 (dt,  $J = 8.9, 4.2$  Hz, 1H), 6.01 (d,  $J = 3.0$  Hz, 1H), 5.94 (s, 1H), 5.42 (s, 1H), 4.43 (d,  $J = 34.5$  Hz, 1H), 4.31 (dd,  $J = 15.7, 6.2$  Hz, 1H), 4.15–3.96 (m, 2H), 3.85–3.67 (m, 1H), 3.67–3.40 (m, 3H), 3.27–3.04 (m, 1H), 2.20 (s, 3H).  $^{13}\text{C}$  NMR (150 MHz, DMSO- $d_6$ ):  $\delta$  169.81, 164.24, 161.68, 151.53, 151.19, 150.43, 149.86, 147.17, 131.99, 130.91, 119.90, 115.74, 114.70, 108.00, 106.76, 99.39, 58.09, 47.48, 43.06, 41.45, 36.25, 13.66. HRMS (ESI)  $m/z$   $[\text{M} + \text{H}]^+$  calcd for  $\text{C}_{22}\text{H}_{21}\text{Cl}_2\text{N}_5\text{O}_5$ , 505.0920; found, 506.0990. HPLC purity: 97.13%.

*N*-((Pyrro-2-yl)methyl)-1-(3,4-dichlorobenzoyl)-4-(2,6-dioxo-1,2,3,6-tetrahydropyrimidine-4-carbonyl) Piperazine-2-carboxamide (GA-25). Light-yellow solid, 77% yield. mp 152–154 °C.  $^1\text{H}$  NMR (600 MHz, DMSO- $d_6$ ):  $\delta$  11.21 (d,  $J = 16.0$  Hz, 1H), 10.48 (d,  $J = 36.5$  Hz, 1H), 8.44 (d,  $J = 37.8$  Hz, 1H), 7.40 (t,  $J = 8.0$  Hz, 1H), 7.03 (d,  $J = 3.1$  Hz, 1H), 6.82 (dd,  $J = 9.2, 2.9$  Hz, 1H), 6.62 (d,  $J = 6.5$  Hz, 1H), 5.94–5.86 (m, 1H), 5.82 (d,  $J = 11.4$  Hz, 1H), 5.46 (s, 1H), 4.43 (d,  $J = 29.7$  Hz, 1H), 4.33–4.15 (m, 2H), 4.15–4.04 (m, 2H), 3.72–3.46 (m, 4H).  $^{13}\text{C}$  NMR (150 MHz, DMSO- $d_6$ ):  $\delta$  169.65, 164.35, 161.79, 151.63, 149.88, 147.39, 132.59, 130.91, 127.21, 118.68, 117.58, 115.84, 114.02, 107.72, 106.42, 99.37, 57.94, 47.50, 43.10, 41.80, 41.36. HRMS (ESI)  $m/z$   $[\text{M} + \text{H}]^+$  calcd for  $\text{C}_{21}\text{H}_{20}\text{Cl}_2\text{N}_6\text{O}_4$ , 490.0923; found, 491.0992. HPLC purity: 96.08%.

*S*-*N*-(Thiophen-2-ylmethyl)-1-(3,4-dichlorobenzoyl)-4-(2,6-dioxo-1,2,3,6-tetrahydropyrimidine-4-carbonyl) Piperazine-2-carboxamide (GA-175) (26). Light-yellow solid, 69% yield. mp 176–178 °C.  $^1\text{H}$  NMR (600 MHz, DMSO- $d_6$ ):  $\delta$  11.29–11.16 (m, 2H), 8.78 (dt,  $J = 19.5, 5.8$  Hz, 1H), 7.43–7.28 (m, 2H), 7.00 (t,  $J = 3.8$  Hz, 1H), 6.96–6.87 (m, 2H), 6.81 (dd,  $J = 9.0, 3.3$  Hz, 1H), 5.42 (d,  $J = 15.3$  Hz, 1H), 4.54 (dd,  $J = 15.4, 6.6$  Hz, 1H), 4.47–4.37 (m, 2H), 4.26 (dd,  $J = 15.4, 5.1$  Hz, 1H), 4.10 (t,  $J = 13.8$  Hz, 1H), 3.81–3.42 (m, 4H), 3.27–3.17 (m, 1H).  $^{13}\text{C}$  NMR (150 MHz, DMSO- $d_6$ ):  $\delta$  168.94, 164.24, 161.70, 152.35, 149.77, 147.14, 142.56, 132.03, 130.22, 127.11, 125.68, 124.38, 119.28, 115.74, 114.00, 100.84, 58.22, 48.07, 43.06, 41.47, 37.86. HRMS (ESI)  $m/z$   $[\text{M} + \text{H}]^+$  calcd for  $\text{C}_{21}\text{H}_{19}\text{Cl}_2\text{N}_5\text{O}_4\text{S}$ , 507.0535; found, 508.0604. HPLC purity: 99.68%.

*N*-Phenyl-1-(3,4-dichlorobenzoyl)-4-(2,6-dioxo-1,2,3,6-tetrahydropyrimidine-4-carbonyl) Piperazine-2-carboxamide (GA-27). Light-yellow solid, 83% yield. mp 179–180 °C.  $^1\text{H}$  NMR (600 MHz, DMSO- $d_6$ ):  $\delta$  11.28 (d,  $J = 42.4$  Hz, 1H), 11.19 (d,  $J = 36.5$  Hz, 1H), 10.10 (d,  $J = 117.8$  Hz, 1H), 7.48 (d,  $J = 8.0$  Hz, 2H), 7.44 (dd,  $J = 9.2, 3.2$  Hz, 1H), 7.28 (dt,  $J = 20.6, 7.7$  Hz, 2H), 7.13 (d,  $J = 7.8$  Hz, 1H), 7.06 (t,  $J = 7.4$  Hz, 1H), 6.89 (d,  $J = 9.1$  Hz, 1H), 5.42 (d,  $J = 71.3$  Hz, 1H), 4.62 (d,  $J = 32.5$  Hz, 1H), 4.22 (dd,  $J = 85.8, 13.5$  Hz, 1H), 3.97–3.76 (m, 1H), 3.69 (t,  $J = 13.7$  Hz, 1H), 3.62–3.43 (m, 2H), 3.22 (t,  $J = 9.6$  Hz, 1H).  $^{13}\text{C}$  NMR (150 MHz, DMSO- $d_6$ ):  $\delta$

168.64, 164.57, 161.77, 152.01, 150.35, 148.24, 146.12, 137.63, 131.02, 129.29, 129.05, 125.17, 124.34, 120.76, 120.32, 116.72, 114.94, 101.33, 58.63, 47.84, 45.66, 41.37. HRMS (ESI)  $m/z$   $[\text{M} + \text{H}]^+$  calcd for  $\text{C}_{22}\text{H}_{19}\text{Cl}_2\text{N}_5\text{O}_4$ , 487.0814; found, 488.0889. HPLC purity: 96.05%.

*R*-*N*-((Furan-2-yl)-methyl)-1-(3,4-dichlorobenzoyl)-4-(2,6-dioxo-1,2,3,6-tetrahydropyrimidine-4-carbonyl) Piperazine-2-carboxamide (GA-13R) (28). White solid, 78% yield. mp 248–251 °C.  $^1\text{H}$  NMR (600 MHz, DMSO- $d_6$ ):  $\delta$  11.22 (d,  $J = 10.3$  Hz, 1H), 9.58 (s, 1H), 8.71 (dt,  $J = 54.8, 5.7$  Hz, 1H), 7.53 (s, 1H), 7.41 (d,  $J = 9.0$  Hz, 1H), 7.00 (t,  $J = 3.4$  Hz, 1H), 6.82 (td,  $J = 9.0, 8.2, 2.9$  Hz, 1H), 6.38–6.34 (m, 1H), 6.14 (d,  $J = 3.1$  Hz, 1H), 5.42 (s, 1H), 4.54–4.44 (m, 1H), 4.36 (dd,  $J = 15.6, 6.3$  Hz, 1H), 4.24 (qd,  $J = 15.8, 5.7$  Hz, 1H), 4.15–4.02 (m, 2H), 3.71 (dd,  $J = 13.8, 4.3$  Hz, 1H), 3.58 (h,  $J = 6.9$  Hz, 4H), 3.54–3.41 (m, 2H), 3.20 (ddd,  $J = 13.5, 9.7, 4.1$  Hz, 1H).  $^{13}\text{C}$  NMR (150 MHz, DMSO- $d_6$ ):  $\delta$  169.96, 164.24, 161.68, 151.51, 149.86, 147.19, 142.58, 132.01, 130.92, 119.89, 115.72, 114.69, 110.86, 107.17, 99.38, 98.63, 53.72, 41.99, 18.44, 17.22, 12.59. HRMS (ESI)  $m/z$   $[\text{M} + \text{H}]^+$  calcd for  $\text{C}_{21}\text{H}_{19}\text{Cl}_2\text{N}_5\text{O}_5$ , 491.0763; found, 492.0836. HPLC purity: 95.90%.

*N*-(4-(Trifluoromethyl)hexyl)-1-(3,4-dichlorobenzoyl)-4-(2,6-dioxo-1,2,3,6-tetrahydropyrimidine-4-carbonyl) Piperazine-2-carboxamide (GA-29). Light-yellow solid, 78% yield. mp 168–170 °C.  $^1\text{H}$  NMR (600 MHz, DMSO- $d_6$ ):  $\delta$  11.21 (d,  $J = 12.4$  Hz, 2H), 8.09 (dd,  $J = 59.5, 6.9$  Hz, 1H), 7.41 (d,  $J = 9.1$  Hz, 1H), 7.07–6.96 (m, 1H), 6.89–6.80 (m, 1H), 5.43 (d,  $J = 24.0$  Hz, 1H), 4.48 (d,  $J = 63.0$  Hz, 1H), 4.16 (dd,  $J = 137.5, 13.8$  Hz, 2H), 3.93–3.69 (m, 2H), 3.69–3.55 (m, 2H), 3.45 (dd,  $J = 11.8, 6.6$  Hz, 1H), 3.30 (s, 1H), 3.20–3.04 (m, 1H), 1.60 (s, 4H), 1.54–1.36 (m, 4H).  $^{13}\text{C}$  NMR (150 MHz, DMSO- $d_6$ ):  $\delta$  169.89, 164.03, 161.41, 151.47, 149.94, 147.09, 132.04, 131.37, 115.58, 114.66, 99.37, 98.80, 56.60, 55.35, 48.24, 43.95, 43.40, 41.44, 28.30, 28.06, 19.89. HRMS (ESI)  $m/z$   $[\text{M} + \text{H}]^+$  calcd for  $\text{C}_{23}\text{H}_{24}\text{Cl}_2\text{F}_3\text{N}_5\text{O}_4$ , 561.1157; found, 562.1235. HPLC purity: 95.56%.

*S*-*N*-((Furan-2-yl)-methyl)-1-(3,4-dichlorobenzoyl)-4-(2,6-dioxo-1,2,3,6-tetrahydropyrimidine-4-carbonyl) Piperazine-2-carboxamide (GA-13S) (30). White solid, 67% yield. mp 216–218 °C.  $^1\text{H}$  NMR (600 MHz, DMSO- $d_6$ ):  $\delta$  9.74–9.36 (m, 2H), 7.52 (d,  $J = 26.3$  Hz, 1H), 7.37 (dd,  $J = 11.5, 9.0$  Hz, 1H), 6.97 (d,  $J = 2.9$  Hz, 1H), 6.79 (dd,  $J = 9.1, 3.1$  Hz, 1H), 6.43–6.28 (m, 1H), 6.14 (dd,  $J = 57.7, 3.2$  Hz, 1H), 5.06 (d,  $J = 44.5$  Hz, 1H), 4.55–4.36 (m, 2H), 4.33–4.04 (m, 3H), 3.66–3.48 (m, 2H), 3.49–3.38 (m, 1H), 3.15–3.02 (m, 1H).  $^{13}\text{C}$  NMR (150 MHz, DMSO- $d_6$ ):  $\delta$  171.29, 170.20, 167.12, 153.04, 152.56, 150.46, 142.38, 142.17, 131.85, 130.04, 120.10, 119.26, 115.16, 114.59, 110.89, 106.88, 106.73, 95.20, 58.43, 47.73, 43.14, 41.19, 36.24. HRMS (ESI)  $m/z$   $[\text{M} + \text{H}]^+$  calcd for  $\text{C}_{21}\text{H}_{19}\text{Cl}_2\text{N}_5\text{O}_5$ , 491.0763; found, 492.0836. HPLC purity: 98.40%.

*S*-*N*-((1*H*-Pyrazol-5-yl)methyl)-1-(3,4-dichlorobenzoyl)-4-(2,6-dioxo-1,2,3,6-tetrahydropyrimidine-4-carbonyl) Piperazine-2-carboxamide (GA-31). White solid, 58% yield. mp 172–174 °C.  $^1\text{H}$  NMR (600 MHz, DMSO- $d_6$ ):  $\delta$  12.56 (s, 1H), 11.27 (d,  $J = 20.7$  Hz, 2H), 8.49 (s, 1H), 7.41 (d,  $J = 13.8$  Hz, 1H), 7.01 (s, 1H), 6.83 (d,  $J = 9.4$  Hz, 1H), 6.01 (d,  $J = 24.9$  Hz, 1H), 5.46 (s, 1H), 4.54–4.32 (m, 2H), 4.10 (q,  $J = 13.3, 12.4$  Hz, 2H), 3.88–3.42 (m, 4H), 3.20 (d,  $J = 9.5$  Hz, 1H).  $^{13}\text{C}$  NMR (150 MHz, DMSO- $d_6$ ):  $\delta$  171.06, 166.06, 162.62, 152.44, 152.31, 149.78, 142.05, 132.00, 130.91, 129.30, 119.69, 115.44, 114.69, 104.21, 99.31, 56.25, 47.39, 45.45, 43.08, 41.13. HRMS (ESI)  $m/z$   $[\text{M} + \text{H}]^+$  calcd for  $\text{C}_{20}\text{H}_{19}\text{Cl}_2\text{N}_7\text{O}_4$ , 491.0876; found, 492.0951. HPLC purity: 95.90%.

*S*-*N*-(Thiazol-5-ylmethyl)-1-(3,4-dichlorobenzoyl)-4-(2,6-dioxo-1,2,3,6-tetrahydropyrimidine-4-carbonyl) Piperazine-2-carboxamide (GA-32). White solid, 68% yield. mp 218–220 °C.  $^1\text{H}$  NMR (600 MHz, DMSO- $d_6$ ):  $\delta$  10.99 (s, 2H), 9.00 (s, 1H), 8.87 (s, 1H), 7.63 (s, 1H), 7.32 (d,  $J = 9.0$  Hz, 1H), 6.92 (d,  $J = 10.4$  Hz, 1H), 6.72 (d,  $J = 9.0$  Hz, 1H), 5.34 (s, 1H), 4.52 (dd,  $J = 15.3, 6.2$  Hz, 1H), 4.38 (d,  $J = 25.6$  Hz, 2H), 4.26 (dd,  $J = 15.3, 5.1$  Hz, 1H), 4.11–3.95 (m, 1H), 3.68–3.49 (m, 2H), 3.38 (dd,  $J = 12.4, 8.8$  Hz, 2H).  $^{13}\text{C}$  NMR (150 MHz, DMSO- $d_6$ ):  $\delta$  170.04, 165.42, 161.86, 154.91, 148.91, 146.42, 141.63, 137.73, 132.62, 130.30, 125.98, 118.51, 116.32, 114.65, 99.46, 58.64, 47.12, 43.01, 41.44, 35.33. HRMS (ESI)  $m/z$

$[M + H]^+$  calcd for  $C_{20}H_{18}Cl_2N_6O_4S$ , 508.0487; found, 509.0561. HPLC purity: 95.43%.

(5)-*N*-(Thiazol-2-ylmethyl)-1-(3,4-dichlorobenzoyl)-4-(2,6-dioxo-1,2,3,6-tetrahydropyrimidine-4-carbonyl) Piperazine-2-carboxamide (**GA-33**). White solid, 75% yield. mp 161–163 °C.  $^1H$  NMR (600 MHz, DMSO- $d_6$ ):  $\delta$  11.31–11.19 (m, 2H), 9.08 (t,  $J = 5.7$  Hz, 1H), 7.70 (d,  $J = 3.3$  Hz, 1H), 7.61 (d,  $J = 3.2$  Hz, 1H), 7.43 (d,  $J = 9.0$  Hz, 1H), 7.03 (d,  $J = 3.0$  Hz, 1H), 6.84 (dd,  $J = 9.1, 3.0$  Hz, 1H), 5.46 (s, 1H), 4.69 (dd,  $J = 16.2, 6.6$  Hz, 1H), 4.62–4.45 (m, 2H), 4.37–4.14 (m, 1H), 3.90–3.64 (m, 2H), 3.60–3.45 (m, 2H), 3.30–3.22 (m, 1H).  $^{13}C$  NMR (150 MHz, DMSO- $d_6$ ):  $\delta$  170.43, 169.44, 164.25, 161.72, 152.28, 149.74, 147.13, 143.26, 132.04, 130.91, 120.44, 119.53, 115.75, 114.67, 100.62, 58.38, 49.07, 47.22, 43.01, 41.02. HRMS (ESI)  $m/z$   $[M + H]^+$  calcd for  $C_{20}H_{18}Cl_2N_6O_4S$ , 508.0487; found, 509.0559. HPLC purity: 95.00%.

(5)-*N*-(Oxazol-5-ylmethyl)-1-(3,4-dichlorobenzoyl)-4-(2,6-dioxo-1,2,3,6-tetrahydropyrimidine-4-carbonyl) Piperazine-2-carboxamide (**GA-34**). White solid, 73% yield. mp 188–190 °C.  $^1H$  NMR (600 MHz, DMSO- $d_6$ ):  $\delta$  11.16 (s, 2H), 8.85–8.66 (m, 1H), 8.16 (s, 1H), 7.34 (d,  $J = 9.0$  Hz, 1H), 6.94 (s, 1H), 6.83 (d,  $J = 6.6$  Hz, 1H), 6.73 (d,  $J = 5.8$  Hz, 1H), 5.33 (d,  $J = 9.1$  Hz, 1H), 4.45–4.31 (m, 2H), 4.15–3.97 (m, 2H), 3.78–3.54 (m, 2H), 3.52–3.34 (m, 3H), 3.12 (t,  $J = 11.5$  Hz, 1H).  $^{13}C$  NMR (150 MHz, DMSO- $d_6$ ):  $\delta$  169.31, 165.26, 162.29, 152.00, 151.53, 149.88, 149.56, 133.55, 130.53, 123.64, 123.05, 119.86, 115.72, 114.34, 99.03, 58.19, 47.30, 43.04, 41.41, 34.65. HRMS (ESI)  $m/z$   $[M + H]^+$  calcd for  $C_{20}H_{18}Cl_2N_6O_5S$ , 492.0716; found, 493.0789. HPLC purity: 94.70%.

**General Synthesis Procedure for the Intermediates in GB Series.** Methyl-1-Boc-4-(2,6-dioxo-1,2,3,6-tetrahydropyrimidine-4-carbonyl)piperazine-2-carboxylate (**8**). To a suspension of orotic acid (3.52 g, 22.6 mmol) in DCM (120 mL), HATU (11.67 g, 30.7 mmol) was added under an ice bath. The mixture was stirred for 10 min and then added with *N,N*-diisopropyl ethylamine (DIPEA, 7.9 g, 61.4 mmol) and compound **7** (5.0 g, 20.5 mmol). The mixture was allowed to warm to room temperature, then stirred for 2.5 h. When the reaction was finished monitoring by TLC, DCM solution was washed with 1 M HCl, water, and saturated NaCl solution successively. The organic phase was dried over anhydrous  $Na_2SO_4$ , filtered, and concentrated in vacuo to yield a brown oil. The resulting crude product was separated through silica gel column (DCM/MeOH = 80:1 to 50:1) to give compound **8** as a light-yellow foam (5.2 g, 13.6 mmol, 66%).  $^1H$  NMR (400 MHz, DMSO- $d_6$ ):  $\delta$  11.23 (d,  $J = 20.4$  Hz, 2H), 5.50 (s, 1H), 4.87–4.53 (m, 1H), 4.15 (dd,  $J = 51.1, 10.1$  Hz, 1H), 3.93–3.73 (m, 1H), 3.67 (s, 3H), 3.14 (d,  $J = 7.8$  Hz, 1H), 3.07–2.66 (m, 2H), 1.41 (d,  $J = 17.7$  Hz, 9H). ESI-MS  $m/z$   $[M + H]^+$  calcd for  $C_{16}H_{22}N_4O_7$ , 382.1; found, 383.2.

1-Boc-4-(2,6-Dioxo-1,2,3,6-tetrahydropyrimidine-4-carbonyl)piperazine-2-carboxylic Acid (**9**). To a stirred solution of compound **8** (5.0 g, 12.9 mmol) in THF/MeOH (60 mL, v/v = 1/1) was added LiOH (2 M aqueous solution, 45.2 mL, 90.3 mmol) dropwise under an ice bath. Then, the mixture was allowed to react under room temperature for 5 h with stirring. When the reaction finished, the mixture was concentrated under reduced pressure to remove volatile solvent. The resulting solution was then cooled under an ice bath and added with 1 M HCl dropwise accompanied with stirring. The resulting suspension was filtered, to afford compound **9** (4.5 g, 12.2 mmol, 95%) as a light-yellow solid.  $^1H$  NMR (400 MHz, DMSO- $d_6$ ):  $\delta$  13.15 (s, 1H), 11.28 (s, 2H), 5.47 (s, 1H), 4.60 (d,  $J = 23.5$  Hz, 1H), 4.25–4.06 (m, 1H), 3.85–3.71 (m, 1H), 3.33 (s, 2H), 3.16 (d,  $J = 9.4$  Hz, 2H), 1.40 (d,  $J = 14.0$  Hz, 9H). ESI-MS  $m/z$   $[M + H]^+$  calcd for  $C_{15}H_{20}N_4O_7$ , 368.1; found, 369.1.

*N*-(Furan-2-ylmethyl)-1-Boc-4-(2,6-dioxo-1,2,3,6-Tetrahydropyrimidine-4-carbonyl) Piperazine-2-carboxamide (**10a**). To a solution of compound **9** (4.01 g, 10.9 mmol) in DCM (70 mL), *O*-(7-azabenzotriazol-1-yl)-*N,N,N',N'*-tetramethyluronium hexafluorophosphate (HATU, 6.2 g, 16.3 mmol) was added under an ice bath and stirred for 30 min. The solution was then added with DIPEA (4.2 g, 32.61 mmol) and furan-2-ylmethanamine (1.27 g, 13.04 mmol). After stirring for 12 h at room temperature, the solution was washed by 1 M HCl, water, and saturated NaCl solution successively, dried over anhydrous  $Na_2SO_4$ , and concentrated in vacuo. The residue was

purified by flash column chromatography on silica gel to afford **10a** (3.65 g, 8.16 mmol, 75%) as a light-yellow foam. ESI-MS  $m/z$   $[M + H]^+$  calcd for  $C_{20}H_{25}N_5O_7$ , 447.2; found, 448.3.

*N*-(Furan-2-ylmethyl)-1-(2,6-dioxo-1,2,3,6-tetrahydropyrimidine-4-carbonyl) Piperazine-3-carboxamide Trifluoroacetate (**11a**). Compound **10a** (3.65 g, 8.16 mmol) was dissolved in 70 mL of DCM under an ice bath and stirring. To the solution was added trifluoroacetic acid (5.5 g, 48.6 mmol) dropwise under 0 °C. The mixture was stirred under room temperature for 8 h, and DCM and trifluoroacetic acid were removed under reduced pressure. The residual brown oil was added with 15 mL of EtOAc and stirred for 10 min. The precipitated solid was separated by filtering and washed with 2 mL of EtOAc to yield compound **11a** (3.32 g, 89%) as a white solid.  $^1H$  NMR (400 MHz, DMSO- $d_6$ ):  $\delta$  11.25 (s, 2H), 9.77–9.03 (m, 3H), 7.50 (s, 1H), 6.37 (d,  $J = 40.9$  Hz, 2H), 5.62 (s, 1H), 4.59 (dd,  $J = 81.7, 12.4$  Hz, 1H), 4.35 (s, 1H), 4.23 (d,  $J = 15.7$  Hz, 1H), 4.09 (s, 1H), 3.93 (t,  $J = 15.7$  Hz, 1H), 3.57 (s, 1H), 3.39 (d,  $J = 11.5$  Hz, 1H), 3.26 (s, 1H), 3.11–2.94 (m, 1H). ESI-MS  $m/z$   $[M + H]^+$  calcd for  $C_{15}H_{17}N_5O_5$ , 347.1; found, 348.2.

**General Procedure for the Target Compounds in GB Series.** Compound **11a** (1.0 equiv) and  $K_2CO_3$  (4.0 equiv) were mixed in 5 mL of methanol and stirred for 5 min until completely dissolved. Various benzyl bromides, benzoyl chlorides, or benzenesulfonyl chlorides were added to the mixture. The mixture was stirred for 8 h under room temperature and monitored by TLC. The mixture was then diluted by DCM and filtered to remove excess  $K_2CO_3$ . The resulting solution was concentrated in vacuo and separated by flash column chromatography on silica gel to give final products of GB series.

*N*-(Furan-2-ylmethyl)-1-(4-chloro-2-fluorobenzyl)-4-(2,6-dioxo-1,2,3,6-tetrahydropyrimidine-4-carbonyl) Piperazine-2-carboxamide (**GB-1**). White solid, 50% yield, mp 169–171 °C.  $^1H$  NMR (600 MHz, DMSO- $d_6$ ):  $\delta$  11.39–10.93 (m, 2H), 8.55 (dt,  $J = 54.1, 5.8$  Hz, 1H), 7.53 (d,  $J = 9.1$  Hz, 1H), 7.50–7.42 (m, 1H), 7.39 (d,  $J = 9.9$  Hz, 1H), 7.27 (dd,  $J = 8.2, 2.1$  Hz, 1H), 6.37 (d,  $J = 8.8$  Hz, 1H), 6.22 (dd,  $J = 16.7, 3.3$  Hz, 1H), 5.51 (s, 1H), 4.40–4.18 (m, 2H), 3.77–3.50 (m, 4H), 3.45 (d,  $J = 13.8$  Hz, 1H), 3.31–3.25 (m, 1H), 3.20–3.02 (m, 1H), 2.99–2.79 (m, 1H), 2.24 (dd,  $J = 25.5, 10.5$  Hz, 1H).  $^{13}C$  NMR (150 MHz, DMSO- $d_6$ ):  $\delta$  171.13, 163.90, 161.92, 160.27, 152.38, 151.59, 147.71, 143.52, 132.57, 129.61, 125.82, 116.34, 116.16, 111.33, 106.86, 98.70, 63.98, 50.95, 47.95, 46.22, 43.93, 35.90. HRMS (ESI)  $m/z$   $[M + H]^+$  calcd for  $C_{22}H_{21}ClFN_5O_5$ , 489.1215; found, 490.1292. HPLC purity: 96.20%.

*N*-(Furan-2-ylmethyl)-1-(4-chloro-3-fluorobenzyl)-4-(2,6-dioxo-1,2,3,6-tetrahydropyrimidine-4-carbonyl) Piperazine-2-carboxamide (**GB-2**). White solid, 55% yield, mp 161–163 °C.  $^1H$  NMR (600 MHz, DMSO- $d_6$ ):  $\delta$  11.17 (d,  $J = 15.4$  Hz, 2H), 8.61 (dt,  $J = 45.5, 5.8$  Hz, 1H), 7.52 (t,  $J = 8.1$  Hz, 2H), 7.41 (t,  $J = 10.1$  Hz, 1H), 7.18 (t,  $J = 9.2$  Hz, 1H), 6.36 (d,  $J = 9.0$  Hz, 1H), 6.21 (dd,  $J = 16.3, 3.2$  Hz, 1H), 5.51 (d,  $J = 8.4$  Hz, 1H), 4.31 (dddd,  $J = 43.8, 20.8, 15.6, 5.8$  Hz, 2H), 3.79–3.61 (m, 2H), 3.55 (dd,  $J = 13.4, 7.3$  Hz, 1H), 3.39 (d,  $J = 32.1$  Hz, 1H), 3.27 (dd,  $J = 32.2, 13.6$  Hz, 2H), 3.08 (ddd,  $J = 57.9, 8.2, 3.7$  Hz, 1H), 2.84 (dd,  $J = 70.0, 11.4$  Hz, 1H), 2.29–2.15 (m, 1H).  $^{13}C$  NMR (150 MHz, DMSO- $d_6$ ):  $\delta$  170.70, 163.25, 161.31, 157.23, 153.39, 151.56, 149.00, 142.51, 131.14, 130.13, 125.55, 118.51, 117.54, 111.35, 107.18, 101.33, 63.12, 57.61, 48.79, 46.22, 44.36, 35.89. HRMS (ESI)  $m/z$   $[M + H]^+$  calcd for  $C_{22}H_{21}ClFN_5O_5$ , 489.1215; found, 490.1286. HPLC purity: 99.34%.

*N*-(Furan-2-ylmethyl)-1-(3,4-dichloro)-4-(2,6-dioxo-1,2,3,6-tetrahydropyrimidine-4-carbonyl) Piperazine-2-carboxamide (**GB-3**). White solid, 63% yield, mp 176–177 °C.  $^1H$  NMR (600 MHz, DMSO- $d_6$ ):  $\delta$  11.30–11.15 (m, 2H), 8.55 (dt,  $J = 68.4, 5.8$  Hz, 1H), 7.63–7.56 (m, 2H), 7.51 (d,  $J = 5.1$  Hz, 1H), 7.42 (dd,  $J = 8.3, 2.2$  Hz, 1H), 6.40–6.30 (m, 1H), 6.19 (dd,  $J = 13.0, 3.2$  Hz, 1H), 5.52 (d,  $J = 2.9$  Hz, 1H), 4.39–4.15 (m, 2H), 3.98–3.70 (m, 1H), 3.69–3.52 (m, 3H), 3.51 (s, 1H), 3.50–3.38 (m, 1H), 3.28–3.12 (m, 1H), 3.03–2.81 (m, 1H), 2.30 (dt,  $J = 32.5, 8.1$  Hz, 1H).  $^{13}C$  NMR (150 MHz, DMSO- $d_6$ ):  $\delta$  170.15, 164.26, 161.35, 152.46, 151.54, 147.47, 142.58, 135.14, 134.48, 132.85, 129.10, 127.77, 110.89, 107.30, 99.12, 98.74, 63.16, 55.04, 49.04, 46.23, 43.87, 35.88. HRMS (ESI)  $m/z$   $[M$

+ H]<sup>+</sup> calcd for C<sub>22</sub>H<sub>21</sub>Cl<sub>2</sub>N<sub>5</sub>O<sub>5</sub>, 505.0920; found, 506.0993. HPLC purity: 98.29%.

*N*-(Furan-2-ylmethyl)-1-(4-chloro-2-nitro)-4-(2,6-dioxo-1,2,3,6-tetrahydropyrimidine-4-carbonyl) Piperazine-2-carboxamide (**GB-4**). White solid, 53% yield, mp 186–188 °C. <sup>1</sup>H NMR (600 MHz, DMSO-*d*<sub>6</sub>): δ 11.19 (s, 1H), 10.73 (s, 1H), 8.75 (dt, *J* = 63.4, 5.5 Hz, 1H), 8.17 (d, *J* = 2.0 Hz, 2H), 7.93 (d, *J* = 8.2 Hz, 1H), 7.49 (d, *J* = 15.7 Hz, 1H), 6.35 (d, *J* = 16.2 Hz, 1H), 6.22 (s, 1H), 5.52 (d, *J* = 10.2 Hz, 1H), 4.39–4.20 (m, 2H), 3.95 (dd, *J* = 149.5, 13.2 Hz, 1H), 3.76–3.65 (m, 1H), 3.58 (d, *J* = 6.6 Hz, 1H), 3.46 (d, *J* = 14.2 Hz, 1H), 3.32–3.26 (m, 2H), 3.20 (d, *J* = 7.5 Hz, 1H), 2.79 (d, *J* = 12.2 Hz, 1H), 2.26 (q, *J* = 12.1, 10.0 Hz, 1H). <sup>13</sup>C NMR (150 MHz, DMSO-*d*<sub>6</sub>): δ 164.24, 160.53, 152.37, 151.52, 149.03, 147.47, 143.30, 142.50, 135.36, 134.36, 130.12, 122.17, 110.90, 107.27, 99.09, 98.72, 64.27, 49.77, 46.21, 43.83, 35.91, 27.02. HRMS (ESI) *m/z* [M + H]<sup>+</sup> calcd for C<sub>22</sub>H<sub>21</sub>ClN<sub>6</sub>O<sub>7</sub>, 516.1160; found, 517.1235. HPLC purity: 99.28%.

*N*-(Furan-2-ylmethyl)-1-((6-chloropyridin-3-yl)methyl)-4-(2,6-dioxo-1,2,3,6-tetrahydropyrimidine-4-carbonyl) Piperazine-2-carboxamide (**GB-5**). White solid, 59% yield, mp 202–204 °C. <sup>1</sup>H NMR (600 MHz, DMSO-*d*<sub>6</sub>): δ 11.24 (s, 1H), 11.18 (d, *J* = 14.6 Hz, 1H), 8.64 (dt, *J* = 51.5, 5.8 Hz, 1H), 8.34 (d, *J* = 9.1 Hz, 1H), 7.81 (t, *J* = 8.3 Hz, 1H), 7.52 (d, *J* = 10.2 Hz, 1H), 7.48 (d, *J* = 8.2 Hz, 1H), 6.37 (d, *J* = 9.4 Hz, 1H), 6.22 (dd, *J* = 16.9, 3.2 Hz, 1H), 5.52 (d, *J* = 7.2 Hz, 1H), 4.31 (dddd, *J* = 46.1, 20.9, 15.6, 5.8 Hz, 2H), 3.78–3.61 (m, 2H), 3.54 (dd, *J* = 13.4, 7.9 Hz, 1H), 3.45 (d, *J* = 13.9 Hz, 1H), 3.25 (dd, *J* = 27.6, 13.5 Hz, 2H), 3.08 (ddd, *J* = 61.8, 8.1, 3.7 Hz, 1H), 2.96–2.75 (m, 1H), 2.30–2.15 (m, 1H). <sup>13</sup>C NMR (150 MHz, DMSO-*d*<sub>6</sub>): δ 170.14, 164.26, 161.32, 152.44, 151.57, 150.60, 149.63, 147.70, 142.55, 140.78, 133.40, 124.38, 110.94, 107.29, 98.70, 64.17, 63.73, 55.10, 48.04, 43.86, 35.90. HRMS (ESI) *m/z* [M + H]<sup>+</sup> calcd for C<sub>21</sub>H<sub>21</sub>ClN<sub>6</sub>O<sub>5</sub>, 472.1262; found, 473.133. HPLC purity: 99.70%.

*N*-(Furan-2-ylmethyl)-1-(naphthalen-2-ylmethyl)-4-(2,6-dioxo-1,2,3,6-tetrahydropyrimidine-4-carbonyl) Piperazine-2-carboxamide (**GB-6**). White solid, 61% yield, mp 230–232 °C. <sup>1</sup>H NMR (600 MHz, DMSO-*d*<sub>6</sub>): δ 11.25 (s, 1H), 11.19 (d, *J* = 25.0 Hz, 1H), 8.63 (dt, *J* = 49.3, 5.9 Hz, 1H), 7.91–7.82 (m, 3H), 7.77 (d, *J* = 9.4 Hz, 1H), 7.52 (dd, *J* = 24.0, 8.1 Hz, 4H), 6.37 (d, *J* = 10.3 Hz, 1H), 6.25 (dd, *J* = 21.0, 3.2 Hz, 1H), 5.52 (d, *J* = 10.5 Hz, 1H), 4.43–4.26 (m, 2H), 3.90 (t, *J* = 12.0 Hz, 1H), 3.78–3.63 (m, 1H), 3.58–3.38 (m, 2H), 3.33–3.21 (m, 2H), 3.11 (ddd, *J* = 50.7, 8.2, 3.7 Hz, 1H), 3.00–2.80 (m, 1H), 2.24 (dt, *J* = 35.0, 9.0 Hz, 1H). <sup>13</sup>C NMR (150 MHz, DMSO-*d*<sub>6</sub>): δ 170.32, 164.24, 161.28, 152.68, 151.53, 147.66, 142.57, 135.79, 133.31, 132.89, 128.21, 128.05, 127.97, 127.79, 126.54, 126.24, 110.94, 107.24, 99.08, 98.72, 64.43, 58.79, 49.63, 46.29, 44.32, 35.92. HRMS (ESI) *m/z* [M + H]<sup>+</sup> calcd for C<sub>26</sub>H<sub>25</sub>N<sub>5</sub>O<sub>5</sub>, 487.1856; found, 488.1930. HPLC purity: 99.04%.

*N*-(Furan-2-ylmethyl)-1-(4-(trifluoromethyl)benzyl)-4-(2,6-dioxo-1,2,3,6-tetrahydropyrimidine-4-carbonyl) Piperazine-2-carboxamide (**GB-7**). White solid, 67% yield, mp 210–216 °C. <sup>1</sup>H NMR (600 MHz, DMSO-*d*<sub>6</sub>): δ 11.18 (s, 1H), 11.12 (d, *J* = 17.3 Hz, 1H), 8.55 (dt, *J* = 48.6, 5.8 Hz, 1H), 7.61 (d, *J* = 7.8 Hz, 2H), 7.52–7.43 (m, 3H), 6.29 (d, *J* = 9.5 Hz, 1H), 6.14 (dd, *J* = 16.4, 3.2 Hz, 1H), 5.45 (d, *J* = 7.4 Hz, 1H), 4.30–4.14 (m, 2H), 3.73 (t, *J* = 14.7 Hz, 1H), 3.68–3.54 (m, 1H), 3.54–3.38 (m, 2H), 3.26–3.17 (m, 2H), 3.03 (ddd, *J* = 54.1, 8.1, 3.7 Hz, 1H), 2.78 (dd, *J* = 72.9, 12.9 Hz, 1H), 2.15 (dt, *J* = 18.8, 8.6 Hz, 1H). <sup>13</sup>C NMR (150 MHz, DMSO-*d*<sub>6</sub>): δ 170.18, 164.24, 161.28, 152.57, 151.54, 147.67, 143.33, 142.55, 130.09, 128.43, 125.49, 123.92, 110.92, 107.20, 99.08, 64.22, 58.02, 46.26, 43.93, 41.04, 35.89. HRMS (ESI) *m/z* [M + H]<sup>+</sup> calcd for C<sub>23</sub>H<sub>22</sub>F<sub>3</sub>N<sub>5</sub>O<sub>5</sub>, 505.1573; found, 506.1649. HPLC purity: 98.72%.

*N*-(Furan-2-ylmethyl)-1-cyclohexylmethyl-4-(2,6-dioxo-1,2,3,6-tetrahydropyrimidine-4-carbonyl) Piperazine-2-carboxamide (**GB-10**). White solid, 58% yield, mp 144–146 °C. <sup>1</sup>H NMR (600 MHz, DMSO-*d*<sub>6</sub>): δ 11.56–11.10 (m, 1H), 8.48–8.31 (m, 1H), 7.61–7.51 (m, 1H), 6.43–6.34 (m, 1H), 6.23 (ddd, *J* = 23.4, 7.8, 3.2 Hz, 1H), 5.73–5.56 (m, 1H), 4.39–4.22 (m, 2H), 3.99–3.79 (m, 1H), 3.68–3.42 (m, 3H), 3.39 (s, 1H), 3.30–3.13 (m, 2H), 3.04 (ddd, *J* = 66.7, 12.9, 9.4 Hz, 1H), 2.95–2.66 (m, 2H), 1.60 (dd, *J* = 32.9, 6.0 Hz, 7H), 1.11 (s, 4H). <sup>13</sup>C NMR (150 MHz, DMSO-*d*<sub>6</sub>): δ 170.37, 163.04, 161.01, 152.60, 151.80, 142.55, 130.13, 110.91,

107.17, 100.19, 57.63, 50.40, 47.65, 43.49, 37.17, 35.93, 30.43, 29.54, 26.25, 25.76. HRMS (ESI) *m/z* [M + H]<sup>+</sup> calcd for C<sub>22</sub>H<sub>29</sub>N<sub>5</sub>O<sub>5</sub>, 443.2169; found, 444.2239. HPLC purity: 95.90%.

*N*-(Furan-2-ylmethyl)-1-cyclopentylmethyl-4-(2,6-dioxo-1,2,3,6-tetrahydropyrimidine-4-carbonyl) Piperazine-2-carboxamide (**GB-11**). White solid, 60% yield, mp 138–140 °C. <sup>1</sup>H NMR (600 MHz, DMSO-*d*<sub>6</sub>): δ 11.44 (d, *J* = 26.7 Hz, 1H), 11.12 (s, 1H), 8.47–8.22 (m, 1H), 7.61–7.49 (m, 1H), 6.38 (dp, *J* = 8.8, 2.1 Hz, 1H), 6.22 (ddd, *J* = 20.4, 8.8, 3.2 Hz, 1H), 5.71–5.45 (m, 1H), 4.36–4.19 (m, 2H), 3.74–3.48 (m, 2H), 3.23–2.79 (m, 3H), 2.23–1.94 (m, 2H), 1.74–1.38 (m, 7H), 1.23 (s, 4H). <sup>13</sup>C NMR (150 MHz, DMSO-*d*<sub>6</sub>): δ 170.71, 162.39, 160.26, 152.68, 151.70, 142.03, 130.13, 110.91, 107.30, 100.09, 56.91, 49.20, 47.65, 44.27, 43.45, 35.92, 30.66, 30.30, 29.77, 25.11, 24.73. HRMS (ESI) *m/z* [M + H]<sup>+</sup> calcd for C<sub>21</sub>H<sub>27</sub>N<sub>5</sub>O<sub>5</sub>, 429.2012; found, 430.2089. HPLC purity: 97.58%.

*N*-(Furan-2-ylmethyl)-1-((1,1'-biphenyl)-4-ylmethyl)-4-(2,6-dioxo-1,2,3,6-tetrahydropyrimidine-4-carbonyl) Piperazine-2-carboxamide (**GB-12**). White solid, 60% yield, mp 208–210 °C. <sup>1</sup>H NMR (600 MHz, DMSO-*d*<sub>6</sub>): δ 11.21 (t, *J* = 23.3 Hz, 2H), 8.60 (dd, *J* = 43.2, 5.9 Hz, 1H), 7.66 (d, *J* = 7.2 Hz, 2H), 7.61 (d, *J* = 7.7 Hz, 2H), 7.55 (d, *J* = 11.0 Hz, 1H), 7.49–7.44 (m, 2H), 7.43–7.34 (m, 3H), 6.38 (d, *J* = 11.9 Hz, 1H), 6.24 (d, *J* = 13.6 Hz, 1H), 5.52 (d, *J* = 8.6 Hz, 1H), 4.43–4.24 (m, 2H), 4.10–3.72 (m, 2H), 3.67–3.39 (m, 2H), 3.31–3.21 (m, 2H), 3.08 (ddd, *J* = 55.2, 8.2, 3.7 Hz, 1H), 2.89 (ddd, *J* = 68.2, 8.0, 4.4 Hz, 1H), 2.22 (dt, *J* = 29.2, 9.1 Hz, 1H). <sup>13</sup>C NMR (150 MHz, DMSO-*d*<sub>6</sub>): δ 169.22, 164.24, 161.26, 152.66, 151.53, 148.07, 142.05, 140.44, 138.99, 138.01, 130.18, 130.07, 129.40, 127.83, 127.08, 110.94, 107.20, 99.07, 64.49, 58.55, 49.60, 48.19, 46.29, 35.92. HRMS (ESI) *m/z* [M + H]<sup>+</sup> calcd for C<sub>28</sub>H<sub>27</sub>N<sub>5</sub>O<sub>5</sub>, 513.2012; found, 514.2088. HPLC purity: 97.58%.

*N*-(Furan-2-ylmethyl)-1-((2'-cyano-[1,1'-biphenyl]-4-yl)methyl)-4-(2,6-dioxo-1,2,3,6-tetrahydropyrimidine-4-carbonyl) Piperazine-2-carboxamide (**GB-14**). White solid, 55% yield, mp 222–224 °C. <sup>1</sup>H NMR (600 MHz, DMSO-*d*<sub>6</sub>): δ 11.18 (d, *J* = 22.3 Hz, 2H), 8.64 (dt, *J* = 43.3, 5.8 Hz, 1H), 7.95 (d, *J* = 7.9 Hz, 1H), 7.79 (t, *J* = 7.7 Hz, 1H), 7.63 (d, *J* = 7.8 Hz, 1H), 7.58 (t, *J* = 7.6 Hz, 1H), 7.56–7.51 (m, 3H), 7.49 (t, *J* = 8.9 Hz, 2H), 6.37 (dt, *J* = 10.2, 2.4 Hz, 1H), 6.23 (dd, *J* = 16.6, 3.2 Hz, 1H), 5.53 (d, *J* = 14.6 Hz, 1H), 4.43–4.23 (m, 2H), 4.12–3.76 (m, 2H), 3.67 (d, *J* = 13.4 Hz, 1H), 3.62–3.53 (m, 1H), 3.45 (d, *J* = 13.4 Hz, 1H), 3.31–3.22 (m, 2H), 3.12 (ddd, *J* = 58.6, 8.2, 3.7 Hz, 1H), 2.96 (d, *J* = 13.0 Hz, 1H), 2.84 (d, *J* = 12.1 Hz, 1H), 2.30–2.16 (m, 1H). <sup>13</sup>C NMR (150 MHz, DMSO-*d*<sub>6</sub>): δ 169.69, 166.64, 161.69, 151.56, 144.78, 142.55, 137.15, 134.39, 134.02, 130.58, 129.80, 129.68, 129.03, 128.63, 119.10, 111.86, 109.95, 107.26, 101.27, 64.11, 57.72, 48.63, 46.26, 44.33, 34.73. HRMS (ESI) *m/z* [M + H]<sup>+</sup> calcd for C<sub>28</sub>H<sub>27</sub>N<sub>5</sub>O<sub>5</sub>, 538.1965; found, 539.2037. HPLC purity: 94.99%.

*N*-(Furan-2-ylmethyl)-1-(3-chloro-4-(4,4,5,5-tetramethyl-1,3,2-dioxaborolan-2-yl)benzyl)-4-(2,6-dioxo-1,2,3,6-tetrahydropyrimidine-4-carbonyl) piperazine-2-carboxamide (**GB-15**). White solid, 65% yield, mp 156–158 °C. <sup>1</sup>H NMR (600 MHz, DMSO-*d*<sub>6</sub>): δ 11.31–11.10 (m, 2H), 8.81 (dt, *J* = 47.4, 5.9 Hz, 1H), 7.57 (dd, *J* = 7.7, 3.6 Hz, 1H), 7.41 (s, 1H), 7.37–7.32 (m, 1H), 7.26 (dd, *J* = 10.7, 8.0 Hz, 1H), 7.01–6.90 (m, 2H), 5.52 (d, *J* = 12.5 Hz, 1H), 4.56–4.40 (m, 2H), 3.93 (s, 1H), 3.78–3.63 (m, 2H), 3.59–3.50 (m, 1H), 3.27–3.13 (m, 2H), 3.03 (ddd, *J* = 56.0, 8.4, 3.5 Hz, 1H), 2.88–2.82 (m, 1H), 2.76–2.71 (m, 1H), 2.23–2.10 (m, 1H), 1.30 (s, 6H), 1.07 (s, 6H). <sup>13</sup>C NMR (150 MHz, DMSO-*d*<sub>6</sub>): δ 170.12, 164.24, 162.03, 151.55, 146.88, 143.46, 142.81, 138.90, 136.73, 130.91, 127.99, 127.13, 125.86, 125.48, 98.24, 84.37, 74.01, 65.12, 58.64, 49.78, 44.50, 38.47, 25.42, 25.03. HRMS (ESI) *m/z* [M + H]<sup>+</sup> calcd for C<sub>28</sub>H<sub>33</sub>BClN<sub>5</sub>O<sub>5</sub>S, 613.1933; found, 614.2019. HPLC purity: 95.34%.

*N*-(Furan-2-ylmethyl)-1-(2,4-dichlorobenzoyl)-4-(2,6-dioxo-1,2,3,6-tetrahydropyrimidine-4-carbonyl) Piperazine-2-carboxamide (**GB-16**). White solid, 62% yield, mp 215–218 °C. <sup>1</sup>H NMR (600 MHz, DMSO-*d*<sub>6</sub>): δ 11.21 (t, *J* = 19.4 Hz, 2H), 8.74 (q, *J* = 37.1, 33.4 Hz, 1H), 7.78 (s, 1H), 7.60–7.25 (m, 3H), 6.96 (d, *J* = 5.0 Hz, 2H), 5.41 (d, *J* = 63.9 Hz, 1H), 5.09 (t, *J* = 27.9 Hz, 1H), 4.73–4.52 (m, 1H), 4.32 (d, *J* = 15.5 Hz, 1H), 4.14 (dd, *J* = 32.6, 13.4 Hz, 1H), 3.67–3.45 (m, 2H), 3.22 (p, *J* = 13.4, 12.6 Hz, 1H), 3.10 (q, *J* = 7.3 Hz, 1H). <sup>13</sup>C NMR (150 MHz, DMSO-*d*<sub>6</sub>): δ 166.78, 164.16, 161.89,



151.52, 147.38, 141.46, 135.14, 134.47, 130.74, 130.12, 129.70, 128.47, 127.21, 127.11, 126.12, 125.04, 99.53, 55.35, 53.74, 42.06, 38.05. HRMS (ESI)  $m/z$   $[M + H]^+$  calcd for  $C_{22}H_{19}Cl_2N_3O_5S$ , 535.0484; found, 536.0577. HPLC purity: 99.11%.

(S)-N-(Furan-2-ylmethyl)-1-((4-chlorophenyl)sulfonyl)-4-(2,6-dioxo-1,2,3,6-tetrahydropyrimidine-4-carbonyl) Piperazine-2-carboxamide (**GB-17**). White solid, 72% yield, mp 236–238 °C.  $^1H$  NMR (600 MHz, DMSO- $d_6$ ):  $\delta$  11.18 (m, 2H), 8.68 (dt, 1H), 7.76 (dd,  $J = 22.7, 8.2$  Hz, 2H), 7.61 (d,  $J = 7.8$  Hz, 2H), 7.41 (d,  $J = 5.1$  Hz, 1H), 7.01–6.86 (m, 2H), 5.31 (s, 1H), 4.58–4.40 (m, 2H), 4.21 (d,  $J = 12.3$  Hz, 1H), 4.14–3.99 (m, 1H), 3.83–3.70 (m, 1H), 3.63 (s, 1H), 3.04 (d,  $J = 12.5$  Hz, 1H), 2.72 (t,  $J = 11.9$  Hz, 1H).  $^{13}C$  NMR (150 MHz, DMSO- $d_6$ ):  $\delta$  170.34, 164.11, 162.05, 152.32, 151.76, 147.99, 142.36, 139.20, 137.76, 129.70, 126.75, 110.07, 107.13, 100.90, 65.99, 51.65, 49.38, 44.72, 35.72. HRMS (ESI)  $m/z$   $[M + H]^+$  calcd for  $C_{22}H_{19}Cl_2N_3O_5S$ , 537.0544; found, 538.0622. HPLC purity: 96.88%.

(S)-N-(Furan-2-ylmethyl)-1-(3,4-dichloro)-4-(2,6-dioxo-1,2,3,6-tetrahydropyrimidine-4-carbonyl) Piperazine-2-carboxamide (**GB-35**). White solid, 62% yield, mp 186–188 °C.  $^1H$  NMR (600 MHz, DMSO- $d_6$ ):  $\delta$  11.31–11.14 (m, 2H), 8.56 (d,  $J = 69.2$  Hz, 1H), 7.66–7.54 (m, 2H), 7.51 (d,  $J = 6.7$  Hz, 1H), 7.42 (d,  $J = 10.5$  Hz, 1H), 6.36 (s, 1H), 6.19 (d,  $J = 12.7$  Hz, 1H), 5.52 (s, 1H), 4.38–4.17 (m, 2H), 3.98–3.71 (m, 1H), 3.70–3.47 (m, 4H), 3.48 (s, 1H), 3.28–3.11 (m, 1H), 3.03–2.80 (m, 1H), 2.40–2.19 (m, 1H).  $^{13}C$  NMR (150 MHz, DMSO- $d_6$ ):  $\delta$  170.15, 164.25, 161.32, 152.91, 151.53, 147.65, 142.56, 135.13, 134.48, 132.85, 132.66, 129.07, 127.77, 110.89, 107.19, 98.74, 63.85, 54.15, 48.21, 43.87, 41.02, 35.88. HRMS (ESI)  $m/z$   $[M + H]^+$  calcd for  $C_{22}H_{21}Cl_2N_3O_5S$ , 505.0920; found, 506.0986. HPLC purity: 95.95%.

(S)-N-(Thiophen-2-ylmethyl)-1-(3,4-dichloro)-4-(2,6-dioxo-1,2,3,6-tetrahydropyrimidine-4-carbonyl) Piperazine-2-carboxamide (**GB-135**). White solid, 62% yield, mp 232–234 °C.  $^1H$  NMR (600 MHz, DMSO- $d_6$ ):  $\delta$  11.19 (d,  $J = 19.3$  Hz, 2H), 8.73 (dt,  $J = 63.6, 5.8$  Hz, 1H), 7.67–7.53 (m, 2H), 7.41 (dd,  $J = 8.4, 2.2$  Hz, 1H), 7.38–7.30 (m, 1H), 6.93 (d,  $J = 17.2$  Hz, 2H), 5.53 (s, 1H), 4.56–4.34 (m, 2H), 3.87 (dd,  $J = 158.4, 13.8$  Hz, 1H), 3.73–3.57 (m, 3H), 3.57–3.50 (m, 1H), 3.46–3.36 (m, 1H), 3.26–3.10 (m, 1H), 3.00–2.80 (m, 1H), 2.35–2.22 (m, 1H).  $^{13}C$  NMR (150 MHz, DMSO- $d_6$ ):  $\delta$  171.97, 163.53, 161.35, 152.16, 148.39, 143.53, 134.90, 132.85, 132.15, 128.71, 127.77, 127.11, 125.85, 125.49, 106.12, 64.11, 53.96, 49.01, 48.02, 43.90, 37.62. HRMS (ESI)  $m/z$   $[M + H]^+$  calcd for  $C_{22}H_{21}Cl_2N_3O_5S$ , 521.0691; found, 522.0563. HPLC purity: 96.11%.

**General Synthesis Procedure for the Intermediates in GC Series. 1-(3,4-Dichlorobenzoyl)-4-Boc Piperazine-2-carboxylic Acid (**12**).** To a stirred solution of compound **3** (4.0 g, 10.3 mmol) in THF/MeOH (60 mL,  $v/v = 1/1$ ) was added LiOH (1 M aqueous solution, 41.2 mL, 41.2 mmol) dropwise under an ice bath. Then, the mixture was allowed to react under room temperature for 7 h with stirring. When the reaction finished, the mixture was concentrated under reduced pressure until less than 50 mL remained. The resulting solution was then cooled under an ice bath and added with 1 M HCl dropwise accompanied with stirring. The water phase was extracted with EtOAc (4  $\times$  40 mL). The organic phase was collected and dried over anhydrous  $Na_2SO_4$  and concentrated in vacuo to give compound **12** (3.59 g, 9.60 mmol, 93%) as a white foam. ESI-MS  $m/z$   $[M + H]^+$  calcd for  $C_{16}H_{20}Cl_2N_2O_4$ , 374.1; found, 375.1.

**N-(Thiophen-2-methyl)-1-(3,4-dichlorobenzoyl)-4-Boc-piperazine-2-carboxamide (**13**).** To a suspension of compound **12** (3.59 g, 9.60 mmol) and DCM (80 mL) was added with HATU (5.59 g, 14.4 mmol) under 0 °C and stirred for 30 min. Then, DIPEA (3.71 g, 28.8 mmol, 3 equiv) and thiophen-2-ylmethanamine (1.30 g, 11.5 mmol, 1.2 equiv) were added to the system together. After stirring for 6 h at room temperature, the solution was filtered to remove any precipitate. The organic phase was washed by 0.5 M HCl, water, and saturated NaCl solution successively, dried over anhydrous  $Na_2SO_4$ , and concentrated in vacuo. The residue was purified by flash column chromatography on silica gel to afford **13** (4.03 g, 8.60 mmol, 89%) as an off-white solid. ESI-MS  $m/z$   $[M + H]^+$  calcd for  $C_{21}H_{25}Cl_2N_3O_3S$ , 469.1; found, 470.1.

**N-(Thiophen-2-methyl)-1-(3,4-dichlorobenzoyl)piperazine-2-carboxamide Trifluoroacetate (**14**).** Compound **13** (4.0 g, 8.53 mmol) was dissolved in DCM (80 mL) under an ice bath and stirring. To the solution was added trifluoroacetic acid (6.8 g, 59.7 mmol) dropwise under 0 °C. The reaction was stirred under room temperature for 8 h, monitored by TLC, and filtered to separate precipitate. The organic solution was evaporated under reduced pressure to remove DCM and trifluoroacetic acid, then added with 30 mL *n*-hexane and stirred for 10 min. The precipitate was separated by filtering and washed with 5 mL *n*-hexane. The solid product acquired from filtration was gathered and dried, giving compound **14** (3.38 g, 7.00 mmol, 82%) as a gray-white solid.  $^1H$  NMR (400 MHz, DMSO- $d_6$ ):  $\delta$  9.09 (s, 1H), 8.49 (s, 1H), 7.58–7.37 (m, 2H), 7.22–7.13 (m, 1H), 7.08–6.87 (m, 3H), 4.71–4.53 (m, 2H), 4.48 (dd,  $J = 25.7, 5.8$  Hz, 1H), 3.69 (dd,  $J = 53.0, 13.3$  Hz, 2H), 3.53 (d,  $J = 11.9$  Hz, 1H), 3.26 (d,  $J = 13.1$  Hz, 2H), 3.10 (d,  $J = 20.9$  Hz, 1H). ESI-MS  $m/z$   $[M + H]^+$  calcd for  $C_{16}H_{17}Cl_2N_3OS$ , 369.0; found, 370.1.

**General Procedure for the Compounds in GC Series (GC-1 to GC-5).** DIPEA (0.128 g, 1.0 mmol, 4.0 equiv) and compound **14** (0.12 g, 0.25 mmol, 1.0 equiv) were added successively into 6 mL DCM and stirred until **14** dissolved completely. The mixture was cooled under an ice bath, then various sulfonyl chlorides (0.30 mmol, 1.2 equiv) were added into the system, and the solution was stirred for 2 h, monitored by TLC. The reaction was quenched with saturated  $NaHCO_3$ , then organic phase was separated, washed with saturated NaCl solution, dried over anhydrous  $Na_2SO_4$ , and concentrated in vacuo. The resulting crude products were separated by flash column chromatography on silica gel to give the final products.

(S)-N-(Thiophen-2-ylmethyl)-1-(3,4-dichlorobenzoyl)-4-(pyridin-3-ylsulfonyl)piperazine-2-carboxamide (**GC-1**). Off-white solid, 55% yield, mp 71–80 °C.  $^1H$  NMR (600 MHz, DMSO- $d_6$ ):  $\delta$  8.94–8.86 (m, 2H), 8.66 (t,  $J = 5.9$  Hz, 1H), 8.16 (dt,  $J = 7.2, 1.6$  Hz, 1H), 7.69 (dd,  $J = 8.1, 4.8$  Hz, 1H), 7.41–7.31 (m, 2H), 6.98 (d,  $J = 2.9$  Hz, 1H), 6.93 (d,  $J = 5.0$  Hz, 2H), 6.78 (dd,  $J = 9.1, 3.0$  Hz, 1H), 4.47 (t,  $J = 3.5$  Hz, 1H), 4.45–4.36 (m, 2H), 4.03 (dt,  $J = 12.0, 2.4$  Hz, 1H), 3.70–3.56 (m, 2H), 3.56–3.47 (m, 1H), 2.88 (dd,  $J = 12.2, 4.4$  Hz, 1H), 2.68 (td,  $J = 11.0, 4.4$  Hz, 1H).  $^{13}C$  NMR (150 MHz, DMSO- $d_6$ ):  $\delta$  169.32, 156.01, 150.67, 148.19, 143.09, 137.42, 133.61, 131.96, 130.85, 127.08, 125.56, 125.36, 124.50, 120.99, 116.47, 115.31, 57.44, 47.25, 45.23, 44.52, 37.51. HRMS (ESI)  $m/z$   $[M + H]^+$  calcd for  $C_{21}H_{20}Cl_2N_4O_3S_2$ , 510.0354; found, 511.0433. HPLC purity: 99.00%.

(S)-N-(Thiophen-2-ylmethyl)-1-(3,4-dichlorobenzoyl)-4-((3-chlorophenyl)sulfonyl) piperazine-2-carboxamide (**GC-2**). Off-white solid, 72% yield, mp 77–80 °C.  $^1H$  NMR (600 MHz, DMSO- $d_6$ ):  $\delta$  8.65 (t,  $J = 5.9$  Hz, 1H), 7.81 (d,  $J = 7.7, 1.8$  Hz, 1H), 7.78–7.65 (m, 3H), 7.41–7.32 (m, 2H), 6.98 (d,  $J = 3.0$  Hz, 1H), 6.93 (d,  $J = 4.7$  Hz, 2H), 6.78 (dd,  $J = 9.0, 3.0$  Hz, 1H), 4.46 (q,  $J = 4.6, 4.0$  Hz, 1H), 4.42 (dd,  $J = 5.9, 3.0$  Hz, 2H), 3.99 (dt,  $J = 12.0, 2.4$  Hz, 1H), 3.63 (dt,  $J = 12.5, 3.5$  Hz, 1H), 3.60–3.47 (m, 2H), 2.83 (dd,  $J = 12.1, 4.4$  Hz, 1H), 2.63 (td,  $J = 11.0, 3.7$  Hz, 1H).  $^{13}C$  NMR (150 MHz, DMSO- $d_6$ ):  $\delta$  169.31, 148.66, 142.70, 137.78, 134.72, 133.85, 132.80, 131.95, 130.85, 127.43, 127.08, 126.68, 125.55, 124.93, 120.27, 116.50, 114.58, 57.42, 48.07, 45.90, 44.55, 37.91. HRMS (ESI)  $m/z$   $[M + H]^+$  calcd for  $C_{22}H_{20}Cl_3N_3O_3S_2$ , 543.0012; found, 544.0085. HPLC purity: 99.19%.

(S)-N-(Thiophen-2-ylmethyl)-1-(3,4-dichlorobenzoyl)-4-(4-fluorophenylsulfonyl) piperazine-2-carboxamide (**GC-3**). Light-yellow solid, 69% yield, mp 85–86 °C.  $^1H$  NMR (600 MHz, DMSO- $d_6$ ):  $\delta$  8.66 (t,  $J = 5.9$  Hz, 1H), 8.42–8.32 (m, 1H), 7.98 (dd,  $J = 10.2, 1.9$  Hz, 1H), 7.79 (dd,  $J = 8.5, 1.9$  Hz, 1H), 7.37 (dd,  $J = 4.9, 1.5$  Hz, 1H), 7.34 (d,  $J = 9.0$  Hz, 1H), 6.97 (d,  $J = 2.9$  Hz, 1H), 6.93 (dd,  $J = 7.8, 2.8$  Hz, 2H), 6.77 (dd,  $J = 9.1, 3.0$  Hz, 1H), 4.46 (t,  $J = 3.9$  Hz, 1H), 4.42 (dd,  $J = 5.9, 2.6$  Hz, 2H), 4.01 (dt,  $J = 12.1, 2.5$  Hz, 1H), 3.66 (dt,  $J = 12.7, 3.6$  Hz, 1H), 3.63–3.58 (m, 1H), 3.54–3.47 (m, 1H), 3.03 (dd,  $J = 12.3, 4.6$  Hz, 1H), 2.83 (td,  $J = 11.3, 3.7$  Hz, 1H).  $^{13}C$  NMR (150 MHz, DMSO- $d_6$ ):  $\delta$  169.33, 155.88, 154.12, 150.24, 142.68, 140.12, 134.18, 130.85, 128.17, 127.07, 125.56, 125.36, 124.54, 120.22, 118.39, 118.24, 116.29, 115.15, 57.47, 46.89, 45.14, 43.89, 37.89. HRMS (ESI)  $m/z$   $[M + H]^+$  calcd for

C<sub>22</sub>H<sub>20</sub>Cl<sub>2</sub>FN<sub>3</sub>O<sub>3</sub>S<sub>2</sub>, 527.0307; found, 528.0381. HPLC purity: 98.90%. HPLC purity: 98.10%.

(5)-*N*-(Thiophen-2-ylmethyl)-1-(3,4-dichlorobenzoyl)-4-((4-nitrophenyl)sulfonyl) Piperazine-2-carboxamide (GC-4). Yellow solid, 71% yield, mp 97–99 °C. <sup>1</sup>H NMR (600 MHz, DMSO-*d*<sub>6</sub>): δ 8.67 (t, *J* = 5.9 Hz, 1H), 8.42 (d, *J* = 8.8 Hz, 2H), 8.01 (d, *J* = 8.9 Hz, 2H), 7.40–7.29 (m, 2H), 6.96 (d, *J* = 3.0 Hz, 1H), 6.94–6.89 (m, 2H), 6.77 (dd, *J* = 9.1, 2.9 Hz, 1H), 4.45 (t, *J* = 3.8 Hz, 1H), 4.43–4.39 (m, 2H), 4.01 (dt, *J* = 12.3, 2.4 Hz, 1H), 3.65 (dt, *J* = 12.8, 3.6 Hz, 1H), 3.59 (dt, *J* = 12.8, 4.0 Hz, 1H), 3.55–3.47 (m, 1H), 2.92 (dd, *J* = 12.2, 4.5 Hz, 1H), 2.72 (td, *J* = 11.2, 3.7 Hz, 1H). <sup>13</sup>C NMR (150 MHz, DMSO-*d*<sub>6</sub>): δ 170.20, 150.57, 149.56, 142.70, 140.85, 131.96, 130.27, 128.95, 127.07, 125.56, 125.35, 124.76, 120.25, 117.37, 115.24, 57.47, 47.06, 45.20, 43.99, 37.41. HRMS (ESI) *m/z* [M + H]<sup>+</sup> calcd for C<sub>22</sub>H<sub>20</sub>Cl<sub>2</sub>N<sub>4</sub>O<sub>3</sub>S<sub>2</sub>, 554.0252; found, 555.0324. HPLC purity: 98.92%.

(5)-*N*-(Thiophen-2-ylmethyl)-1-(3,4-dichlorobenzoyl)-4-((4-cyanophenyl)sulfonyl) Piperazine-2-carboxamide (GC-5). Yellow solid, 65% yield, mp 98–100 °C. <sup>1</sup>H NMR (600 MHz, DMSO-*d*<sub>6</sub>): δ 8.65 (t, *J* = 5.9 Hz, 1H), 8.12 (d, *J* = 8.4 Hz, 2H), 7.92 (d, *J* = 8.5 Hz, 2H), 7.41–7.32 (m, 2H), 6.97 (d, *J* = 3.0 Hz, 1H), 6.96–6.90 (m, 2H), 6.77 (dd, *J* = 9.1, 3.0 Hz, 1H), 4.45 (t, *J* = 3.7 Hz, 1H), 4.41 (dd, *J* = 5.9, 3.3 Hz, 2H), 3.99 (dt, *J* = 12.2, 2.3 Hz, 1H), 3.67–3.60 (m, 1H), 3.60–3.54 (m, 1H), 3.50 (td, *J* = 12.4, 11.6, 3.7 Hz, 1H), 2.89 (dd, *J* = 12.2, 4.4 Hz, 1H), 2.75–2.64 (m, 1H). <sup>13</sup>C NMR (150 MHz, DMSO-*d*<sub>6</sub>): δ 169.29, 150.69, 142.70, 140.27, 133.45, 131.96, 130.85, 128.64, 127.08, 125.56, 125.36, 121.01, 118.04, 116.85, 116.22, 115.28, 57.46, 47.17, 45.24, 44.09, 37.91. HRMS (ESI) *m/z* [M + H]<sup>+</sup> calcd for C<sub>23</sub>H<sub>20</sub>Cl<sub>2</sub>N<sub>4</sub>O<sub>3</sub>S<sub>2</sub>, 534.0354; found, 535.0433. HPLC purity: 98.53%.

(5)-1-(3,4-Dichlorophenyl)-4-((3-fluoro-4-nitrophenyl)sulfonyl)-*N*-(thiophen-2-ylmethyl)piperazine-2-carboxamide (GC-7). Yellow solid, 61% yield, mp 92–94 °C. <sup>1</sup>H NMR (600 MHz, DMSO-*d*<sub>6</sub>): δ 8.66 (t, *J* = 5.9 Hz, 1H), 8.42–8.32 (m, 1H), 7.98 (dd, *J* = 10.2, 1.9 Hz, 1H), 7.79 (dd, *J* = 8.5, 1.9 Hz, 1H), 7.37 (dd, *J* = 4.9, 1.5 Hz, 1H), 7.34 (d, *J* = 9.0 Hz, 1H), 6.97 (d, *J* = 2.9 Hz, 1H), 6.93 (dd, *J* = 7.8, 2.8 Hz, 2H), 6.77 (dd, *J* = 9.1, 3.0 Hz, 1H), 4.46 (t, *J* = 3.9 Hz, 1H), 4.42 (dd, *J* = 5.9, 2.6 Hz, 2H), 4.01 (dt, *J* = 12.1, 2.5 Hz, 1H), 3.66 (dt, *J* = 12.7, 3.6 Hz, 1H), 3.63–3.58 (m, 1H), 3.54–3.47 (m, 1H), 3.03 (dd, *J* = 12.3, 4.6 Hz, 1H), 2.83 (td, *J* = 11.3, 3.7 Hz, 1H). <sup>13</sup>C NMR (150 MHz, DMSO-*d*<sub>6</sub>): δ 169.33, 155.88, 154.12, 142.68, 140.12, 130.85, 128.17, 127.07, 125.56, 125.36, 124.54, 120.22, 118.39, 118.24, 116.29, 115.15, 57.47, 46.89, 45.14, 43.89, 37.89. HRMS (ESI) *m/z* [M + H]<sup>+</sup> calcd for C<sub>22</sub>H<sub>20</sub>Cl<sub>2</sub>FN<sub>4</sub>O<sub>3</sub>S<sub>2</sub>, 572.0158; (M + H)<sup>+</sup>, 573.0231. HPLC purity: 96.98%.

**General Procedure for GC-9 to GC-17 and GC-34.** Various acetic acids (0.30 mmol, 1.2 equiv) and *O*-(7-azabenzotriazol-1-yl)-*N,N,N',N'*-tetramethyluronium hexafluorophosphate (0.40 mmol, 1.6 equiv) were mixed in 8 mL of DCM under an ice bath. The mixture was stirred for 10 min and then added with DIPEA (0.128 g, 1.0 mmol, 4.0 equiv) and compound **14** (0.12 g, 0.25 mmol, 1.0 equiv). The solution was allowed to warm to room temperature for 2 h and monitored by TLC. Then, the mixture was washed with 1 M HCl, saturated NaHCO<sub>3</sub>, and saturated NaCl solution successively. The organic phase was dried over anhydrous Na<sub>2</sub>SO<sub>4</sub>, filtered, and concentrated in vacuo. The resulting crude product was separated through silica gel column to give final compounds GC-9 to GC-17 and GC-34.

(5)-*N*-(Thiophen-2-ylmethyl)-1-(3,5-dichlorobenzoyl)-4-(2-(benzo[*d*][1,2,3]triazol-1-yl)acetyl) Piperazine-2-carboxamide (GC-9). White solid, 71% yield, mp 186–188 °C. <sup>1</sup>H NMR (600 MHz, DMSO-*d*<sub>6</sub>): δ 8.86 (dt, *J* = 46.0, 6.0 Hz, 1H), 8.05 (d, *J* = 8.3 Hz, 1H), 7.65 (dd, *J* = 48.3, 8.3 Hz, 1H), 7.52 (td, *J* = 7.4, 3.2 Hz, 1H), 7.46–7.37 (m, 2H), 7.34 (t, *J* = 4.8 Hz, 1H), 7.10 (d, *J* = 3.0 Hz, 1H), 6.97 (dd, *J* = 26.7, 2.6 Hz, 1H), 6.92–6.85 (m, 2H), 5.98–5.83 (m, 1H), 5.69 (dd, *J* = 68.6, 17.2 Hz, 1H), 4.65–4.45 (m, 2H), 4.43 (d, *J* = 11.2 Hz, 1H), 4.36 (d, *J* = 15.3 Hz, 1H), 4.01 (dd, *J* = 31.8, 14.0 Hz, 1H), 3.79–3.72 (m, 1H), 3.67 (d, *J* = 12.9 Hz, 1H), 3.53–3.36 (m, 1H), 3.18 (ddd, *J* = 13.2, 9.5, 3.7 Hz, 1H). <sup>13</sup>C NMR (150 MHz, DMSO-*d*<sub>6</sub>): δ 170.55, 164.69, 149.58, 145.62, 142.68, 135.52,

132.10, 130.94, 127.64, 127.09, 125.76, 125.52, 125.30, 124.21, 119.49, 116.79, 114.90, 111.24, 58.83, 49.14, 45.55, 43.54, 41.52, 38.08. HRMS (ESI) *m/z* [M + H]<sup>+</sup> calcd for C<sub>24</sub>H<sub>22</sub>Cl<sub>2</sub>N<sub>6</sub>O<sub>2</sub>S, 528.0902; found, 529.0977. HPLC purity: 99.68%.

(5)-*N*-(Thiophen-2-ylmethyl)-1-(3,5-dichlorobenzoyl)-4-(4-fluoro-2-(trifluoromethyl) benzoyl) Piperazine-2-carboxamide (GC-10). White solid, 61% yield, mp 132–134 °C. <sup>1</sup>H NMR (600 MHz, DMSO-*d*<sub>6</sub>): δ 8.65 (t, *J* = 6.0 Hz, 1H), 7.80–7.55 (m, 3H), 7.39 (d, *J* = 9.4 Hz, 2H), 7.03–6.88 (m, 3H), 6.79 (d, *J* = 12.8 Hz, 1H), 4.74–4.55 (m, 1H), 4.49 (d, *J* = 4.0 Hz, 1H), 4.26 (dd, *J* = 15.8, 4.6 Hz, 1H), 3.75–3.50 (m, 3H), 3.28 (d, *J* = 32.3 Hz, 3H). <sup>13</sup>C NMR (150 MHz, DMSO-*d*<sub>6</sub>): δ 169.80, 166.19, 160.98, 151.05, 142.23, 133.47, 133.41, 132.05, 131.10, 130.91, 127.09, 125.84, 125.56, 120.04, 119.90, 115.88, 115.64, 114.79, 114.59, 57.36, 47.42, 42.55, 41.05, 37.90. HRMS (ESI) *m/z* [M + H]<sup>+</sup> calcd for C<sub>24</sub>H<sub>19</sub>Cl<sub>2</sub>F<sub>4</sub>N<sub>3</sub>O<sub>2</sub>S, 559.0511; found, 560.0588. HPLC purity: 95.28%.

(5)-*N*-(Thiophen-2-ylmethyl)-1-(3,4-dichlorobenzoyl)-4-(furan-2-carbonyl)piperazine-2-carboxamide (GC-11). Off-white solid, 55% yield, mp 211–213 °C. <sup>1</sup>H NMR (600 MHz, DMSO-*d*<sub>6</sub>): δ 8.81 (s, 1H), 7.84 (s, 1H), 7.40 (dd, *J* = 9.0, 2.3 Hz, 1H), 7.32 (d, *J* = 5.0 Hz, 1H), 7.00 (s, 1H), 6.93 (s, 1H), 6.91–6.87 (m, 1H), 6.85 (s, 1H), 6.75 (d, *J* = 9.0 Hz, 1H), 6.63 (d, *J* = 2.9 Hz, 1H), 4.57 (d, *J* = 13.2 Hz, 1H), 4.40 (s, 1H), 4.39–4.33 (m, 2H), 4.05 (s, 1H), 3.62 (h, *J* = 4.9 Hz, 2H), 3.30 (d, *J* = 2.3 Hz, 2H). <sup>13</sup>C NMR (150 MHz, DMSO-*d*<sub>6</sub>): δ 170.61, 160.03, 149.67, 147.39, 145.39, 142.72, 132.98, 131.42, 127.88, 125.90, 125.28, 118.38, 117.04, 115.17, 113.70, 111.82, 59.00, 43.43, 40.63, 37.89. HRMS (ESI) *m/z* [M + H]<sup>+</sup> calcd for C<sub>21</sub>H<sub>19</sub>Cl<sub>2</sub>N<sub>3</sub>O<sub>3</sub>S, 463.0524; found, 464.0593. HPLC purity: 97.29%.

(5)-*N*-(Thiophen-2-ylmethyl)-1-(3,4-dichlorobenzoyl)-4-((*R,R*)-5-oxopyrrolidine-2-carbonyl) Piperazine-2-carboxamide (GC-12). White solid, 57% yield, mp 121–123 °C. <sup>1</sup>H NMR (600 MHz, DMSO-*d*<sub>6</sub>): δ 8.84 (t, *J* = 6.1 Hz, 1H), 7.67 (s, 1H), 7.38 (dd, *J* = 19.1, 6.7 Hz, 2H), 6.97–6.86 (m, 3H), 6.76 (t, *J* = 6.2 Hz, 1H), 4.48–4.33 (m, 4H), 3.91–3.82 (m, 1H), 3.76–3.49 (m, 3H), 2.10–2.00 (m, 2H), 1.90–1.73 (m, 1H), 1.27 (dd, *J* = 12.1, 6.7 Hz, 3H). <sup>13</sup>C NMR (150 MHz, DMSO-*d*<sub>6</sub>): δ 177.83, 171.28, 170.48, 149.66, 142.60, 133.12, 130.89, 127.05, 125.74, 124.98, 118.75, 115.28, 114.22, 59.20, 51.63, 45.10, 42.99, 37.92, 29.63, 24.93, 16.20. HRMS (ESI) *m/z* [M + H]<sup>+</sup> calcd for C<sub>23</sub>H<sub>20</sub>Cl<sub>2</sub>N<sub>4</sub>O<sub>3</sub>S<sub>2</sub>, 480.0790; found, 481.0865. HPLC purity: 98.02%.

(5)-*N*-(Thiophen-2-ylmethyl)-1-(3,4-dichlorobenzoyl)-4-picolinoylpiperazine-2-carboxamide (GC-13). White solid, 65% yield, mp 105–107 °C. <sup>1</sup>H NMR (600 MHz, DMSO-*d*<sub>6</sub>): δ 8.64–8.60 (m, 1H), 7.96–7.89 (m, 1H), 7.52–7.46 (m, 2H), 7.40–7.33 (m, 2H), 6.95–6.90 (m, 2H), 6.83–6.73 (m, 2H), 4.40 (ddd, *J* = 21.5, 15.4, 6.0 Hz, 1H), 4.23–4.18 (m, 2H), 3.70–3.58 (m, 2H), 3.39 (ddd, *J* = 12.6, 8.3, 4.1 Hz, 1H), 1.44 (d, *J* = 6.8 Hz, 1H), 1.24 (d, *J* = 5.6 Hz, 1H), 1.10 (t, *J* = 6.4 Hz, 1H). <sup>13</sup>C NMR (150 MHz, DMSO-*d*<sub>6</sub>): δ 169.57, 167.51, 153.90, 149.83, 148.51, 142.58, 137.77, 132.02, 130.90, 127.04, 125.53, 125.28, 124.20, 121.35, 119.64, 114.96, 114.32, 58.70, 47.55, 43.10, 41.91, 38.72. HRMS (ESI) *m/z* [M + H]<sup>+</sup> calcd for C<sub>22</sub>H<sub>20</sub>Cl<sub>2</sub>N<sub>4</sub>O<sub>2</sub>S, 474.0684; found, 475.0758. HPLC purity: 96.72%.

(5)-*N*-(Thiophen-2-ylmethyl)-1-(3,4-dichlorobenzoyl)-4-nicotinoylpiperazine-2-carboxamide (GC-14). White solid, 75% yield, mp 101–103 °C. <sup>1</sup>H NMR (600 MHz, DMSO-*d*<sub>6</sub>): δ 8.66 (d, *J* = 3.3 Hz, 1H), 8.54 (d, *J* = 2.1 Hz, 1H), 7.72 (dt, *J* = 7.9, 2.0 Hz, 1H), 7.52–7.44 (m, 1H), 7.40 (d, *J* = 9.0 Hz, 1H), 7.37–7.34 (m, 1H), 6.97 (d, *J* = 2.9 Hz, 1H), 6.92 (dd, *J* = 5.1, 3.3 Hz, 1H), 6.86 (s, 1H), 6.78 (dd, *J* = 9.0, 3.0 Hz, 1H), 4.48 (dd, *J* = 15.0, 5.9 Hz, 1H), 4.26 (s, 2H), 3.93–3.75 (m, 1H), 3.69–3.50 (m, 3H), 3.39 (d, *J* = 10.9 Hz, 1H), 3.20–3.01 (m, 1H). <sup>13</sup>C NMR (150 MHz, DMSO-*d*<sub>6</sub>): δ 169.81, 166.52, 151.41, 149.75, 147.07, 143.40, 137.42, 132.05, 131.94, 130.93, 127.62, 125.68, 125.42, 123.36, 121.27, 116.40, 114.51, 52.85, 34.74, 18.58, 15.55, 12.87. HRMS (ESI) *m/z* [M + H]<sup>+</sup> calcd for C<sub>22</sub>H<sub>20</sub>Cl<sub>2</sub>N<sub>4</sub>O<sub>2</sub>S, 474.0684; found, 475.0759. HPLC purity: 99.21%.

(5)-*N*-(Thiophen-2-ylmethyl)-1-(3,5-dichlorobenzoyl)-4-(3,5-dichlorobenzoyl) Piperazine-2-carboxamide (GC-15). White solid, 63% yield, mp 169–171 °C. <sup>1</sup>H NMR (600 MHz, DMSO-*d*<sub>6</sub>): δ 8.76 (d, *J* = 7.7 Hz, 1H), 7.74 (s, 1H), 7.40 (d, *J* = 9.0 Hz, 1H), 7.36 (d, *J*

= 5.0 Hz, 3H), 6.98 (d,  $J = 2.6$  Hz, 1H), 6.92 (dd,  $J = 5.1, 3.3$  Hz, 1H), 6.86 (s, 1H), 6.78 (d,  $J = 8.4$  Hz, 1H), 4.51 (dd,  $J = 15.2, 6.2$  Hz, 1H), 4.27 (s, 2H), 3.90–3.72 (m, 1H), 3.62 (d,  $J = 34.7$  Hz, 3H), 3.31 (s, 2H).  $^{13}\text{C}$  NMR (150 MHz, DMSO- $d_6$ ):  $\delta$  170.49, 166.87, 149.72, 142.13, 140.26, 136.13, 133.02, 130.93, 129.73, 127.06, 126.22, 125.67, 125.43, 120.34, 118.14, 116.57, 115.62, 114.54, 57.33, 49.31, 42.62, 41.78, 37.01. HRMS (ESI)  $m/z$   $[M + H]^+$  calcd for  $\text{C}_{23}\text{H}_{19}\text{Cl}_4\text{N}_3\text{O}_2\text{S}$ , 540.9952; found, 542.0023. HPLC purity: 95.08%.

(*S*)-*N*-(Thiophen-2-ylmethyl)-1-(3,5-dichlorobenzoyl)-4-(6-oxo-3,6-dihydropyrimidine-4-carbonyl) Piperazine-2-carboxamide (**GC-16**). White solid, 52% yield, mp 130–132 °C.  $^1\text{H}$  NMR (600 MHz, DMSO- $d_6$ ):  $\delta$  12.74 (s, 1H), 8.72 (dt,  $J = 61.4, 5.9$  Hz, 1H), 8.25 (s, 1H), 7.51–7.27 (m, 2H), 6.97 (dd,  $J = 6.5, 3.0$  Hz, 1H), 6.92 (q,  $J = 2.9, 2.5$  Hz, 1H), 6.86 (d,  $J = 3.4$  Hz, 1H), 6.78 (dd,  $J = 9.1, 3.2$  Hz, 1H), 6.30 (d,  $J = 21.5$  Hz, 1H), 4.59–4.37 (m, 2H), 4.31–4.20 (m, 1H), 4.16–4.03 (m, 1H), 3.79–3.69 (m, 1H), 3.64 (ddd,  $J = 18.9, 11.8, 5.6$  Hz, 1H), 3.61–3.54 (m, 1H), 3.52–3.42 (m, 1H), 3.31–3.27 (m, 1H).  $^{13}\text{C}$  NMR (150 MHz, DMSO- $d_6$ ):  $\delta$  170.44, 170.11, 166.62, 161.44, 150.65, 149.42, 142.59, 133.07, 130.89, 127.08, 125.58, 125.39, 124.44, 119.76, 115.53, 114.49, 58.51, 47.14, 43.05, 41.51, 37.88. HRMS (ESI)  $m/z$   $[M + H]^+$  calcd for  $\text{C}_{21}\text{H}_{19}\text{Cl}_2\text{N}_5\text{O}_3\text{S}$ , 491.0586; found, 492.0656. HPLC purity: 96.18%.

(*S*)-*N*-(Thiophen-2-ylmethyl)-1-(3,5-dichlorobenzoyl)-4-(2,6-dichloropyrimidine-4-carbonyl) Piperazine-2-carboxamide (**GC-17**). White solid, 58% yield, mp 178–180 °C.  $^1\text{H}$  NMR (600 MHz, DMSO- $d_6$ ):  $\delta$  8.70 (dt,  $J = 141.7, 5.9$  Hz, 1H), 7.72 (d,  $J = 74.6$  Hz, 1H), 7.43–7.31 (m, 2H), 7.00 (dd,  $J = 14.9, 2.9$  Hz, 1H), 6.96–6.90 (m, 1H), 6.85 (dd,  $J = 26.2, 3.2$  Hz, 1H), 6.80 (dd,  $J = 11.5, 2.9$  Hz, 1H), 4.64–4.43 (m, 2H), 4.44–4.36 (m, 1H), 4.22 (dd,  $J = 15.2, 5.1$  Hz, 1H), 4.05 (d,  $J = 14.0$  Hz, 1H), 3.78–3.68 (m, 1H), 3.59–3.52 (m, 1H), 3.52–3.45 (m, 1H), 3.32 (ddd,  $J = 13.5, 9.8, 4.1$  Hz, 1H).  $^{13}\text{C}$  NMR (150 MHz, DMSO- $d_6$ ):  $\delta$  170.36, 169.67, 165.81, 163.98, 159.97, 150.21, 143.57, 132.01, 130.87, 127.09, 125.69, 125.48, 121.04, 116.32, 114.75, 58.93, 47.20, 43.06, 41.77, 37.94. HRMS (ESI)  $m/z$   $[M + H]^+$  calcd for  $\text{C}_{21}\text{H}_{17}\text{Cl}_4\text{N}_5\text{O}_2\text{S}$ , 542.9857; found, 543.9931. HPLC purity: 98.68%.

(*S*)-*N*-(Thiophen-2-ylmethyl)-1-(3,5-dichlorobenzoyl)-4-(isoquinoline-4-carbonyl) Piperazine-2-carboxamide (**GC-34**). White solid, 65% yield, mp 157–159 °C.  $^1\text{H}$  NMR (600 MHz, DMSO- $d_6$ ):  $\delta$  9.40 (d,  $J = 3.2$  Hz, 1H), 8.41 (s, 1H), 8.23 (d,  $J = 8.1$  Hz, 2H), 7.89–7.75 (m, 3H), 7.39 (d,  $J = 9.1$  Hz, 2H), 7.03–6.84 (m, 3H), 6.78 (dd,  $J = 14.9, 7.7$  Hz, 1H), 4.56 (dd,  $J = 29.7, 4.1$  Hz, 2H), 4.18 (s, 1H), 3.79–3.67 (m, 2H), 3.61 (s, 2H), 3.52 (p,  $J = 6.4$  Hz, 2H).  $^{13}\text{C}$  NMR (150 MHz, DMSO- $d_6$ ):  $\delta$  166.82, 153.90, 149.80, 140.56, 132.05, 130.91, 128.63, 128.50, 127.09, 125.73, 125.60, 125.40, 124.35, 119.77, 115.80, 115.47, 114.71, 114.44, 57.72, 45.87, 44.14, 43.28, 41.54. HRMS (ESI)  $m/z$   $[M + H]^+$  calcd for 524.0841; found, 525.0920. HPLC purity: 99.10%.

## ■ ASSOCIATED CONTENT

### Supporting Information

The Supporting Information is available free of charge at <https://pubs.acs.org/doi/10.1021/acs.jmedchem.2c01146>.

Procedures for in vitro activity experiment, co-crystallization and data, pharmacokinetics study method, and spectral data of the target compounds (PDF)

Molecular formula strings (CSV)

### Accession Codes

SARS-CoV-2  $\text{M}^{\text{Pro}}$  complexes: GA-17S, PDB entry: 8ACD; GC-14, PDB entry: 8ACL.

## ■ AUTHOR INFORMATION

### Corresponding Authors

Ann E. Tollefson – Department of Molecular Microbiology and Immunology, Saint Louis University School of Medicine, St. Louis, Missouri 63103, United States; Saint Louis University Institute for Drug and Biotherapeutic Innovation,

St. Louis, Missouri 63103, United States;

Email: [ann.tollefson@health.slu.edu](mailto:ann.tollefson@health.slu.edu)

Christa E. Müller – PharmaCenter Bonn & Pharmaceutical Institute, Department of Pharmaceutical & Medicinal Chemistry, University of Bonn, Bonn 53113, Germany; [orcid.org/0000-0002-0013-6624](https://orcid.org/0000-0002-0013-6624); Phone: +49-(0)228-73-2301; Email: [christa.mueller@uni-bonn.de](mailto:christa.mueller@uni-bonn.de)

Xinyong Liu – Department of Medicinal Chemistry, Key Laboratory of Chemical Biology, Ministry of Education, School of Pharmaceutical Sciences, Shandong University, Ji'nan 250012, China; [orcid.org/0000-0002-7302-2214](https://orcid.org/0000-0002-7302-2214); Phone: 086-531-88380270; Email: [xinyongl@sdu.edu.cn](mailto:xinyongl@sdu.edu.cn)

Peng Zhan – Department of Medicinal Chemistry, Key Laboratory of Chemical Biology, Ministry of Education, School of Pharmaceutical Sciences, Shandong University, Ji'nan 250012, China; [orcid.org/0000-0002-9675-6026](https://orcid.org/0000-0002-9675-6026); Email: [zhanpeng1982@sdu.edu.cn](mailto:zhanpeng1982@sdu.edu.cn)

## Authors

Shenghua Gao – Department of Medicinal Chemistry, Key Laboratory of Chemical Biology, Ministry of Education, School of Pharmaceutical Sciences, Shandong University, Ji'nan 250012, China; Shenzhen Research Institute of Shandong University, Guangdong 518057, P. R. China

Katharina Sylvester – PharmaCenter Bonn & Pharmaceutical Institute, Department of Pharmaceutical & Medicinal Chemistry, University of Bonn, Bonn 53113, Germany

Letian Song – Department of Medicinal Chemistry, Key Laboratory of Chemical Biology, Ministry of Education, School of Pharmaceutical Sciences, Shandong University, Ji'nan 250012, China

Tobias Claff – PharmaCenter Bonn & Pharmaceutical Institute, Department of Pharmaceutical & Medicinal Chemistry, University of Bonn, Bonn 53113, Germany

Lanlan Jing – Department of Medicinal Chemistry, Key Laboratory of Chemical Biology, Ministry of Education, School of Pharmaceutical Sciences, Shandong University, Ji'nan 250012, China

Molly Woodson – Department of Molecular Microbiology and Immunology, Saint Louis University School of Medicine, St. Louis, Missouri 63103, United States; Saint Louis University Institute for Drug and Biotherapeutic Innovation, St. Louis, Missouri 63103, United States

Renato H. Weiße – Institute of Bioanalytical Chemistry, Center for Biotechnology and Biomedicine, Leipzig University, Leipzig 04103, Germany; [orcid.org/0000-0002-1736-8085](https://orcid.org/0000-0002-1736-8085)

Yusen Cheng – Department of Medicinal Chemistry, Key Laboratory of Chemical Biology, Ministry of Education, School of Pharmaceutical Sciences, Shandong University, Ji'nan 250012, China

Laura Schäkel – PharmaCenter Bonn & Pharmaceutical Institute, Department of Pharmaceutical & Medicinal Chemistry, University of Bonn, Bonn 53113, Germany

Marvin Petry – PharmaCenter Bonn & Pharmaceutical Institute, Department of Pharmaceutical & Medicinal Chemistry, University of Bonn, Bonn 53113, Germany

Michael Gütschow – PharmaCenter Bonn & Pharmaceutical Institute, Department of Pharmaceutical & Medicinal Chemistry, University of Bonn, Bonn 53113, Germany; [orcid.org/0000-0002-9376-7897](https://orcid.org/0000-0002-9376-7897)

- Anke C. Schiedel – PharmaCenter Bonn & Pharmaceutical Institute, Department of Pharmaceutical & Medicinal Chemistry, University of Bonn, Bonn 53113, Germany
- Norbert Sträter – Institute of Bioanalytical Chemistry, Center for Biotechnology and Biomedicine, Leipzig University, Leipzig 04103, Germany; [orcid.org/0000-0002-2001-0500](https://orcid.org/0000-0002-2001-0500)
- Dongwei Kang – Department of Medicinal Chemistry, Key Laboratory of Chemical Biology, Ministry of Education, School of Pharmaceutical Sciences, Shandong University, Ji'nan 250012, China; [orcid.org/0000-0001-9232-953X](https://orcid.org/0000-0001-9232-953X)
- Shujing Xu – Department of Medicinal Chemistry, Key Laboratory of Chemical Biology, Ministry of Education, School of Pharmaceutical Sciences, Shandong University, Ji'nan 250012, China
- Karoly Toth – Department of Molecular Microbiology and Immunology, Saint Louis University School of Medicine, St. Louis, Missouri 63103, United States; Saint Louis University Institute for Drug and Biotherapeutic Innovation, St. Louis, Missouri 63103, United States
- John Tavis – Department of Molecular Microbiology and Immunology, Saint Louis University School of Medicine, St. Louis, Missouri 63103, United States; Saint Louis University Institute for Drug and Biotherapeutic Innovation, St. Louis, Missouri 63103, United States; [orcid.org/0000-0002-8711-4240](https://orcid.org/0000-0002-8711-4240)

Complete contact information is available at:  
<https://pubs.acs.org/10.1021/acs.jmedchem.2c01146>

#### Author Contributions

P.Z. and X.L. conceived the project and designed the experiments. S.G. and L.S. synthesized the compounds. S.G. and L.J. performed enzymatic experiments. L.S. and S.G. carried out computational experiments. A.T., K.T., M.W., and J.T. completed the antiviral activity evaluation and cytotoxicity studies in Vero E6 cells. C.E.M. supervised co-crystallization experiments, structure determination, and enzyme inhibition assays. M.G. designed and provided the fluorogenic substrate; K.S., M.P., and L.S. expressed enzymes and performed assays; K.S. performed the co-crystallization experiments; R.H.W. measured the X-ray diffraction data; T.C., L.S., M.P., A.C.S., N.S., and C.E.M. analyzed the biological and X-ray data; S.G. prepared the manuscript with input from all authors.

#### Notes

The authors declare no competing financial interest.

#### ACKNOWLEDGMENTS

We gratefully acknowledge financial support from the Major Basic Research Project of Shandong Provincial Natural Science Foundation (no. ZR2021ZD17), Guangdong Basic and Applied Basic Research Foundation (no. 2021A1515110740), China Postdoctoral Science Foundation (no. 2021M702003), Science Foundation for Outstanding Young Scholars of Shandong Province (no. ZR2020JQ31), and Foreign Cultural and Educational Experts Project (no. GXL20200015001). C.E.M., M.G., and N.S. were supported by the Volkswagen Foundation. We acknowledge DESY (Hamburg, Germany), a member of the Helmholtz Association HGF, and the EMBL for the provision of experimental facilities at synchrotron beamlines P13 and P14 and the MX Laboratory at the Helmholtz Zentrum Berlin (BESSY II) for beam time. We

thank Selina Storm and Isabel Bento for assistance in using the EMBL beamlines.

#### ABBREVIATIONS

3CL<sup>pro</sup>, 3C-like protease; AUC, area under curve; CL, clearance rate; C<sub>max</sub>, maximum concentration; COVID-19, coronavirus disease 2019; ACE2, angiotensin-converting enzyme 2; DCM, dichloromethane; DIPEA, *N,N*-diisopropyl ethylamine; THF, tetrahydrofuran; FRET, fluorescence resonance energy transfer; HATU, *O*-(7-azabenzotriazol-1-yl)-*N,N,N',N'*-tetramethyluronium hexafluorophosphate; HPLC, high-performance liquid chromatography; M<sup>pro</sup>, main protease; MRT, mean residence time; PLP<sup>pro</sup>, papain-like protease; SAR, structure–activity relationship; SARS-CoV-2, severe acute respiratory syndrome coronavirus 2; TFA, trifluoroacetic acid; TLC, thin-layer chromatography; T<sub>max</sub>, time-to-maximum concentration; TMS, tetramethyl silane

#### REFERENCES

- (1) Zhou, P.; Yang, X. L.; Wang, X. G.; Hu, B.; Zhang, L.; Zhang, W.; Si, H. R.; Zhu, Y.; Li, B.; Huang, C. L.; Chen, H. D.; Chen, J.; Luo, Y.; Guo, H.; Jiang, R. D.; Liu, M. Q.; Chen, Y.; Shen, X. R.; Wang, X.; Zheng, X. S.; Zhao, K.; Chen, Q. J.; Deng, F.; Liu, L. L.; Yan, B.; Zhan, F. X.; Wang, Y. Y.; Xiao, G. F.; Shi, Z. L. A Pneumonia Outbreak Associated With a New Coronavirus of Probable Bat Origin. *Nature* **2020**, *579*, 270–273.
- (2) WHO Coronavirus (COVID-19) Dashboard. <https://covid19.who.int/> (accessed July, 2022).
- (3) Hu, B.; Guo, H.; Zhou, P.; Shi, Z. L. Characteristics of SARS-CoV-2 and COVID-19. *Nat. Rev. Microbiol.* **2021**, *19*, 141–154.
- (4) Stasi, C.; Fallani, S.; Voller, F.; Silvestri, C. Treatment for COVID-19: An Overview. *Eur. J. Pharmacol.* **2020**, *889*, 173644.
- (5) Feikin, D. R.; Higdson, M. M.; Abu-Raddad, L. J.; Andrews, N.; Araos, R.; Goldberg, Y.; Groome, M. J.; Huppert, A.; O'Brien, K. L.; Smith, P. G.; Wilder-Smith, A.; Zeger, S.; Deloria Knoll, M.; Patel, M. K. Duration of Effectiveness of Vaccines Against SARS-CoV-2 Infection and Covid-19 Disease: Results of a Systematic Review and Meta-Regression. *Lancet* **2022**, *399*, 924–944.
- (6) Chen, J.; Wang, R.; Gilby, N. B.; Wei, G. W. Omicron Variant (B.1.1.529): Infectivity, Vaccine Breakthrough, and Antibody Resistance. *J. Chem. Inf. Model.* **2022**, *62*, 412–422.
- (7) Cele, S.; Jackson, L.; Khoury, D. S.; Khan, K.; Moyo-Gwete, T.; Tegally, H.; San, J. E.; Cromer, D.; Scheepers, C.; Amoako, D. G.; Karim, F.; Bernstein, M.; Lustig, G.; Archary, D.; Smith, M.; Ganga, Y.; Jule, Z.; Reedoy, K.; Hwa, S. H.; Giandhari, J.; Blackburn, J. M.; Gosnell, B. I.; Abdool Karim, S. S.; Hanekom, W.; Davies, S. A.; Hsiao, A.; Martin, J. N.; Mlisana, R. J.; Wibmer, M. S.; Williamson, M. P.; York, T.; Harrichandras, P. L.; Herbst, A.; COMMIT-KZN Team. Omicron Extensively but Incompletely Escapes Pfizer BNT162b2 Neutralization. *Nature* **2022**, *602*, 654–656.
- (8) Xiang, R.; Yu, Z.; Wang, Y.; Wang, L.; Huo, S.; Li, Y.; Liang, R.; Hao, Q.; Ying, T.; Gao, Y.; Yu, F.; Jiang, S. Recent Advances in Developing Small-molecule Inhibitors Against SARS-CoV-2. *Acta Pharm. Sin. B* **2022**, *12*, 1591–1623.
- (9) Kneller, D. W.; Phillips, G.; O'Neill, H. M.; Jędrzejczak, R.; Stols, L.; Langan, P.; Joachimiak, A.; Coates, L.; Kovalevsky, A. Structural Plasticity of SARS-CoV-2 3CL M<sup>pro</sup> Active Site Cavity Revealed by Room Temperature X-ray Crystallography. *Nat. Commun.* **2020**, *11*, 3202.
- (10) Zhang, L.; Lin, D.; Sun, X.; Curth, U.; Drosten, C.; Sauerhering, L.; Becker, S.; Rox, K.; Hilgenfeld, R. Crystal Structure of SARS-CoV-2 Main Protease Provides a Basis for Design of Improved  $\alpha$ -ketoamide Inhibitors. *Science* **2020**, *368*, 409–412.
- (11) Gao, S.; Huang, T.; Song, L.; Xu, S.; Cheng, Y.; Cherukupalli, S.; Kang, D.; Zhao, T.; Sun, L.; Zhang, J.; Zhan, P.; Liu, X. Medicinal Chemistry Strategies Towards the Development of Effective SARS-CoV-2 inhibitors. *Acta Pharm. Sin. B* **2022**, *12*, 581–599.

- (12) Konno, S.; Kobayashi, K.; Senda, M.; Funai, Y.; Seki, Y.; Tamai, I.; Schäkel, L.; Sakata, K.; Pillaiyar, T.; Taguchi, A.; Taniguchi, A.; Gütschow, M.; Müller, C. E.; Takeuchi, K.; Hirohama, M.; Kawaguchi, A.; Kojima, M.; Senda, T.; Shirasaka, Y.; Kamitani, W.; Hayashi, Y. 3CL Protease Inhibitors with an Electrophilic Arylketone Moiety as Anti-SARS-CoV-2 Agents. *J. Med. Chem.* **2022**, *65*, 2926–2939.
- (13) Breidenbach, J.; Lemke, C.; Pillaiyar, T.; Schäkel, L.; Al Hamwi, G.; Dielt, M.; Gedschold, R.; Geiger, N.; Lopez, V.; Mirza, S.; Namasivayam, V.; Schiedel, A. C.; Sylvester, K.; Thimm, D.; Vielmuth, C.; Phuong Vu, L.; Zylina, M.; Bodem, J.; Gütschow, M.; Müller, C. E. Targeting the Main Protease of SARS-CoV-2: From the Establishment of High Throughput Screening to the Design of Tailored Inhibitors. *Angew. Chem., Int. Ed. Engl.* **2021**, *60*, 10423–10429.
- (14) Dampalla, C. S.; Rathnayake, A. D.; Kankanamalage, A. C.; Kim, Y.; Perera, K. D.; Nguyen, H. N.; Miller, M. J.; Madden, T. K.; Picard, H. R.; Thurman, H. A.; Kashipathy, M. M.; Liu, L.; Battaile, K. P.; Lovell, S.; Chang, K. O.; Groutas, W. C. Structure-Guided Design of Potent Spirocyclic Inhibitors of Severe Acute Respiratory Syndrome Coronavirus-2 3C-like Protease. *J. Med. Chem.* **2022**, *65*, 7818–7832.
- (15) Owen, D. R.; Allerton, C. M. N.; Anderson, A. S.; Aschenbrenner, L.; Avery, M.; Berritt, S.; Boras, B.; Cardin, R. D.; Carlo, A.; Coffman, K. J.; Dantonio, A.; Di, L.; Eng, H.; Ferre, R.; Gajiwala, K. S.; Gibson, S. A.; Greasley, S. E.; Hurst, B. L.; Kadar, E. P.; Kalgutkar, A. S.; Lee, J. C.; Lee, J.; Liu, W.; Mason, S. W.; Noell, S.; Novak, J. J.; Obach, R. S.; Ogilvie, K.; Patel, N. C.; Pettersson, M.; Rai, D. K.; Reese, M. R.; Sammons, M. F.; Sathish, J. G.; Singh, R. S. P.; Steppan, C. M.; Stewart, A. E.; Tuttle, J. B.; Updyke, L.; Verhoest, P. R.; Wei, L.; Yang, Q.; Zhu, Y. An Oral SARS-CoV-2 M<sup>pro</sup> Inhibitor Clinical Candidate for the Treatment of COVID-19. *Science* **2021**, *374*, 1586–1593.
- (16) Boras, B.; Jones, R. M.; Anson, B. J.; Arenson, D.; Aschenbrenner, L.; Bakowski, M. A.; Beutler, N.; Binder, J.; Chen, E.; Eng, H.; Hammond, H.; Hammond, J.; Haupt, R. E.; Hoffman, R.; Kadar, E. P.; Kania, R.; Kimoto, E.; Kirkpatrick, M. G.; Lanyon, L.; Lendy, E. K.; Lillis, J. R.; Logue, J.; Luthra, S. A.; Ma, C.; Mason, S. W.; McGrath, M. E.; Noell, S.; Obach, R. S.; O'Connor, M. N.; Ogilvie, R.; Owen, K.; Pettersson, D.; Reese, M.; Rogers, M. R.; Rosales, T. F.; Rossulek, R.; Sathish, M. I.; Shirai, J. G.; Steppan, N.; Ticehurst, C.; Updyke, M.; Weston, L. W.; Zhu, S.; White, Y.; Garcia-Sastre, K. M.; Wang, A.; Chatterjee, J.; Mesecar, A. K.; Frieman, A. D.; Anderson, M. B.; Allerton, A. S.; Allerton, C. Preclinical Characterization of an Intravenous Coronavirus 3CL Protease Inhibitor for the Potential Treatment of COVID19. *Nat. Commun.* **2021**, *12*, 6055.
- (17) Cáceres, C. J.; Cardenas-Garcia, S.; Carnaccini, S.; Seibert, B.; Rajao, D. S.; Wang, J.; Perez, D. R. Efficacy of GC-376 Against SARS-CoV-2 Virus Infection in the K18 hACE2 Transgenic Mouse Model. *Sci. Rep.* **2021**, *11*, 9609.
- (18) Dai, W.; Zhang, B.; Jiang, X. M.; Su, H.; Li, J.; Zhao, Y.; Xie, X.; Jin, Z.; Peng, J.; Liu, F.; Li, C.; Li, Y.; Bai, F.; Wang, H.; Cheng, X.; Cen, X.; Hu, S.; Yang, X.; Wang, J.; Liu, X.; Xiao, G.; Jiang, H.; Rao, Z.; Zhang, L. K.; Xu, Y.; Yang, H.; Liu, H. Structure-Based Design of Antiviral Drug Candidates Targeting the SARS-CoV-2 Main Protease. *Science* **2020**, *368*, 1331–1335.
- (19) Pillaiyar, T.; Flury, P.; Krüger, N.; Su, H.; Schäkel, L.; Da Silva, D.; Eppler, E.; Kronenberger, O.; Nie, T.; Luedtke, T.; Rocha, S.; Sylvester, C.; Petry, K.; McKerrow, M. R. I.; Poso, J. H.; Pöhlmann, A.; Gütschow, S.; O'Donoghue, M.; Xu, A. J.; Müller, Y.; Laufer, C. E.; Laufer, S. A. Small-Molecule Thioesters as SARS-CoV-2 Main Protease Inhibitors: Enzyme Inhibition, Structure-Activity Relationships, Antiviral Activity, and X-ray Structure Determination. *J. Med. Chem.* **2022**, *65*, 9376–9395.
- (20) Hattori, S. I.; Higshi-Kuwata, N.; Raghavaiah, J.; Das, D.; Bulut, H.; Davis, D. A.; Takamatsu, Y.; Matsuda, K.; Takamune, N.; Kishimoto, N.; Okamura, T.; Misumi, S.; Yarchoan, R.; Maeda, K.; Ghosh, A. K.; Mitsuya, H. GRL-0920, an Indole Chloropyridinyl Ester, Completely Blocks SARS-CoV-2 Infection. *mBio* **2020**, *11*, No. e01833-20.
- (21) Ma, X. R.; Alugubelli, Y. R.; Ma, Y.; Vatanserver, E. C.; Scott, D. A.; Qiao, Y.; Yu, G.; Xu, S.; Liu, W. R. MPI8 is Potent against SARS-CoV-2 by Inhibiting Dually and Selectively the SARS-CoV-2 Main Protease and the Host Cathepsin L. *ChemMedChem* **2022**, *17*, No. e202100456.
- (22) Ma, C.; Xia, Z.; Sacco, M. D.; Hu, Y.; Townsend, J. A.; Meng, X.; Choza, J.; Tan, H.; Jang, J.; Gongora, M. V.; Zhang, X.; Zhang, F.; Xiang, Y.; Marty, M. T.; Chen, Y.; Wang, J. Discovery of Di- and Trihaloacetamides as Covalent SARS-CoV-2 Main Protease Inhibitors with High Target Specificity. *J. Am. Chem. Soc.* **2021**, *143*, 20697–20709.
- (23) Bai, B.; Arutyunova, E.; Khan, M. B.; Lu, J.; Joyce, M. A.; Saffran, H. A.; Shields, J. A.; Kandadai, A. S.; Belovodskiy, A.; Hena, M.; Vuong, W.; Lamer, T.; Young, H. S.; Vederas, J. C.; Tyrrell, D. L.; Lemieux, M. J.; Nieman, J. A. Peptidomimetic Nitrile Warheads as SARS-CoV-2 3CL Protease Inhibitors. *RSC Med. Chem.* **2021**, *12*, 1722–1730.
- (24) Deshmukh, M. G.; Ippolito, J. A.; Zhang, C. H.; Stone, E. A.; Reilly, R. A.; Miller, S. J.; Jorgensen, W. L.; Anderson, K. S. Structure-Guided Design of a Perampanel-Derived Pharmacophore Targeting the SARS-CoV-2 Main Protease. *Structure* **2021**, *29*, 823–833.
- (25) Kitamura, N.; Sacco, M. D.; Ma, C.; Hu, Y.; Townsend, J. A.; Meng, X.; Zhang, F.; Zhang, X.; Ba, M.; Szeto, T.; Kukuljac, A.; Marty, M. T.; Schultz, D.; Cherry, S.; Xiang, Y.; Chen, Y.; Wang, J. Expedited Approach toward the Rational Design of Noncovalent SARS-CoV-2 Main Protease Inhibitors. *J. Med. Chem.* **2022**, *65*, 2848–2865.
- (26) Unoh, Y.; Uehara, S.; Nakahara, K.; Nobori, H.; Yamatsu, Y.; Yamamoto, S.; Maruyama, Y.; Taoda, Y.; Kasamatsu, K.; Suto, T.; Kouki, K.; Nakahashi, A.; Kawashima, S.; Sanaki, T.; Toba, S.; Uemura, K.; Mizutare, T.; Ando, S.; Sasaki, M.; Orba, Y.; Sawa, H.; Sato, A.; Sato, T.; Kato, T.; Tachibana, Y. Discovery of S-217622, a Noncovalent Oral SARS-CoV-2 3CL Protease Inhibitor Clinical Candidate for Treating COVID-19. *J. Med. Chem.* **2022**, *65*, 6499–6512.
- (27) Clyde, A.; Galanie, S.; Kneller, D. W.; Ma, H.; Babuji, Y.; Blaiszik, B.; Brace, A.; Brettin, T.; Chard, K.; Chard, R.; Coates, L.; Foster, I.; Hauner, D.; Kertesz, V.; Kumar, N.; Lee, H.; Li, Z.; Merzky, A.; Schmidt, J. G.; Tan, L.; Titov, M.; Trifan, A.; Turilli, M.; Van Dam, H.; Chennubhotla, S. C.; Jha, S.; Kovalevsky, A.; Ramanathan, A.; Head, M. S.; Stevens, R. High-Throughput Virtual Screening and Validation of a SARS-CoV-2 Main Protease Noncovalent Inhibitor. *J. Chem. Inf. Model.* **2022**, *62*, 116–128.
- (28) Ju, H.; Murugan, N. A.; Hou, L.; Li, P.; Guizzo, L.; Zhang, Y.; Bertagnin, C.; Kong, X.; Kang, D.; Jia, R.; Ma, X.; Du, R.; Poongavanam, V.; Loregian, A.; Huang, B.; Liu, X.; Zhan, P. Identification of C5-NH2 Modified Oseltamivir Derivatives as Novel Influenza Neuraminidase Inhibitors with Highly Improved Antiviral Activities and Favorable Druggability. *J. Med. Chem.* **2021**, *64*, 17992–18009.
- (29) Qiao, J.; Li, Y. S.; Zeng, R.; Liu, F. L.; Luo, R. H.; Huang, C.; Wang, Y. F.; Zhang, J.; Quan, B.; Shen, C.; Mao, X.; Liu, X.; Sun, W.; Yang, W.; Ni, X.; Wang, K.; Xu, L.; Duan, Z. L.; Zou, Q. C.; Zhang, H. L.; Qu, W.; Long, Y. H.; Li, M. H.; Yang, R. C.; Liu, X.; You, J.; Zhou, Y.; Yao, R.; Li, W. P.; Liu, J. M.; Chen, P.; Liu, Y.; Lin, G. F.; Yang, X.; Zou, J.; Li, L.; Hu, Y.; Lu, G. W.; Li, W. M.; Wei, Y. Q.; Zheng, Y. T.; Lei, J.; Yang, S. SARS-CoV-2 M<sup>pro</sup> Inhibitors with Antiviral Activity in a Transgenic Mouse Model. *Science* **2021**, *371*, 1374–1378.
- (30) Wilcken, R.; Zimmermann, M. O.; Lange, A.; Joerger, A. C.; Boeckler, F. M. Principles and Applications of Halogen Bonding in Medicinal Chemistry and Chemical Biology. *J. Med. Chem.* **2013**, *56*, 1363–1388.
- (31) Han, S. H.; Goins, C. M.; Arya, T.; Shin, W. J.; Maw, J.; Hooper, A.; Sonawane, D. P.; Porter, M. R.; Bannister, B. E.; Crouch, R. D.; Lindsey, A. A.; Lakatos, G.; Martinez, S. R.; Alvarado, J.; Akers, W. S.; Wang, N. S.; Jung, J. U.; Macdonald, J. D.; Stauffer, S. R.

Structure-Based Optimization of ML300-Derived, Noncovalent Inhibitors Targeting the Severe Acute Respiratory Syndrome Coronavirus 3CL Protease (SARS-CoV-2 3CLpro). *J. Med. Chem.* **2022**, *65*, 2880–2904.

(32) Leung, S. S.; Mijalkovic, J.; Borrelli, K.; Jacobson, M. P. Testing Physical Models of Passive Membrane Permeation. *J. Chem. Inf. Model.* **2012**, *52*, 1621–1636.

(33) Leung, S. S.; Sindhikara, D.; Jacobson, M. P. Simple Predictive Models of Passive Membrane Permeability Incorporating Size-Dependent Membrane-Water Partition. *J. Chem. Inf. Model.* **2016**, *56*, 924–929.

(34) Zhang, C. H.; Stone, E. A.; Deshmukh, M.; Ippolito, J. A.; Ghahremanpour, M. M.; Tirado-Rives, J.; Spasov, K. A.; Zhang, S.; Takeo, Y.; Kudalkar, S. N.; Liang, Z.; Isaacs, F.; Lindenbach, B.; Miller, S. J.; Anderson, K. S.; Jorgensen, W. L. Potent Noncovalent Inhibitors of the Main Protease of SARS-CoV-2 from Molecular Sculpting of the Drug Perampanel Guided by Free Energy Perturbation Calculations. *ACS Cent. Sci.* **2021**, *7*, 467–475.